

In vitro and In vivo Bioimaging and Photoelectronic Applications of Graphitic Carbon Nitride (g-C₃N₄) Composite in Drug Delivery Systems for Cancer Cells Treatment

Loutfy H. Madkour

Chemistry Department, Faculty of Science, Tanta University, 31527, Tanta, Egypt.

*Corresponding Author: Loutfy H. Madkour, Chemistry Department, Faculty of Science, Tanta University, 31527, Tanta, Egypt.

Received date: January 08, 2025; Accepted date: January 21, 2025; Published date: February 04, 2025

Citation: Loutfy H. Madkour, (2025), In vitro and In vivo Bioimaging and Photoelectronic Applications of Graphitic Carbon Nitride (g-C₃N₄) Composite in Drug Delivery Systems for Cancer Cells Treatment, *J. Biotechnology and Bioprocessing*, 6(1); DOI:10.31579/2766-2314/150

Copyright: © 2025, Loutfy H. Madkour. This is an open access article distributed under the Creative Commons Attribution License, which permits unrestricted use, distribution, and reproduction in any medium, provided the original work is properly cited.

Abstract

Recently, nanomaterials have been widely applied as biosensors with distinctive features. Graphite phase carbon nitride (g-C₃N₄) is a two-dimensional (2D) carbon-based nanostructure that has received attention in biosensing. Biocompatibility, biodegradability, semiconductivity, high photoluminescence yield, low-cost synthesis, easy production process, antimicrobial activity, and high stability are prominent properties that have rendered g-C₃N₄ a promising candidate to be used in electrochemical, optical, and other kinds of biosensors. These applications encompass a meticulous exploration of detecting biomolecules, drug molecules. Graphitic carbon nitride (g-C₃N₄) has garnered much attention as a promising 2D material in the realm of electrochemical sensors. It contains a polymeric matrix that can serve as an economical and non-toxic electrode material for the detection of a diverse range of analytes. However, its performance is impeded by a relatively limited active surface area and inherent instability. Although electrochemistry involving metal-doped g-C₃N₄ nanomaterials is rapidly progressing, it remains relatively unexplored. The metal doping of g-C₃N₄ augments the electrochemically active surface area of the resulting electrode, which has the potential to significantly enhance electrode kinetics and bolster catalytic activity. Consequentially, the main objective of this chapter is to provide insight into the intricacies of synthesizing and characterizing metal-doped g-C₃N₄. Furthermore, we comprehensively delve into the fundamental attributes of electrochemical sensors based on metal-doped g-C₃N₄, with a specific focus on healthcare and environmental applications. Graphitic carbon nitride (g-C₃N₄) belongs to an older age class of 2-D semiconducting materials that are affordable, metal-free, indispensable towards sensing applications due to identifiable changes in their conductivity after analyte exposure especially when they are in the nano-regime. This review presents the g-C₃N₄ unique features, synthesis methods, and g-C₃N₄-based nanomaterials. In addition, recent relevant studies on using g-C₃N₄ in biosensors in regard to improving treatment pathways are reviewed.

Key Words: g-C₃N₄ modifications; biosensing; bioimaging; drug delivery; cancer therapy; biomedical and healthcare applications

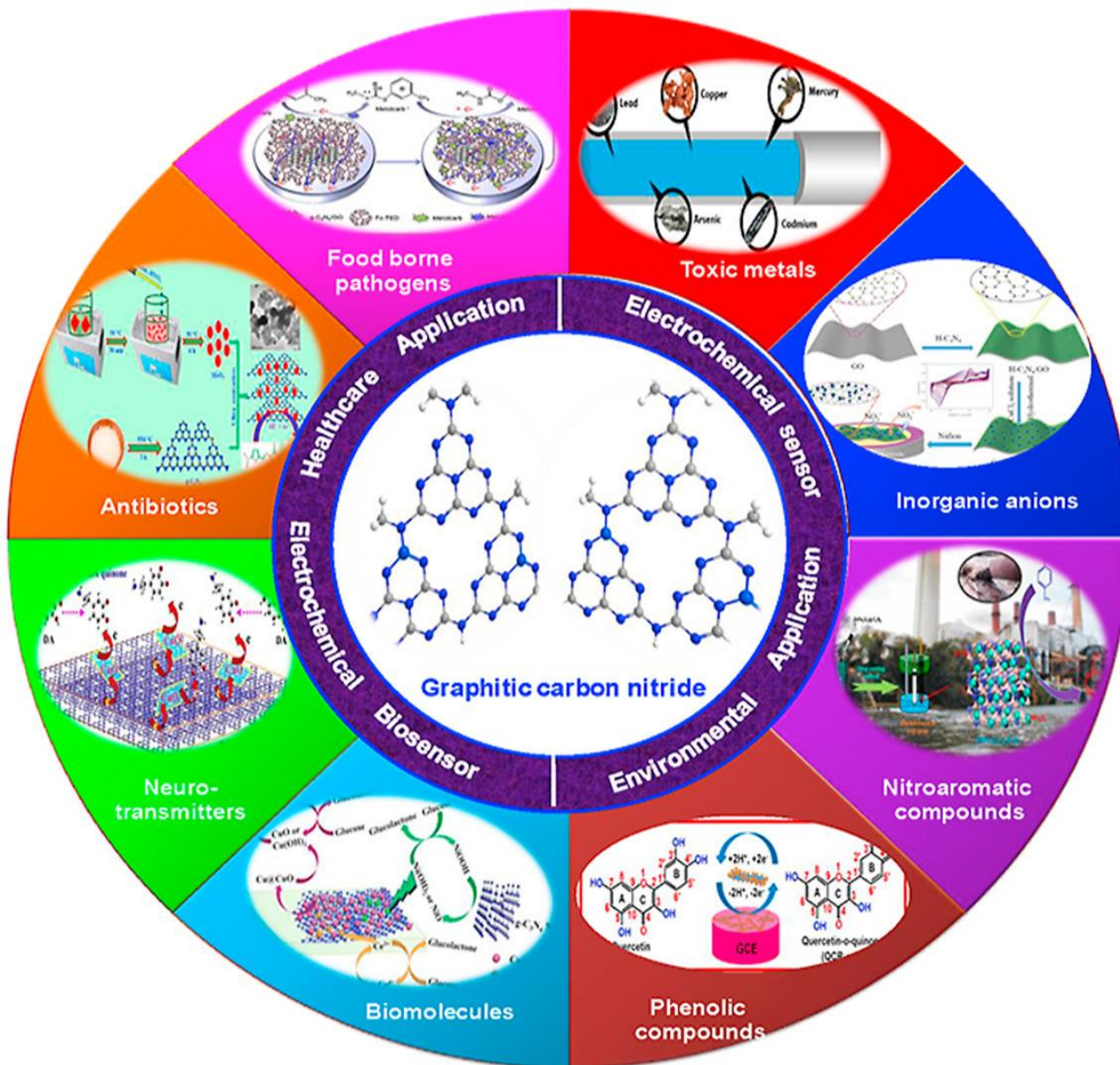
1. Background of Graphitic carbon nitride (g-C₃N₄)

Graphitic carbon nitride (g-C₃N₄, composed of the sp² hybridization with highly delocalized π -conjugated electronic structures) is typical metal-free polymer semiconductor, which has currently been attracted wide attention in energy conversion/storage and environmental remediation due to its various advantages such as high physicochemical stability, unique electronic band structure of visible light responsive sensitivity, and "earth-abundant" nature [1]. More than 25,400 scientific papers concerning carbon nitride or g-C₃N₄ were searched in Web of Science (1/1/2018–23/4/2023). The g-C₃N₄ is comprised of only carbon and nitrogen elements, which are very abundant on the Earth. Importantly, the g-C₃N₄ materials can be easily fabricated by thermal polymerization of abundant nitrogen-rich precursors such as melamine [2,3], dicyandiamide [4], cyanamide [5], urea [4,6], thiourea [7,8],

ammonium thiocyanate [9], etc. Because the band gap of g-C₃N₄ is 2.7 eV, it can absorb visible light shorter than 450 nm effectively, implying broad prospects in solar energy conversion applications. Due to the aromatic C-N heterocycles, g-C₃N₄ is thermally stable up to 600 °C in air. Moreover, g-C₃N₄ is insoluble in acids, bases or organic solvents, exhibiting good chemical stability. The well-known 2D material, graphitic carbon nitride (g-C₃N₄) with stable allotrope, has shown its wider applications in catalysis, photoelectrochemical sensing [10], energy related photoelectronic devices, electrochemical sensor [11], biomedical imaging, biosensor [12] and spectroscopic detections [13]. In brief, graphitic carbon nitride (g-C₃N₄) emphasized the analog skeleton to graphite, found to be promising and fascinating material containing its sturdy C–N covalent bonds instead of C–

C in graphite and the layers that are linked by van der Waals forces [10]. The incorporation of heteroatoms such as nitrogen atom into carbon-based materials can enhance the properties of existing material whereby, the nitrogen atom act as the strong electron donor sites for catalytic conductivity due to the chemical nature of the nitrogen atom [14]. The tri-s-triazine present in the ring structure as well as the high degree of condensation provide ascend to a medium bandgap polymer and indirect semiconductor that was utilized in the field of energy storage [15], electrocatalysis [16], sorbents, heavy metals detection, pesticides detection, photocatalysis, photoelectrocatalysis [10,16] and sensing applications [10,17]. The g-C₃N₄ nanostructures play a vital role in the development of g-C₃N₄ based materials for electrochemical sensing [10]. Apart from catalytic activity and conductivity, the important driving force of the electrode materials will offer the facile interactions through chemical and biological analytes and the control of the functional moieties to extremely selective sensing and limit of detection [10]. Scan of literature from the 'Web of Science' showed the

maximum number of articles on g-C₃N₄ are found to be increased year by year in the field of sensors and plausible modifications towards hybrids or composites with other than carbon-based nanomaterials such as metals, semiconductors, graphene, etc. and also real time samples also were detected [17]. Several reviews explored the synthesis, characterization of g-C₃N₄ [10]. Some of the reviews establish the g-C₃N₄ applications in the field of catalyst, imaging, and LEDs and beyond photocatalyst, few reviews are reported with structural, morphological, sensing properties of g-C₃N₄ [10,18]. Though several domains have employed g-C₃N₄ material, they play an indispensable role in electrochemical detection. Fortunately, a variety of articles on g-C₃N₄ based electrochemical sensors and biosensors have risen [10], but, no specific reviews were highlighted to show the importance of sensor point of view with real-time monitoring. A systematic description of the g-C₃N₄ based nanomaterials used for an electrochemical sensor for environmental application and biosensor for healthcare applications has been shown in Scheme 1



Scheme 1. Graphitic carbon nitride based electrochemical and biosensors for environmental and healthcare applications [10].

To obtain g-C₃N₄ structures with well-defined morphology applicable for fabricating a sensor, pyrolysis technique is generally used with different nitrogen-rich precursors. such as melamine, urea, thiourea, dicyandiamide, cyanamide, and guanidine hydrochloride were developed and applied it for

electrochemical catalysis with a remarkable detection limit for various analytes.

Thus, recent research has highlighted the potential of g-C₃N₄ composites in effectively removing various pollutants from wastewater, such as dyes, oil spills, heavy metal ions, pesticides, microplastics, phenols, and

pharmaceuticals [19-23]. Moreover, there is increasing research interest in utilizing g-C₃N₄-composites for hydrogen generation [24]. The number of publications focusing on pollutant removal and H₂-production using g-C₃N₄ nanocomposites has shown a notable increase over the last few years, as seen in Fig. 1. Initially, there were only a few publications per year, indicating limited attention to the topic. However, since 2017, there has been a rapid upward trend in both citations and publications, signifying a growing interest in the field, where documents on photocatalysis were almost five times

higher than those on H₂-production. Most of these publications consist of journal articles (93%), with a smaller fraction being reviews (4.9%), and conference articles (1.1%), as shown in Fig. 1. This indicates a scarcity of dedicated and updated review papers, which are essential for providing interested researchers and the scientific community with a comprehensive and up-to-date evaluation of g-C₃N₄-composites' application as photocatalysts.

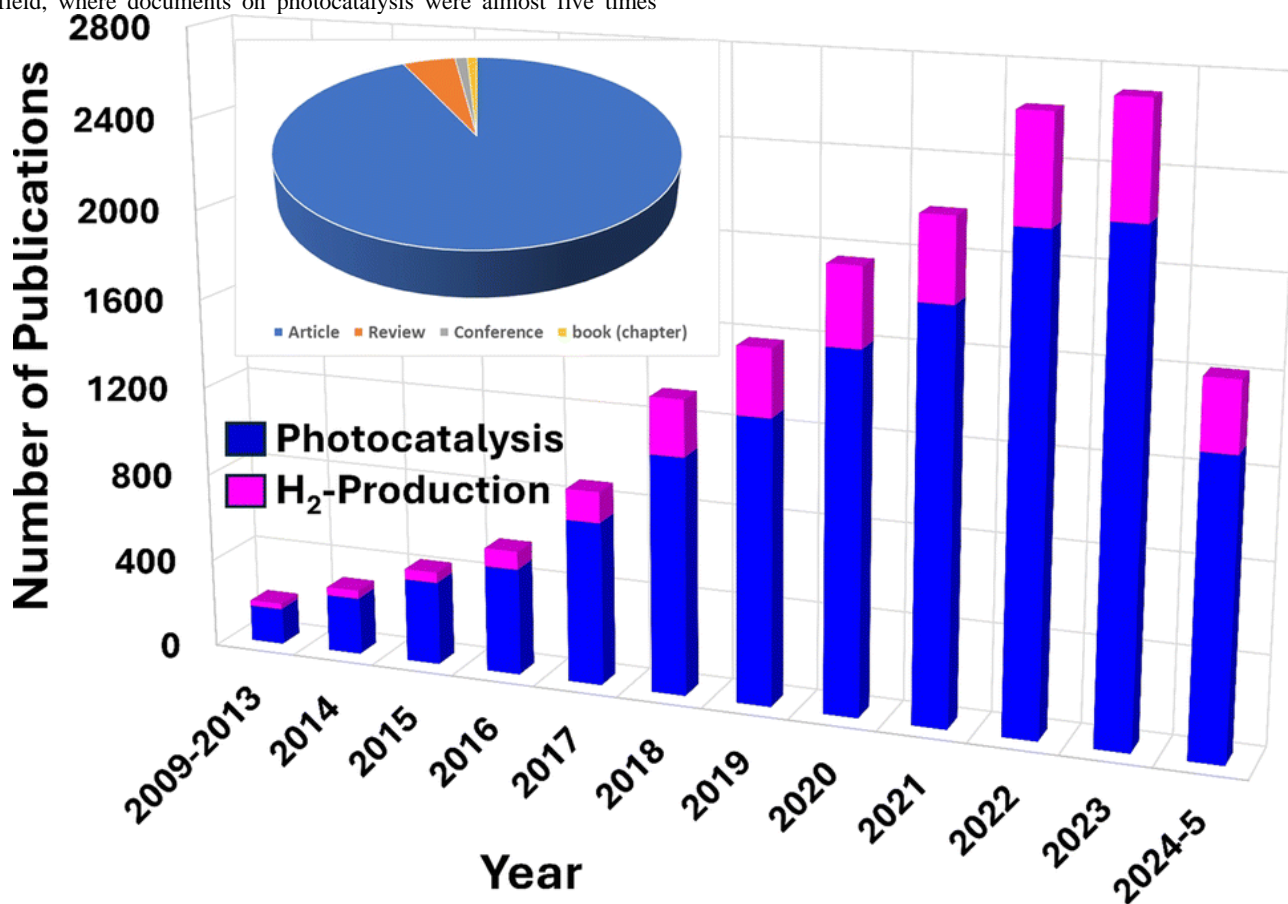


Figure 1: Number of publications in Scopus database reporting g-C₃N₄-based composites for photocatalytic and H₂-production applications: keywords “(g-C₃N₄) and ((photocataly*) or (hydrogen production))”.

Recently, g-C₃N₄ has drawn increasing attention in constructing biosensors owing to its appealing properties such as responsive to visible light, facile synthesis from inexpensive raw materials with modifiable electronic structures, remarkable thermal and physicochemical stability, abundant functional groups on the surface, and excellent photoelectrochemical features.

One of the emerged semiconductors photocatalysts which have received much global attention is the two-dimensional Graphitic Carbon Nitride (g-C₃N₄) nanomaterial. It is an earth-abundant metal-free semiconductor with easily tunable optical, electronic, and good visible-light harvesting properties. With a reasonable bandgap energy of 2.7 eV (460 nm), g-C₃N₄ is physically and chemically robust. It also has the appropriate Conduction Band (CB) and Valence Band (VB) edge positions for both reduction and oxidation reactions [25-27]. Based on these unique properties, g-C₃N₄ has been applied in various fields such as photocatalysis (removal of environmental pollutants, energy conversion systems, energy generation, etc.), photovoltaics, sensors, and electrochemical devices among others [28-30].

Graphitic carbon nitride (g-C₃N₄) has a chemical composition of only carbon and nitrogen, having unique optoelectronic features, electrochemical performance, appropriate band gap, chemical inertness, superior mechanical and thermal stability, two-dimensional structure, outstanding chemical

stability and configurable electronic structure, and has received significant research attention. These properties resulted in increasing research exploration for diverse applications and the foundation for the development of various products. A scientometric analysis of g-C₃N₄-based materials reveals a current shift in applications of the materials from energy conversion systems, hydrogen production, photoelectrochemical, and other disciplines to diverse disciplines. In recent years, g-C₃N₄-based materials have been used in a variety of new fields such as medicine, food safety, mathematics, and computer science. As a result, this chapter was conducted in an attempt to summarize the new emerging disciplines of applications of g-C₃N₄-based materials as a reference base and to provide information for further exploration and expansion of research areas. It was predicted that g-C₃N₄-based materials could be used in sensors and actuators, automotive systems, biomimicry technology, and other multidisciplinary fields.

The early detection of the biomarkers of the diseases plays a significant role in their treatment and control. It is essential to detect biomarkers associated with a disease early and with the high precision for diagnosis, treatment, and prognosis of fatal diseases, such as cancer, which causes a high mortality rate yearly, and neurodegenerative disorders [31-34]. There are some current conventional diagnostic methods, such as blood tests, imaging, and biopsies, which can be expensive and time-consuming with low sensitivity. Moreover, they require trained personnel, limiting their availability to low-income patients [33].

Today, biosensors are used for detection approaches, such as the high-resolution imaging, fast detection, and monitoring of diseases. Biosensors consist of three main components: recognition, signal transducer, and processor, designed to determine specific biomolecules [35]. These biomolecules can be macromolecules, such as nucleic acid and proteins, or small molecules, such as glucose. Various cancer biomarkers, such as BRCA1, BRCA2, CA 15-3, and CA 125 for breast cancer and PSA for prostate cancer, can be detected as well [36]. In this sense, biosensors based on nanomaterials have accurate detection, efficient monitoring, and fast but reliable imaging [37,38]. The physicochemical properties of nanomaterials, such as photoemission, high specific surface leading to extra bioreceptor immobilization, as well as electrical and heat conductivities, make them perfect candidates for biosensor construction [39-43]. Graphene/graphene oxide, carbon quantum dots, gold nanoparticles, carbon nanotubes, porous carbon, and fullerene are nanostructures that have been investigated as the biosensing platforms studied over the years [44-53]. Carbon nanostructure-based sensors are utilized due to their potential to quench fluorescently-labeled probes [37-41,54]. Thus, developing a user-friendly and highly sensitive biosensor is essential. Graphitic carbon nitride (g-C₃N₄) nanosheet is another widely used carbon nanostructure to design biosensors [55-60]. g-C₃N₄ nanosheets have high fluorescence quantum yield, superior chemical and thermal stability, are easy to synthesize with low toxicity, and have a low price and high biocompatibility together with unique

photoelectrochemical and electroluminescent characteristics [61,62]. Furthermore, the optical properties and conductivity of g-C₃N₄ have made it applicable in optical and electrochemical biosensing approaches. For instance, sulfur-doped graphitic carbon nanosheets (s-g-C₃N₄) as a dual (electrochemical and fluorescence) biosensing platform were used for the detection of cancer biomarkers even at very low concentrations (CA15-3) [63]. This chapter summarizes the properties and synthesis methods of graphitic carbon nitride nanosheets, which make them highly suitable candidates for the next generation of biosensors for healthcare and biomedical applications.

2. Historical progress of g-C₃N₄

Table 1 depicts the historical progress of g-C₃N₄ and was adapted from a study conducted by Ajiboye et al. (2020) [64]. The discovery of “melon” by Liebig and Berzelius in the 1830s sparked interest in g-C₃N₄ research. The melon contains a tri-s-triazines monomer that is interconnected by a tertiary amine. The historical evolutionary trend in Table 1 shows that several authors have studied g-C₃N₄ with its introduction as a heterogeneous catalyst in the year 2006. Specifically, its application as a photocatalyst was reported by Wang et al. (2009) for water splitting. Following this breakthrough, several studies involving g-C₃N₄ were conducted and applied in a variety of disciplines and fields.

Year	Works on g-C ₃ N ₄
1834	Berzelius made synthetic polymer which was a derivative of carbon nitride. It was named as “melon” in 1834 by Liebig
1835	Sulfur and potassium ferricyanide was heated together in a crucible to make potassium hydromelanote by Gmelin
1922	The term “carbonic nitride” was introduced and it was found to be formed as the last product of several ammonocarbonic acids using melon as the starting material by Franklin
1937	Tri-s-triazine was suggested as repeat monomer unit of graphitic carbon nitride by Sturdivant and Pauling
1940	Resemblance between graphite and melon was pointed out by Lucas and Redemann. They were both planar and very large
1982	Derivative of cyameluric was obtained as the pioneer crystal structure by Leonard et al.
1990	Sp ³ -bonded β-C ₃ N ₄ was theoretically predicted to have hardness and bulk modulus that is either equal or greater than that of diamond
1996	Although by calculation methods, graphitic carbon nitride was shown to have five structural types by Hemley and Teter
2001	Species having high crystallinity which was believed to be melon possessing high molecular weight was reported by Komatsu
2003	Melam and melem derivatives were isolated and identified as the crystalline structure of heptazine by Schnick et al.
2006	g-C ₃ N ₄ was discovered to be a heterogeneous photocatalyst without containing metals
2007	Milan et al., converted dicyandiamide to imide phase carbon nitride
2009	Semiconductor without metal-based hydrogen generation by Wang using g-C ₃ N ₄

Table 1: Historical summary of progress on g-C₃N₄. Source: Ajiboye et al. [64]

3. Allotropes of g-C₃N₄

The primary allotropes of C₃N₄ include beta-g-C₃N₄ (β-g-C₃N₄) and triazine-based g-C₃N₄ (T-g-C₃N₄), graphitic-C₃N₄, cubic-C₃N₄ and pseudo-cubic-C₃N₄. The diamond-like α-g-C₃N₄ is the most stable allotrope of g-C₃N₄, where four nitrogen atoms in a tetrahedral configuration are bonded to each carbon atom. Its light absorption capacity is limited to the ultraviolet region due to its wide band gap of about 4.8 eV. Further, it has little electrical conductivity and low photocatalytic efficiency. The graphite-like structure i.e., β-g-C₃N₄ is a metastable allotrope of g-C₃N₄, where carbon and nitrogen atoms are arranged in hexagonal rings forming layered sheets. It has a small band gap of about 2.7 eV, which ranges its light absorption capacity to the visible light region. Its electrical conductivity and photocatalytic activity are also higher than α-g-C₃N₄. g-C₃N₄ is a general term for the graphitic carbon nitride-based materials that have a graphite-like structure but with altered degrees of porosity, crystallinity, and imperfection [65].

4. Structural Properties of g-C₃N₄

g-C₃N₄ is a polymeric nanosheet with a graphene-like structure consisting of sp² bonded carbon and nitrogen atoms with abundant amino groups on its surface and suitable bandgap energy of 2.7 eV [66]. Thanks to the g-C₃N₄ electronic band structure with sp² hybridization, it is considered a photon-harvesting semiconductor material that plays a critical role in detecting biomolecules by photoelectrochemical (PEC) biosensors [67]. Due to the presence of melamine in the π-conjugated nanosheets, g-C₃N₄ is fluorescent with high photoluminescence quantum yield with high and minor absorption at 365 nm and visible light region, respectively [68,69], which can be quenched by materials, such as metal ions, nitrobenzene derivative, or biomolecules, such as heparin and sialic acid, which allow its use as a fluorescent probe biosensor [70] with high photostability and no obvious photobleaching under UV light excitation for 10 h [71]. Furthermore, the g-C₃N₄ ability to convert light and electricity makes it a suitable option for electrochemiluminescence-based and photoelectrochemistry-based biosensing [60]. Various precursors have been proposed for g-C₃N₄ synthesis through thermal condensation. These compounds are rich in nitrogen and

contain a tri-s-triazine ring structure, such as dicyandiamide, urea, cyanamide, or thiourea [72]. For instance, if cyanamide is selected as the precursor, thermal heating results in dicyandiamide, melamine, melem, and g-

C_3N_4 , respectively. The molecular structures of the g- C_3N_4 precursors and the corresponding temperatures for their thermal condensation are depicted in Figure 2.

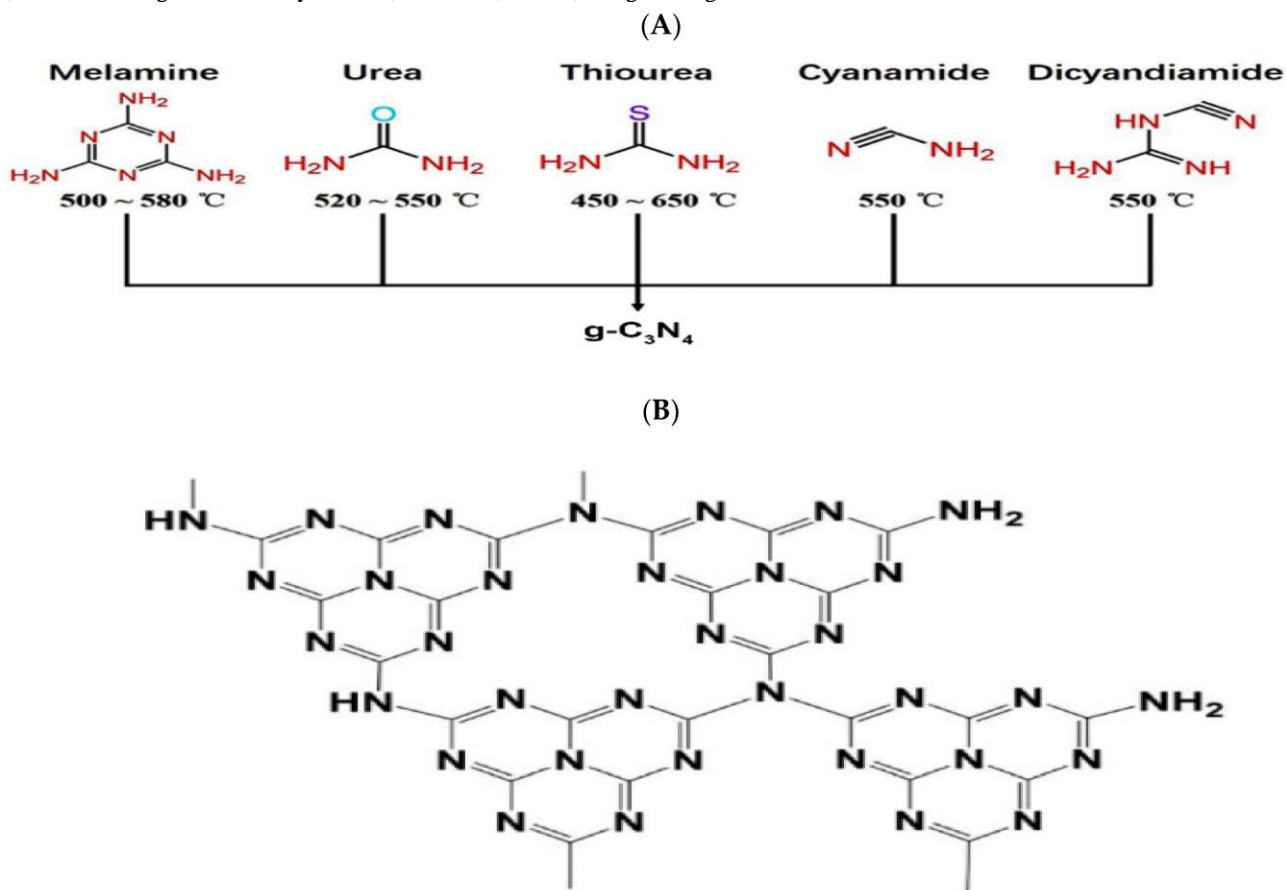


Figure 2: (A) Various g- C_3N_4 precursors and the corresponding temperatures for their thermal condensation into g- C_3N_4 , [73]. (B) g- C_3N_4 structure, [74].

In addition, g- C_3N_4 has been reported to display antimicrobial activity. A number of parameters, including the g- C_3N_4 band gap, intermediate defect states, dispersed surface area, absorbance in suspension, and charge separation influence its photocatalytic bacterial inactivation [60]. Thus, the modification of these properties influences the production of reactive oxygen species, hence the antibacterial activity. The bactericidal rates of more than 99% have been successfully achieved for eight kinds of foodborne pathogenic bacteria with 8 h incubation in the dark. Cell rupture caused by direct mechanical contact between g- C_3N_4 and cell membranes has been observed. Molecular dynamics simulations further indicated that the presence of large defects in g- C_3N_4 enhanced the electrostatic attraction between inherent pores and lipid heads, resulting in enhanced antibacterial activity. The thermal and chemical stability of biosensors is crucial for long shelf lives. g- C_3N_4 nanosheets show high thermal stability in the air (up to 600 °C) thanks to the graphitic graphene-like structure with sp^2 bonds between carbon and nitrogen, providing high chemical stability [75]. g- C_3N_4 has low cytotoxicity and good biocompatibility due to its metal-free structure. Moreover, it has a low production cost, a simple synthesis process, a large specific surface area, easy functionalization, and increased penetration coefficient, allowing the efficient immobilization of molecules

in the matrix for biosensing [76]. As g- C_3N_4 materials are increasingly used in biomedicine, improving their biocompatibility and biodegradability properties is a necessity. Therefore, modifications are applied to enhance the biocompatibility, biodegradability, and further development of g- C_3N_4 materials. For instance, Kang et al. showed that successfully inserting abundant disulfide bonds into g- C_3N_4 endowed more biodegradability and biocompatibility, boosting its application in biomedical fields [77]. In another study that was recently conducted for glucose detection in diabetic patients, the addition of metal co-catalysts (Fe(III), Cu(II)) to the structure via adsorption noticeably enhanced the sensitivity compared to the pristine g- C_3N_4 [78]. Thanks to its easy functionalization, g- C_3N_4 can be adapted to various targets with high sensitivity. For instance, a platform based on proton-functionalized ultrathin g- C_3N_4 nanosheets with a positive charge has been developed for heparin (as a biomolecule with a high negative charge) detection in human serum [79]. Graphitic carbon nitride (g- C_3N_4) exhibits a unique two-dimensional structure composed of carbon and nitrogen atoms, which imparts distinctive structural properties crucial for its photocatalytic performance [80,81]. Understanding these properties is essential for tailoring g- C_3N_4 materials to specific applications and optimizing their efficiency. The key structural attributes are provided in Figure 3.

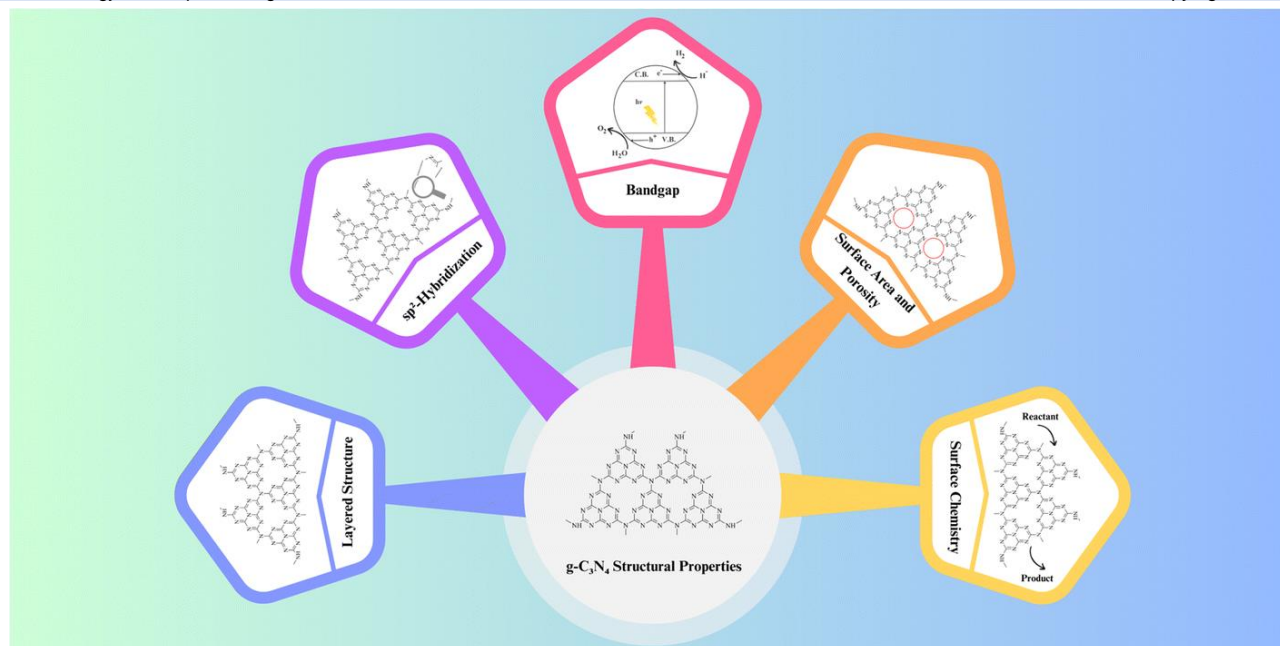


Figure 3: Structural properties of pristine $g\text{-C}_3\text{N}_4$.

4.1. Layered structure

At its core, $g\text{-C}_3\text{N}_4$ consists of stacked layers of carbon and nitrogen atoms arranged in a planar, hexagonal lattice. This layered structure resembles that of graphite, giving rise to its name, “graphitic”. Each layer is composed of tri-s-triazine (C_3N_3) units, and the layers are held together by weak van der Waals forces. This layered configuration provides a large surface area for potential reactant adsorption and photocatalytic reactions, making $g\text{-C}_3\text{N}_4$ an attractive material for various applications [82]

4.2. sp^2 -hybridization

The carbon atoms within the $g\text{-C}_3\text{N}_4$ lattice adopt sp^2 -hybridization, resulting in trigonal planar geometry. This sp^2 -hybridized carbon configuration is responsible for the formation of delocalized π -bonds, contributing to the material's excellent electrical conductivity and optical properties. This electron-rich network facilitates charge carrier mobility and separation, which are essential for efficient photocatalysis [83].

4.3. Bandgap

The electronic band structure of $g\text{-C}_3\text{N}_4$ plays a pivotal role in its photocatalytic activity. It exhibits a moderate bandgap typically around 2.7 to 2.8 eV, making it responsive to visible light. Photons with energy equal to or greater than the bandgap can excite electrons from the valence band to the conduction band, initiating the photocatalytic process. The bandgap value allows $g\text{-C}_3\text{N}_4$ to harness a substantial portion of the solar spectrum, rendering it effective for solar-driven applications. [84].

4.4. Surface area and porosity

The layer-by-layer structure of $g\text{-C}_3\text{N}_4$ results in a high surface area, providing ample sites for reactant adsorption and subsequent photocatalytic reactions. The interlayer spacing between $g\text{-C}_3\text{N}_4$ layers can be tuned to create mesopores and micropores, further enhancing its surface area and porosity. These structural features facilitate efficient mass transport and reactant accessibility, promoting photocatalytic efficiency [85].

4.5. Surface chemistry

The surface of $g\text{-C}_3\text{N}_4$ can be modified through functionalization, which introduces various functional groups such as amino, hydroxyl, and carboxyl groups. These modifications can influence the material's surface charge,

hydrophilicity, and chemical reactivity, thus tailoring its suitability for specific photocatalytic applications. Surface functionalization also enables the attachment of co-catalysts, enhancing charge separation and overall photocatalytic performance [84]. Moving to structural properties, $g\text{-C}_3\text{N}_4$'s layered structure, sp^2 -hybridization, moderate bandgap, high surface area, and porosity are key features. The layered structure provides a large surface area for reactions, while sp^2 -hybridization contributes to electrical conductivity. The moderate bandgap (2.7–2.8 eV) enables responsiveness to visible light, crucial for solar-driven applications. High surface area and porosity, achieved through the layer-by-layer structure and tuned interlayer spacing, facilitate efficient mass transport and reactant accessibility. Surface chemistry, modified through functionalization, further tailors' properties for specific applications [86]. Understanding these structural properties allows researchers to design and engineer $g\text{-C}_3\text{N}_4$ materials with optimized characteristics for diverse photocatalytic applications. By tailoring the layer spacing, bandgap, and surface chemistry, $g\text{-C}_3\text{N}_4$ can be fine-tuned to address specific environmental and energy challenges, contributing to a sustainable and cleaner future.

5. Synthesis Methods

The synthesis of graphitic carbon nitride ($g\text{-C}_3\text{N}_4$) has undergone significant development over the years, offering researchers a versatile toolkit to tailor its properties for specific photocatalytic applications. The following sections explore several key synthesis methods, each with its own advantages and limitations.

5.1. Thermal polymerization

One of the most widely employed methods for $g\text{-C}_3\text{N}_4$ synthesis is thermal polymerization of low-cost precursors, such as melamine, urea, cyanamide, dicyanamide, thiourea, cyanuric acid etc. This process typically involves the heating of these precursors at moderate temperatures (around 500–600 °C) under inert gas atmospheres (Fig. 4). The thermal polymerization route generates a layered $g\text{-C}_3\text{N}_4$ structure with a high surface area, making it suitable for various photocatalytic applications. The method's simplicity and cost-effectiveness have contributed to its popularity [87-89].

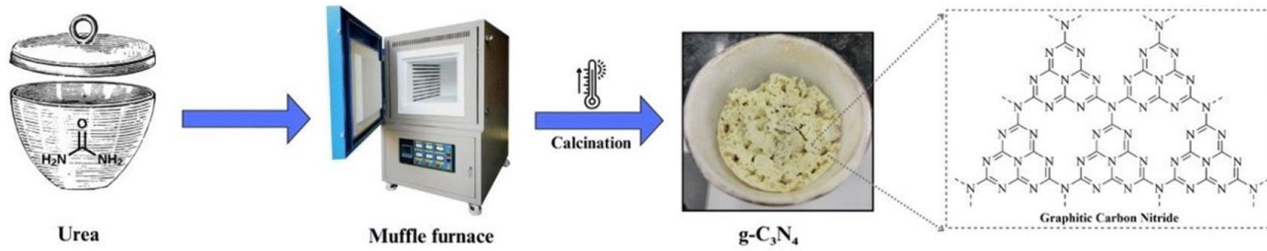


Figure 4 Synthesis of $g-C_3N_4$ via thermal polymerization method.

5.2. Chemical vapor deposition (CVD)

CVD represents an alternative approach to $g-C_3N_4$ synthesis, offering precise control over the material's thickness and morphology. In CVD, volatile precursors, such as cyanamide, are introduced into a high-temperature

reactor, where they decompose and deposit as $g-C_3N_4$ on substrates (shown in Figure. 5). This method allows for the growth of thin films and nanostructures, enabling applications in photovoltaics and optoelectronics. However, CVD may require more specialized equipment and is often associated with higher production costs [90-93].

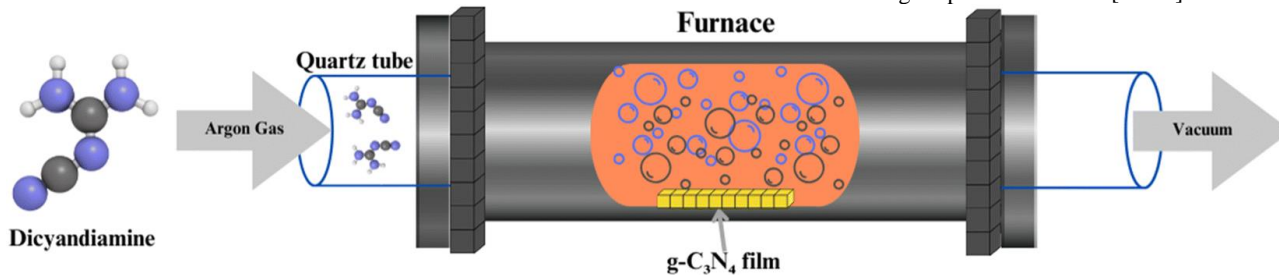


Figure 5: Synthesis of $g-C_3N_4$ via CVD method.

5.3. Solvothermal and hydrothermal methods

Solvothermal and hydrothermal routes involve the reaction of precursors in high-pressure, high-temperature aqueous or organic solvents (Fig. 6). These methods offer control over the morphology and structure of $g-C_3N_4$ by adjusting reaction conditions. Solvent selection plays a crucial role in

influencing the final product's properties. Hydrothermal synthesis is particularly effective in producing hierarchical $g-C_3N_4$ structures with enhanced photocatalytic activity. These methods are advantageous for tailoring $g-C_3N_4$ for specific applications and have gained prominence in recent years [94-98].

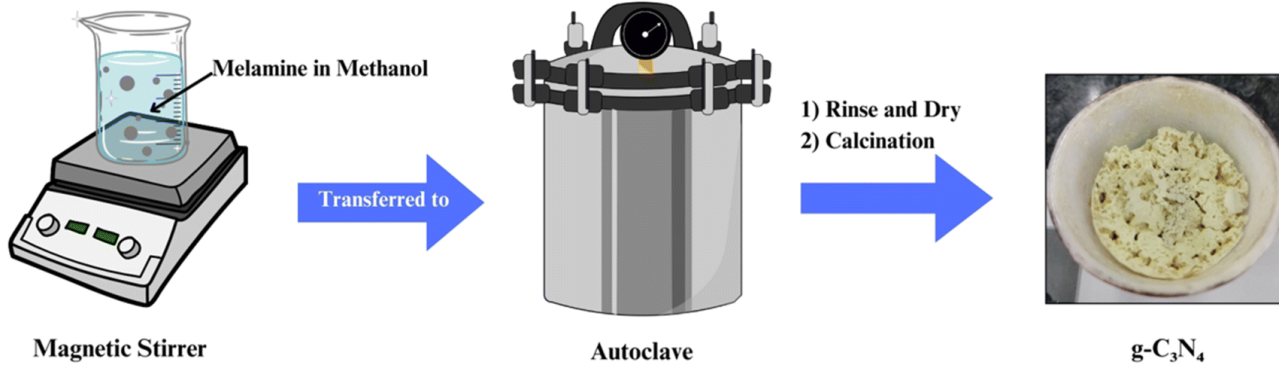


Figure 6: Hydrothermal synthesis of $g-C_3N_4$ particles.

5.4. Template-assisted synthesis

Template-assisted synthesis involves the use of templates, such as mesoporous silica or carbonaceous materials, to guide the formation of $g-C_3N_4$ with specific structures (Figure. 7). By using templates with desired pore sizes and shapes, researchers can control the surface area and porosity

of $g-C_3N_4$, which are critical factors affecting its photocatalytic performance. This approach enables the creation of $g-C_3N_4$ materials with finely tuned properties for applications like pollutant removal and solar energy conversion [99-103].

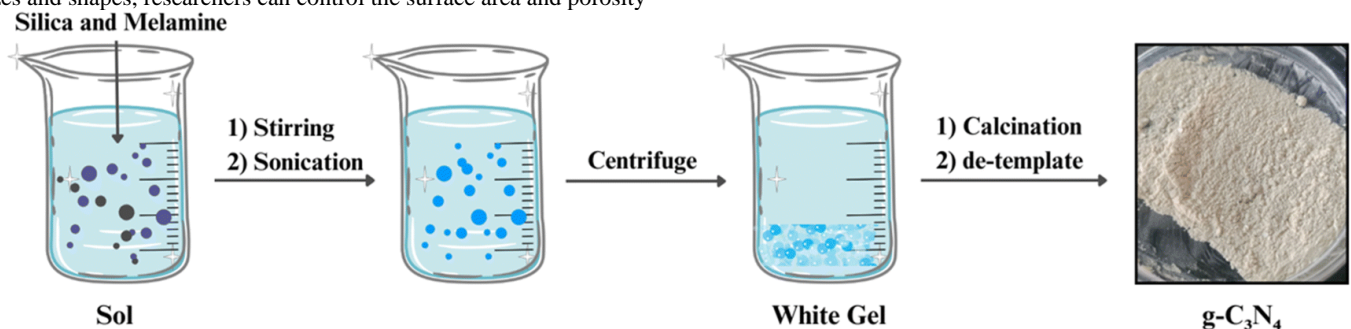


Figure 7: Template-assisted synthesis of $g-C_3N_4$ particles.

5.5. Doping and co-doping strategies

To further enhance the photocatalytic activity of g-C₃N₄, doping and co-doping with other elements, such as sulfur, boron, and metals, have been explored (as shown in Fig. 8). Doping introduces impurities into the g-C₃N₄

lattice, modifying its electronic structure and creating additional active sites for photocatalytic reactions. Co-doping involves the simultaneous incorporation of two or more elements to achieve synergistic effects. These strategies play a pivotal role in improving g-C₃N₄'s efficiency and selectivity in various photocatalytic processes [104-108].

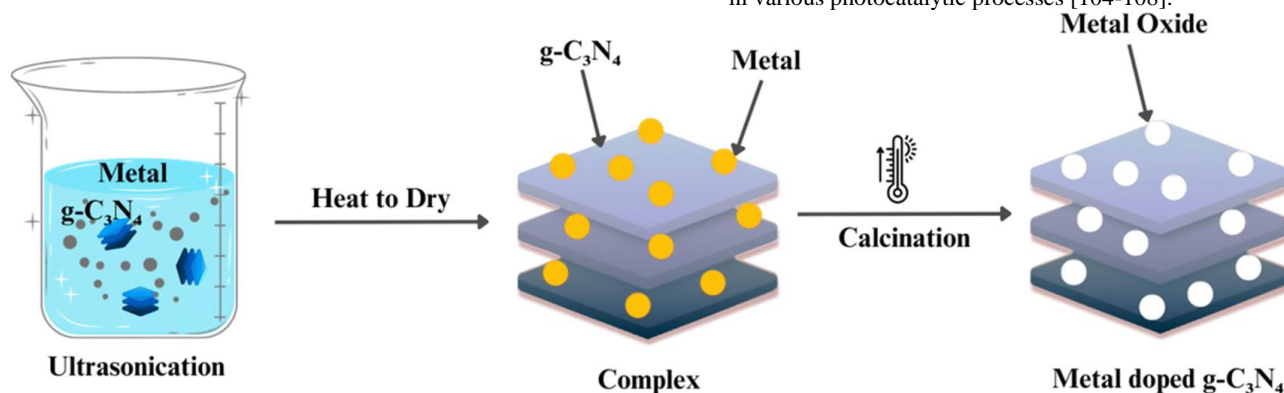


Figure 8: Metal/metal oxide doped g-C₃N₄ synthesis via doping strategies.

The synthesis of graphitic carbon nitride (g-C₃N₄) has advanced significantly, providing a diverse set of methods with distinct advantages and limitations. Thermal polymerization, involving low-cost precursors like melamine, offers simplicity and cost-effectiveness, resulting in a layered g-C₃N₄ structure suitable for various applications. Chemical vapor deposition (CVD) allows precise control over thickness and morphology but may entail higher production costs and specialized equipment. Solvothermal and hydrothermal methods, utilizing high-pressure and high-temperature conditions, provide morphology control and have gained popularity for tailoring g-C₃N₄ properties. Template-assisted synthesis uses templates to guide specific structures, influencing surface area and porosity critical for photocatalytic performance. Doping and co-doping strategies enhance photocatalytic activity by modifying the electronic structure.

Comparing these methods reveals trade-offs in terms of cost, complexity, and yield. Thermal polymerization is cost-effective and straightforward but might lack precision. CVD offers control but at higher costs. Solvothermal and hydrothermal methods provide control over morphology but involve specialized conditions. Template-assisted synthesis allows tailored structures but might be more intricate. Doping strategies enhance

performance but add complexity. The choice depends on desired properties and applications, influencing cost-effectiveness and efficiency [86].

In summary, the choice of synthesis methods for g-C₃N₄ is influenced by the desired properties and intended applications. Researchers and engineers can select from these diverse synthesis techniques to tailor g-C₃N₄ materials that meet the specific demands of sustainable environmental applications, from water purification to renewable energy production.

6. Synthesis Methods of g-C₃N₄-Based Materials

The cyanamide is infiltrated and polymerized in the narrow void of SNSs to form porous g-C₃N₄, and then the SNSs is removed by HF treatment, as shown in Figure 9a. Therefore, the resulting g-C₃N₄ has an anti-opal structure, and the size of the spherical hole indicates the size of the SNSs used, as shown in the SEM images of Figure 9b-e. In this study, the pore size of g-C₃N₄ was between 50 and 80 nm. In spite of the silica hard template, Chen et al. reported the synthesis of porous g-C₃N₄ by using multi-walled carbon nanotube (CNT) as a novel hard template [109]. Unlike other hard templates, CNT can be easily removed and recovered by ultrasonic methods, resulting in a relatively simple preparation of porous g-C₃N₄.

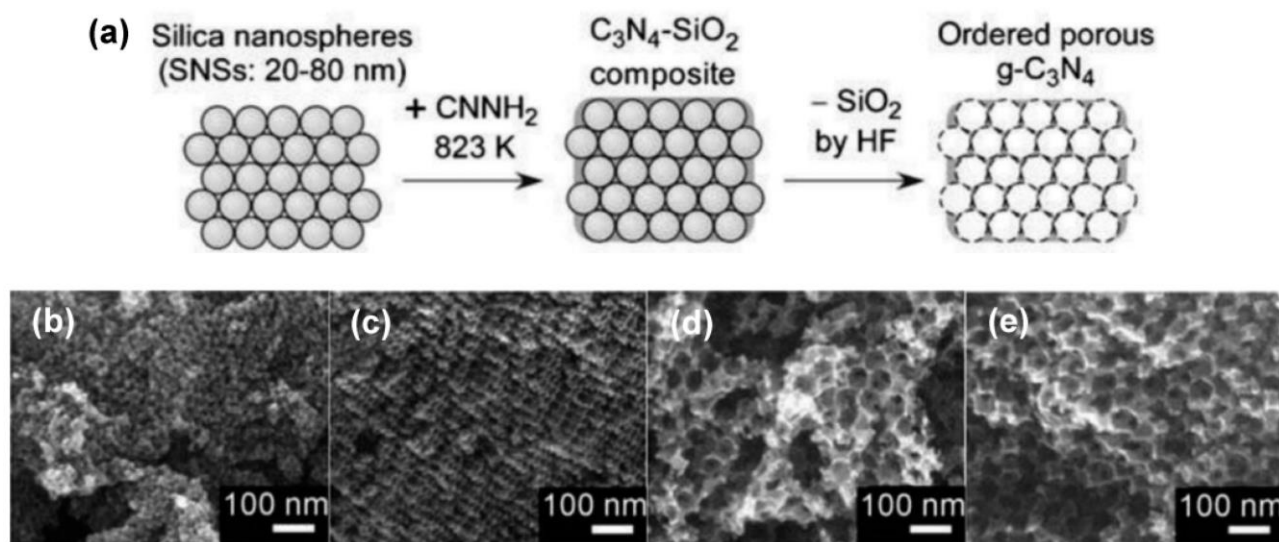


Figure 9 (a) Synthesis procedure of ordered porous g-C₃N₄. Field emission SEM (FESEM) images of porous g-C₃N₄ prepared using silica spheres with various diameters: (b) 20, (c) 30, (d) 50, and (e) 80 nm [110].

The synthesis of $g\text{-C}_3\text{N}_4$ is normally through the polymerization using various synthesis techniques such as chemical vapor deposition (CVD), solid-state reaction, physical vapor deposition (PVD), solvothermal method and thermal nitridation [25,111]. Unfortunately, the product obtained is bulk $g\text{-C}_3\text{N}_4$ which normally exhibits poor optoelectronic properties and hence cannot be utilized and applied in many fields in that form. Thus, to overcome this challenge various nanostructured $g\text{-C}_3\text{N}_4$ such as ultrathin nanosheets, hollows, nanorods, nano leaves, etc. have been prepared with improved optical and electronic properties [112]. Furthermore, nanostructured and nanocomposites of $g\text{-C}_3\text{N}_4$ have enhanced properties such as low electron-hole recombination rate, large surface area, and so on, making them suitable for applications in a variety of fields. Over 400 reviews on $g\text{-C}_3\text{N}_4$ have been conducted, according to Vinoth et al. (2021), with applications including energy conversion systems, hydrogen production, and photoelectrochemical studies, among others.

The structural limitations, including low surface area and insufficient porosity, reduce catalytic activity while ensuring the stability of Z-scheme interfaces and preventing back electron transfer remains complex. Moreover, scaling up production and achieving cost-effective synthesis are ongoing hurdles. Addressing these challenges requires innovations in bandgap engineering, composite formation, and morphology control, along with the development of green and scalable synthesis methods.

6.1. Synthesis of $g\text{-C}_3\text{N}_4$ Nanosheets

The classification of the synthesis methods based on the synthesis procedure can be divided into bottom-up and top-down categories. The “bottom-up” approach generally applies small-sized particles to assemble complex structures. However, the “top-down” procedure is based on splitting large-sized and thick bulks into small particles and thin nanosheets [113,114]. The bottom-up procedure includes ionic liquid, supramolecular pre-assembly, and hydrothermal methods [114]. In the bottom-up approach, $g\text{-C}_3\text{N}_4$ sheets are synthesized on a large scale via thermal polymerization (pyrolysis) or the carbonization of small organic compounds (that contain hydroxyl, carboxyl, carbonyl, and primary amine functional groups) [115], such as melamine, cyanamide, Dicyanamide, or urea [116]. Dante et al. obtained $g\text{-C}_3\text{N}_4$ from the pyrolysis of melamine cyanurate at 650 °C for 50 min (in the crucible with atmosphere condition), which was used for glucose sensing [78]. On the other hand, chemical exfoliation and ultrasonic exfoliation methods have been utilized for the top-down approach. Chemical exfoliation is more common for large-scale production due to its high efficiency and the easier tuning of the $g\text{-C}_3\text{N}_4$ structure [117]. For example, Hatamie et al. used $g\text{-C}_3\text{N}_4$ as a label-free fluoro-sensor to analyze the amount of metronidazole in biological fluids and drug samples. $g\text{-C}_3\text{N}_4$ ultrathin nanosheets were synthesized in bulk via the thermal polymerization method from melamine, possessing a highly π -conjugated structure at 600 °C. The exfoliation procedure was performed through ultrasonication in water media [118].

6.2. Synthesis of $g\text{-C}_3\text{N}_4$ -Based Composites

$g\text{-C}_3\text{N}_4$ properties can be enhanced through its fabrication with other materials into composites. In the modification techniques, metal loading is critical for increasing the potential application of $g\text{-C}_3\text{N}_4$ biosensors due to outstanding electrochemical qualities. Metal/ $g\text{-C}_3\text{N}_4$ composites are produced with solvothermal treatment, photo-deposition, precipitation, and thermal polymerization methods [119]. Generally, there are numerous ways to prepare $g\text{-C}_3\text{N}_4$ -based nanocomposites. The simple pyrolysis method, solution (sonication) mixing, the hydrothermal method, the simple calcination method, the hydrolysis method, sol-gel, and microwave irradiation are some synthesis methods that have been applied in the formation of nanocomposites based on $g\text{-C}_3\text{N}_4$ - and have been utilized for different applications [66]. The pyrolysis method is a common way to produce $g\text{-C}_3\text{N}_4$ -based composites in diagnosis applications where the mixture of the precursor of $g\text{-C}_3\text{N}_4$ and the other components is calcinated in a crucible for a while with a specific heating rate and initial temperature to prepare the nanocomposite. Then, the product is cooled at 25 °C. For example, a sensitive electrochemical sensor for dopamine detection was fabricated by firstly preparing calcium stannate (CaSnO_3) nanoparticles from

CaCl_2 and $\text{SnCl}_2 \cdot 2\text{H}_2\text{O}$ via the hydrothermal method, then $\text{CaSnO}_3\text{-}g\text{-C}_3\text{N}_4$ nanohybrid was produced through the pyrolysis of melamine, $(\text{NH}_4)_2\text{SO}_4$, and CaSnO_3 mixture at 550 °C in a crucible [120]. In another study for glucose detection, $\text{Cu(II)-Fe(III)-}g\text{-C}_3\text{N}_4$ was prepared through the sonication method (2 h sonication of a suspension of 416 mg of $g\text{-C}_3\text{N}_4$ in a 20 mL aqueous solution containing Cu(II) and Fe(III) ions), which led to the adsorption of ions on the $g\text{-C}_3\text{N}_4$ structure [78]. A highly selective glucose-sensing (in human blood) biosensor based on ultrathin $g\text{-C}_3\text{N}_4$ nanosheets doped with niobium (Nb) metal was synthesized by the pyrolysis method from urea [121]. A biosensor for 4-nitrophenol detection was developed by Vinoth et al. 4-nitrophenol is a very poisonous chemical compound released into the water during the production of some drugs, dyes, and leather, posing human health at high risk. So, for 4-nitrophenol monitoring, the biosensor based on $\text{BaSnO}_3\text{-}g\text{-C}_3\text{N}_4$ nanostructure was synthesized by sonication method from prepared BaSnO_3 and $g\text{-C}_3\text{N}_4$ [122].

7. Synthesis of $g\text{-C}_3\text{N}_4$ -Based Biosensors

7.1. $g\text{-C}_3\text{N}_4$ -Based Surface Plasmon Resonance (SPR) Biosensors

Surface plasmon resonance (SPR) sensing is a powerful probe of the interplays between protein–ligand, protein–DNA, protein–protein, and protein–membrane binding [123]. SPR biosensors are a very effective tool for measuring many biomarkers [124]. The main advantages of these biosensors are their fast response and ability to detect various analytes concurrently [125]. Moreover, among various new techniques available, SPR biosensors are the best optical biosensors for label-free, fast, and in situ diagnosis of molecules [61]. SPR is a physical optics phenomenon that can detect biomarkers because of the high sensitivity of surface plasmons to the dielectric medium [126]. In these biosensors, receptors are immobilized on the metal surface, interacting with the analytes and leading to dielectric alteration. This phenomenon affects the resonance condition of surface plasmons with specific surface plasmon waves (SPWs), allowing the transmission of photon’s energy to the surface plasmons at the resonance angle resulting in the decrease of the light reflectance and thus the SPR curve [127]. Based on the characteristic of light, the SPR biosensors can be categorized into angular, wavelength, or intensity-modulated systems [128–130]. The Kretschmann configuration is the most recent version of SPR based on attenuated total reflection [77]. At an angle, part of light energy is transmitted to the surface plasmon, and the reflectance can be shown in the angular scanning. The presence of adsorbed molecules on the biosensor surface varies the refractive index, and the SPR angle is changed accordingly [131].

Two-dimensional (2D) materials with large surface areas, such as $g\text{-C}_3\text{N}_4$, can act as the sensitive layers for SPR [61]. Duan et al. designed a surface plasmon resonance (SPR) biosensor based on a 2D nanocomposite of $g\text{-C}_3\text{N}_4$ nanosheets and molybdenum disulfide quantum dots (MoS_2QDs), adorned with chitosan-stabilized Au nanoparticles (CS-AuNPs) to detect prostate specific antigen (PSA) selectively. In this work, the MoS_2QDs easily aggregated and reduced the sensitivity, but as a support for MoS_2QDs , the $g\text{-C}_3\text{N}_4$ nanosheets improved the biosensing performance for PSA detection. Additionally, the $\text{MoS}_2\text{QDs}@g\text{-C}_3\text{N}_4@CS\text{-AuNPs}$ -based SPR apt sensor showed a very low limit of detection (LOD), 0.77 ng·mL⁻¹, with good linearity range at PSA concentrations in the range of 1.0–250 ng·mL⁻¹ [61].

7.2. $g\text{-C}_3\text{N}_4$ -Based Electrochemical Biosensors

Electrochemical biosensors have been recognized as powerful diagnostic tests over the past years thanks to their unique advantages, such as simplicity, high sensitivity, and accuracy [132]. Three vital components are necessary to develop electrochemical biosensors: (I) a bioreceptor to link with analyte, (II) an electrode, and (III) a read-out system [133]. An electrochemical sensor requires a working reference and an auxiliary electrode; the working electrode in the electrochemical biosensor acts as a transducer in the reaction between the bioreceptor and the analyte. It generates a biological signal which changes into an electronic signal and is processed with high sensitivity [134]. On the other hand, Ag/AgCl -based reference electrode is kept at the site of the reaction to maintain a particular potential. The auxiliary electrode

links the electrolytic solution and must be conductive; thus, gold or platinum are suitable candidates [135]. Some electrochemical methods for marker detection include voltammetric techniques (cyclic, square wave, or stripping), impedimetric, and amperometry. Of these techniques, cyclic voltammetry (CV) is preferred [133].

In an electrochemical biosensor, an electrode is the main component for immobilizing electron motion and biomolecules [136]. Nanomaterials have piqued attention due to their unique electronic characteristics [137]. The carbon allotropes can be applied as electrodes due to their effective electron transfer rate and high active surface area. Additionally, carbon nanostructured materials are significant in research due to their unparalleled properties, such as chemical stability and good conductivity [138]. $g\text{-C}_3\text{N}_4$ is a polymeric semiconductor with a specific structure and high stability, making it a good nanocomposite for electrochemical biosensors [139]. $g\text{-C}_3\text{N}_4$ is known as the most thermal stable allotrope of carbon nitrides [140],

which can be used in the diagnosis system based on its catalytic ability [141]. Due to the low electron conductivity of $g\text{-C}_3\text{N}_4$, it has been used with other materials to enhance its surface conductivity. The $g\text{-C}_3\text{N}_4$ derivatives can electrically connect to the redox center of biomolecules on the surface of the electrode. The electronic integration of the $g\text{-C}_3\text{N}_4$ with various carbon types notably increases the surface area and conductivity [141]. The chemical exfoliation of bulk $g\text{-C}_3\text{N}_4$ has been used to develop $g\text{-C}_3\text{N}_4$ nanosheets for the detection of neurotransmitters, such as dopamine (DA). Kathiresan et al. developed a glassy carbon electrode (GCE) doped with bulk $g\text{-C}_3\text{N}_4$. The electrochemical activation of bulk $g\text{-C}_3\text{N}_4$ was performed with a potential of 1.75 V in neutral pH conditions (pH 7.0). In the electrode oxidation reaction, the two-electron process is followed by the transfer of two protons, resulting in 5-HTquinoneimine. Figure 10 illustrates the redox reaction. Oxidation leads to the transfer of protons to form 5-HTquinoneimine and the reduction occurs in the quinone group on 5-HT quinonimine [142].

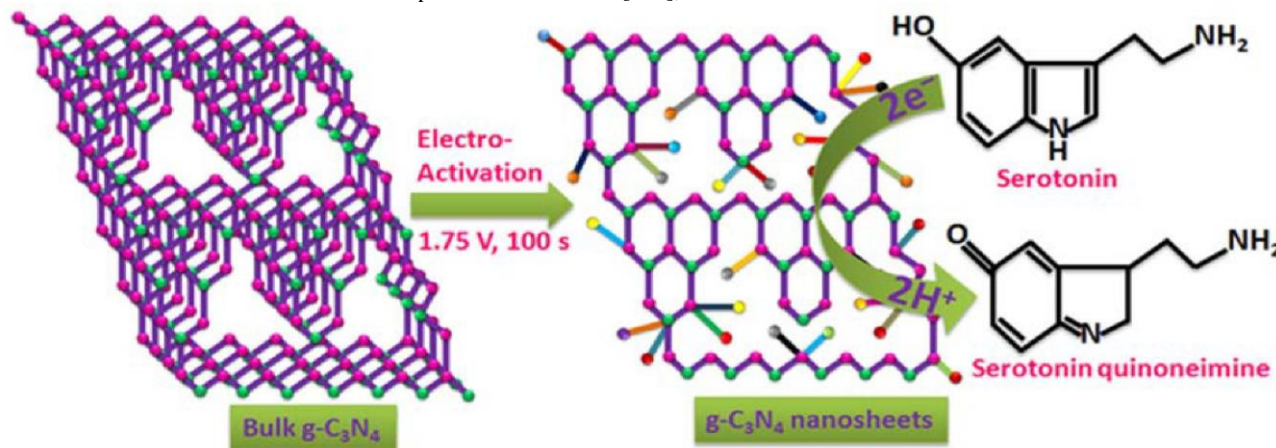


Figure 10: Activation of $g\text{-C}_3\text{N}_4$ on glassy carbon electrode and the redox reaction on the developed electrochemical biosensor for serotonin (5-HT)-. [142].

7.3. $g\text{-C}_3\text{N}_4$ -Based Photoelectrochemical (PEC) Biosensors

The photoelectrochemical (PEC) detection method is a hopeful technique for biological assays [143], which is also a low-cost approach to transforming chemical energy into electricity under a flash of light [144], and PEC biosensors have become prominent due to their capability of biomolecules diagnosis. This method has had much consideration because of its high sensitivity, simplicity, and fast response [145]. In the PEC diagnosis system, light is used as an excitation source [146], allowing for a high sensitivity with low background signals [144]. The PEC cell includes three main components: (a) a light-harvesting semiconductor, (b) a metal electrocatalyst, and (c) adequate electrolytes among the working electrode and auxiliary electrode to generate PEC signals using redox reaction. Upon illumination, the redox reactions lead to a signal between the working and the auxiliary electrodes [147]. PEC biosensors use wide bandgap semiconductors as photoactive materials [119], changing optical energy to electrical and chemical energy [148]. $g\text{-C}_3\text{N}_4$ is a responsive photocatalyst with a bandgap (2.7 eV) [149]. Additionally, one of the promising approaches is a photocatalytic reaction which can absorb visible light [138]. $g\text{-C}_3\text{N}_4$, as an inorganic polymeric semiconductor, possesses a graphite-like layer structure [150]. So, PEC biosensors show advantages over electrochemical and optical biosensors with high sensitivity and low cost. Hence research in the PEC biosensor for analyte detection has increased. Biomarkers detected using photoelectrochemical biosensors are summarized in [151]. For instance, Li et al. developed a PEC biosensor based on coral-like $g\text{-C}_3\text{N}_4$ nanostructures to detect the metronidazole biomarker. Although metronidazole is a common antibacterial drug, it causes carcinogenic and genotoxic issues. Hence, the sensitive and facile detection of metronidazole's residues in typical oral medicine samples is an effective approach in health care. According to the results, coral-like $g\text{-C}_3\text{N}_4$ nanostructures in the biosensor platform boosted the facility of signal amplification in the PEC

sensing [152]. In the other study, Mao et al. applied the photosensitive $\text{CuO-g-C}_3\text{N}_4$ nanostructures as an efficient photocathode in the PEC sensing of aflatoxin B1 (as a food contaminator and class 1 carcinogen). The conjugation of CuO to $g\text{-C}_3\text{N}_4$ efficiently extended the optical absorption toward the visible region. The $\text{CuO-g-C}_3\text{N}_4$ nanocomposite enhanced the PEC signaling for the sensitive detection of aflatoxin B1 [153].

7.4. $g\text{-C}_3\text{N}_4$ -Based Fluorescent Biosensors

Fluorescent biosensors have been used in biological assays, owing to their high sensitivity, simple readout systems, lower response time, and visualization [154]. Fluorescent biosensors possess a specific ability to monitor biological cell targets [155,156]. Fluorescence spectroscopy has been widely applied to determine cancer and heavy metal ions [157,158]. Accordingly, the important advantages of this type of biosensor are that it is non-invasive, its capability to use fluorescence intensity, and its fluorescence lifetime. Additionally, using fluorescent nanomaterials, biomarker diagnosis can be highly selective and sensitive [159]. Fluorescent biosensors function by absorbing electromagnetic radiation, which is absorbed by fluorophores or fluorescently labeled molecules. Fluorescent biosensors can be divided into four types according to the signal-producing technique, including FRET (Förster Resonance Energy Transfer), FLIM (Fluorescence Lifetime Imaging), FI (Fluorescence Intensity and its change), and FCS (Fluorescence Correlation Spectroscopy) [160]. The fluorescence biosensors have a single signal for detection and can easily be disturbed by environmental and instrumental conditions [161]. In luminescence, light is produced by excitation without increasing the temperature. Fluorescence is a type of luminescence that occurs over a short period and is created by electromagnetic excitation [162]. Moreover, in fluorescence, the time interval between absorption and emission is short [163]. Figure 11 shows the various schemes of fluorescent reagent-less protein-based biosensors [164].

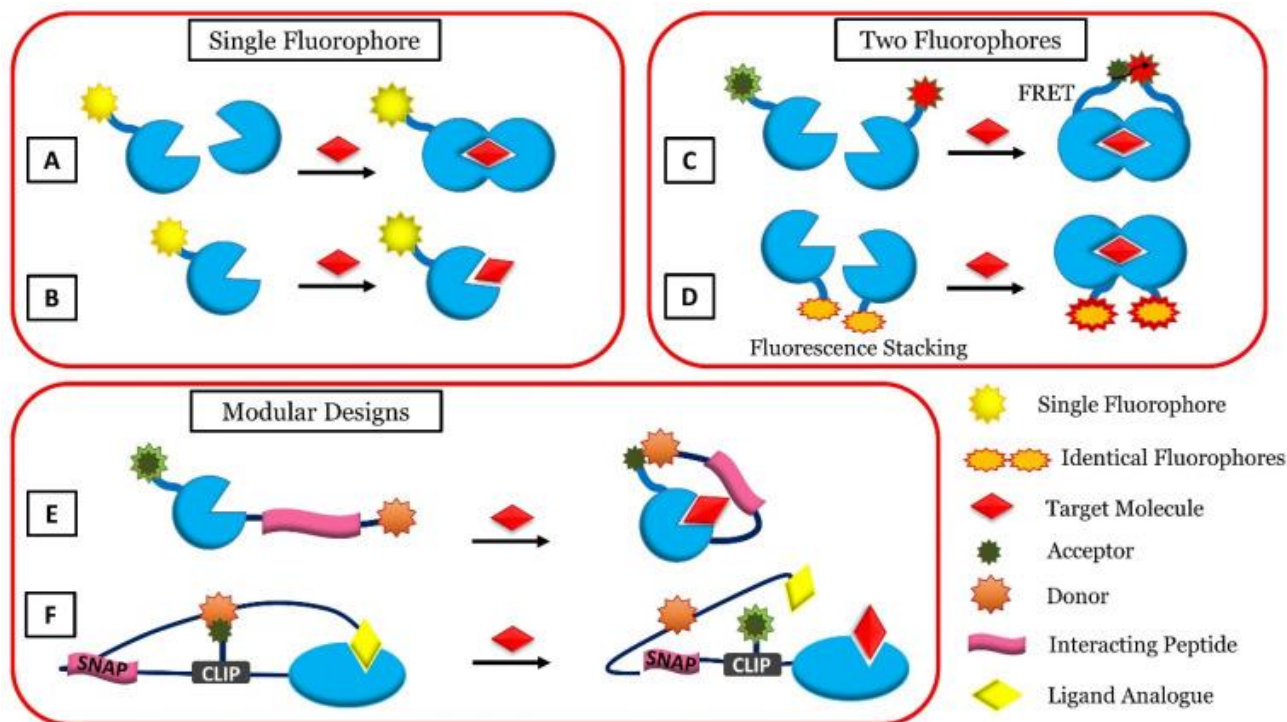


Figure 11: Different schemes of fluorescent reagent-less protein-based biosensors. Single-fluorophore-based biosensors: Change in conformation (A) or target interaction (B) changes the environment of fluorophore. Two-fluorophore-based biosensors: In between two different fluorophores, FRET is recorded (fluorescent proteins) (C), or by breaking the stack of two fluorescent dyes which are identical (D). Modular design-based biosensors: a part in the merged system with the recognition element can interact with either the target bound (E) or the target-free state (F) so that when the target binds, the signal is transduced, [164].

Nanomaterials have introduced an attractive method of developing low-cost and portable fluorescent devices [165]. In recent decades, a new group of 2D nanomaterials has attracted research attention. g-C₃N₄ nanosheets supply an iterating choice for bioimaging and bioprobes applications [166,167]. Additionally, the N-containing structure for the g-C₃N₄ nanosheet provides the potency for coordination with proton or metal ions [168]. The mentioned unique characteristics of g-C₃N₄ nanosheets make this useful for developing fluorescent biosensors or bioprobes. Some of the developed fluorescent biosensors for detecting different biomarkers have been explained through reference [151].

Hatamie et al. applied g-C₃N₄ nanosheets to develop a label-free bioassay system for diagnosing metronidazole in biological fluids. The switch-off green fluorescence biosensor provided rapid sensing with a linear detection range from 0.01 to 0.10 $\mu\text{g mL}^{-1}$ [118]. Dopamine is a neurotransmitter with substantial biological functions in neuroendocrine regulations, and its abnormal content in the human serum leads to Parkinson's and Alzheimer's disease. Lv et al. investigated the g-C₃N₄ nanofibers in the fluorescent probe for dopamine sensing. It provided a sensitive detection platform with a limit of detection (LOD) lower than 17 nM [169].

7.5. g-C₃N₄-Based Electrochemiluminescent (ECL) Biosensors

Over the past several decades, many studies on electrochemiluminescence (ECL) biosensors have been conducted in various fields, such as chemical analysis and clinical diagnostics or food analysis. Electrochemiluminescence, or electrochemical chemiluminescence, is the light emission produced from molecular types by an electron transfer process. Additionally, ECL is triggered by an electrochemical reaction of the luminophores on an electrode surface. Moreover, the significant advantages of ECL are its high sensitivity and selectivity. In ECL biosensors,

electrochemically generated intermediates endure an extremely exergonic reaction to turn out into an electronically excited state. ECL-based biosensors utilize specific biological diagnosis elements, such as enzymes, antibodies, aptamers, peptides, and proteins to selectively recognize a particular analyte and generate an ECL signal [170]. The basis of the method is on diagnosis interaction among biological cognizance elements and the corresponding targets by ECL release alterations. Accordingly, two main components are needed in standard ECL detection: ECL active types and biological cognizance elements.

Depending on the reaction that induces the ECL signal emission, there are several sensing systems for medical applications.

In systems that are based on the chemical reactions of the luminophores and co-reactants, the chemical reaction between the luminophore and the co-reactant and is used for detecting diverse biomarkers.

The second type is systems that involve the co-reaction accelerator-involved reactions. In these systems, the reaction mixture is mixed with co-reaction accelerators. These accelerators are involved in generating electrochemiluminescent reactions in terms of facilitating the ECL reaction rate of co-reactant to produce several intermediates.

In systems that incorporate resonance energy transfer (RET) reactions, instead of using only one luminophore, the signal is emitted via two different emitters by incorporating a RET.

For systems that incorporate an enzyme reaction-based signal amplification, binding events between target analytes and probe DNAs initiate. High sensitivity and extension of the dynamic range of the modulation are some of the benefits of these systems [171]. Figure 12 represents the mentioned types of ECL biosensors based on the reactions leading to ECL signal emission.

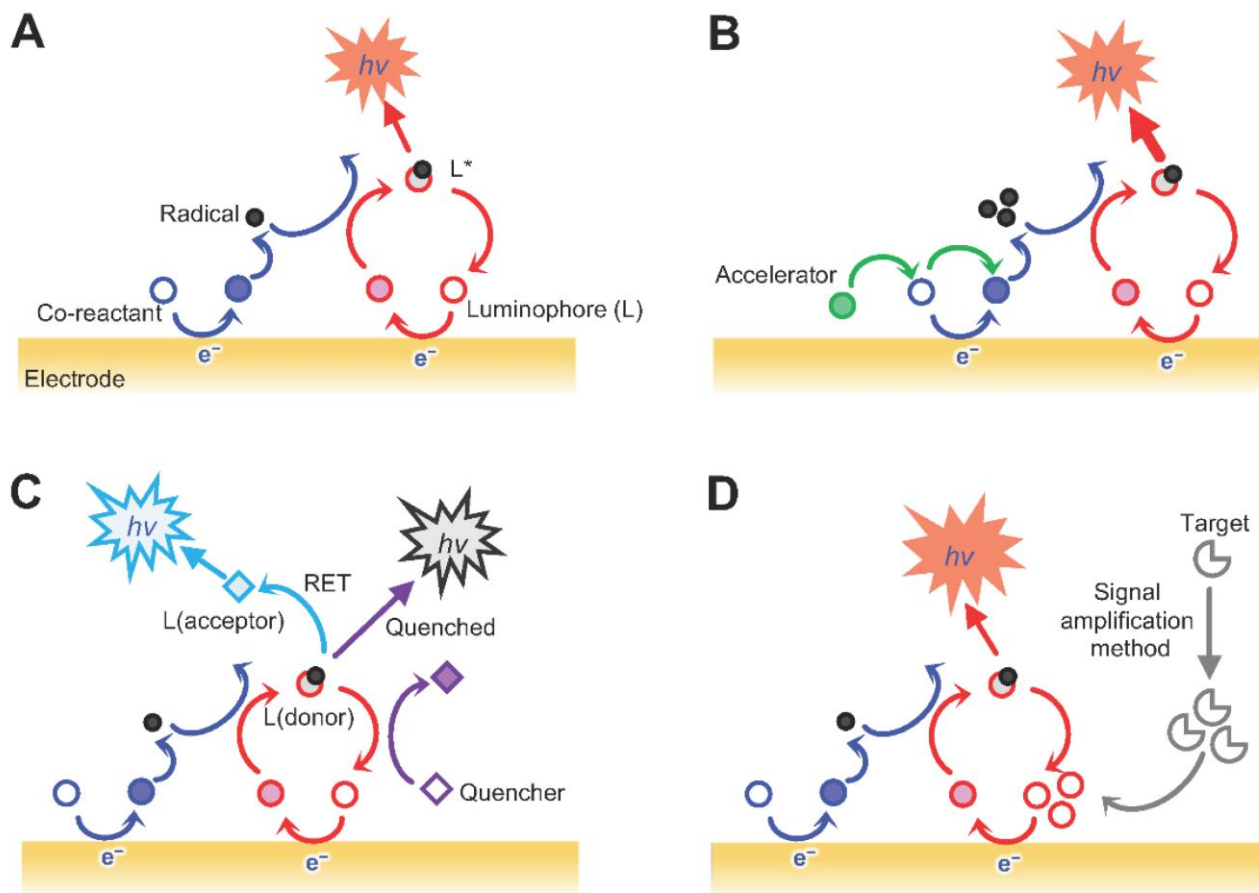


Figure 12: Different categories of ECL systems. (A) Luminophore and co-reactant-involved reaction-based system; (B) co-reaction accelerator-involved reaction-mediated system; (C) resonance energy transfer (RET) reactions-incorporated system; and a (D) signal amplification method-incorporated system. [171].

$g-C_3N_4$ has a large surface area, and this carbon-based material can enable more sites to sequester charge carriers. Additionally, $g-C_3N_4$ has high electron conductivity, and they can successfully separate and then transfer charge carriers [170]. Some of the electrochemiluminescent biosensors are represented in [151].

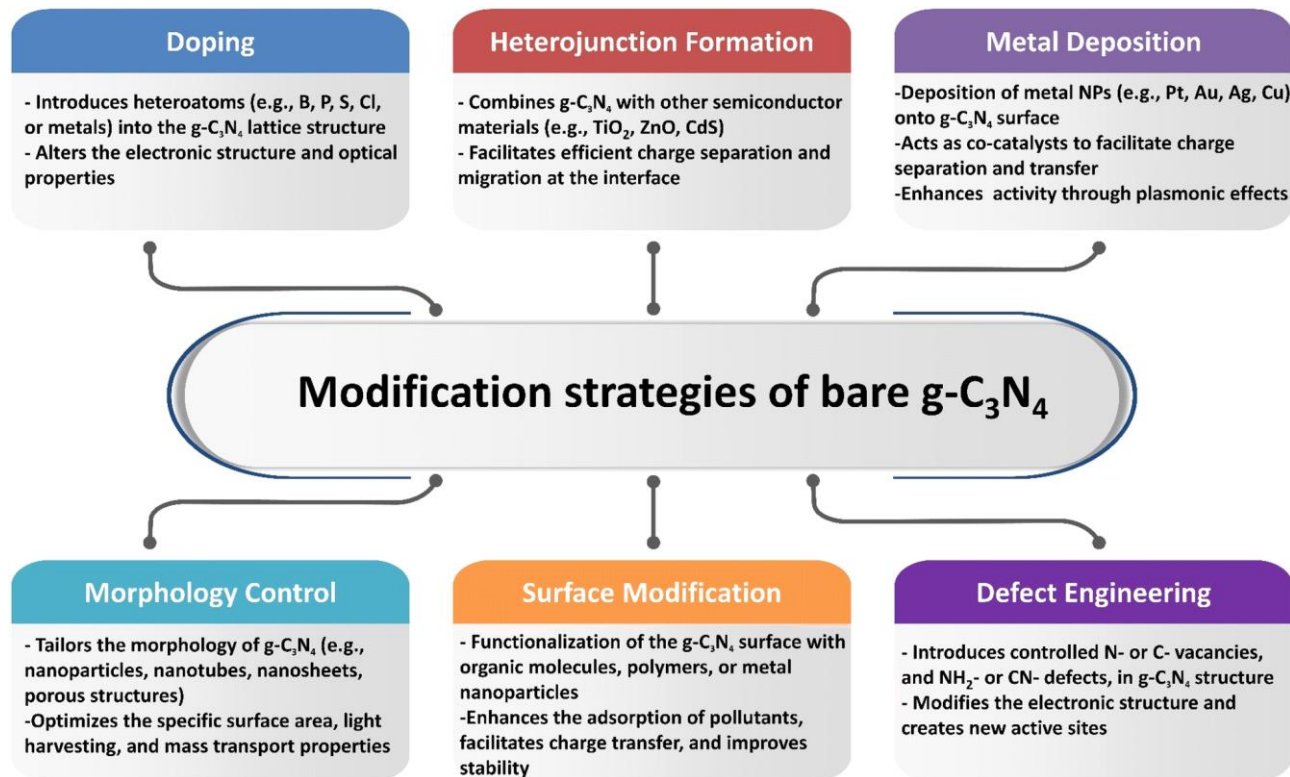
Wu et al. developed an ECL immunosensor to detect the cancer biomarker CA125; nevertheless, its relatively low concentration in human body fluids limits the conventional methods. The disposable and label-free biosensor provided a sensitive detection via ECL emission when multifunctional $g-C_3N_4$ captures the CA125 tumor marker in the range from 0.001 to 5 U/mL, with a LOD of 0.4 mU/mL [172]. Wang et al. proposed a novel ECL bioassay system for detecting the HL-60 cancer cells based on $g-C_3N_4$ nanosheets and Ag-PAMAM-luminol nanocomposites (Ag-PAMAM-luminol NCs), where $g-C_3N_4$ nanosheets were applied as a reductive-oxidative ECL emitter. The overlapping of the ECL spectrum of $g-C_3N_4$ nanosheets and the adsorption spectrum of Ag nanoparticles as well as luminol oxidative-reductive ECL emissions simultaneously contributing to the sensitive detection of the HL-60 cancer cells, with 150 cells as the limit of detection [173].

8. Modification of $g-C_3N_4$ for improved photocatalytic activity

It is an important strategy used for the modification of $g-C_3N_4$ to enhance its photocatalytic efficiency. Due to the poor light harvesting and rapid recombination of electrons and holes, the $g-C_3N_4$ needs to be modified with different types of elements which can increase its efficiency. There have been a lot of ways to modify the $g-C_3N_4$ including elemental doping, heterostructure construction, noble metal loading and nanoarchitecture.

Composite $g-C_3N_4$ photocatalysts have gained significant attention in recent years due to their potential for efficient and sustainable energy conversion and environmental remediation. The $g-C_3N_4$ modification with other materials allows for improved light absorption, better charge separation, and boosted catalytic performance, resulting in enhanced photocatalytic activity.

Several approaches have been applied to modify pristine graphitic carbon nitride and improve its photocatalytic performance, such as creating heterojunctions, doping with non-metallic and metallic materials, co-catalyst loading, tuning catalyst morphology, metal deposition, and nitrogen-defect engineering, as shown in Scheme 2 [174-179]. When it comes to the fabrication of $g-C_3N_4$ composites as photocatalysts, two main approaches are commonly employed based on the crystallization process: in situ crystallization and ex situ crystallization.



Scheme 2: Modification methods of g-C₃N₄ to enhance its photocatalytic performance.

9. Modification of g-C₃N₄ by metal-deposition

Metal deposition involves the introduction of metal nanoparticles or tiny thin films onto the surface of g-C₃N₄ through various deposition techniques, such as physical vapor deposition or chemical methods (e.g., impregnation, electrochemical deposition) [180]. In this process, the metal species are not incorporated into the lattice structure of g-C₃N₄ but rather exist as separate entities on the surface. The incorporation of metals onto g-C₃N₄ as a composite photocatalyst offers critical prospects for improving its light absorption, charge separation, catalytic activity, and overall photocatalytic performance. The localized surface plasmon resonances, catalytic properties, and synergistic effects of noble metals contribute to the enhanced efficiency and selectivity of photocatalytic reactions. For instance, a facile immobilization of noble metals (Ag, Au, and Pd) onto g-C₃N₄ using a simple ultrasonication technique was described [181]. In this method, g-C₃N₄ (0.5 g) was dispersed in DI water through ultrasonication for 1 hour. The metal precursor was then mixed with the previous suspension, followed by reduction using NaBH₄ with continuous stirring for 1 hour. After noble metals' deposition, XRD examination showed a modest drop in the diffraction intensity of the g-C₃N₄ (100) plane. This implies that the presence of metal atoms prevented the formation of g-C₃N₄ crystals [181]. Furthermore, Ag/g-C₃N₄ photocatalyst was synthesized by using an infrared-assisted heating strategy to deposit AgNO₃ salt onto the g-C₃N₄. The presence of Ag nanoparticles on the surface of g-C₃N₄ facilitates the capture of electrons generated by g-C₃N₄ and their subsequent utilization in degrading methyl orange or producing H₂ from H⁺ [182]. In another investigation, researchers employed ultrasonication-assisted liquid exfoliation to create g-C₃N₄ nanosheets from bulk g-C₃N₄. [183]. After that Au was deposited on g-C₃N₄ via green photoreduction of Au(III). TEM analysis verified the good exfoliation of bulk g-C₃N₄ (Fig. 13a). However, numerous Au NPs ranging from 5 to 20 nm were formed on the nanosheets, as depicted in (Fig. 13b). Additionally, DRS results demonstrated that the Au NPs/g-C₃N₄ composite exhibited an absorption peak at 550 nm, indicative of the surface plasmon resonance band specific to colloidal gold (Fig. 13c). Hence, the presence of Au NPs served as electron sinks, facilitating the separation of photogenerated electron/hole pairs [183]. Moreover, Ag NPs/g-C₃N₄ composite was synthesized using an

environmentally friendly chemical approach, as depicted in (Fig. 13d) [184]. The deposition of Ag NPs onto the g-C₃N₄ surface resulted in a slight reduction in the BET surface area, as shown in (Fig. 13d). XPS analysis further confirmed the existence of metallic silver on the g-C₃N₄ surface. Furthermore, chemical impregnation of single Pd atoms onto g-C₃N₄ enhanced its photocatalytic activity [186]. The presence of single Pd atoms and their coordination structure in the composite were confirmed using HAADF-STEM (high-angle annular dark-field scanning transmission electron microscopy) and XAFS (X-ray absorption fine structure) analyses. The powerful interaction between the Pd- and surrounding N-atoms facilitated the production of photogenerated electrons, leading to the promotion of the photocatalytic performance of the composite [186]. However, the noble metal's cost prevents its extensive use in real applications. Studies have been performed on various transition metals, including Fe, Cu, W, Zn, Mo, Zr, etc [187-191]. For example, the incorporation of cobalt into g-C₃N₄ through a one-step thermal polycondensation approach suppressed the growth of the g-C₃N₄ crystals and resulted in a larger specific surface area with the formation of abundant Co-N_x active sites [192]. It also reduced the band gap energy and facilitated more efficient separation of photogenerated electrons and holes [192]. Furthermore, the Fe/g-C₃N₄ composites were fabricated with various initial concentrations of FeCl₃, resulting in samples labeled FCN-0.5, FCN-1, FCN-2, and FCN-3 representing 0.5%, 1%, 2%, and 3% Fe, respectively [185]. The DRS revealed an enhanced visible-light range absorption and a redshift for Fe/g-C₃N₄ composites. As the Fe content increased, the optical band gap gradually shifted to lower energy, indicating the incorporation of Fe ions into the g-C₃N₄ lattice and altering its electronic structure. This redshift in absorption promoted the production of more electron-hole pairs under sunlight, ultimately enhancing the photocatalytic features. Additionally, the Nyquist plots illustrated clear differences in the semicircle diameter between bulk g-C₃N₄, pure g-C₃N₄, and FCN-2 nanosheets, with the FCN-2 nanosheets displaying a significantly smaller semicircle diameter compared to the others (Fig. 13e) [185]. Moreover, the Co/g-C₃N₄ composite was fabricated through an in-situ calcination strategy [193]. Initially, 30 g of melamine was mixed with 50 mL of DI water. Subsequently, Co(NO₃)₂ was added to the suspension under sonication for 10 minutes, maintaining a

weight ratio of 30 : 0.5. The resulting mixture was then calcined in a Muffle furnace at 550 °C for 1 hour at a heating rate of 10 °C min⁻¹[193]. Co/g-C₃N₄ had a surface area of 25.6 m² g⁻¹, featuring a larger amount of mesopores

compared to g-C₃N₄ (surface area: 18.2 m² g⁻¹). The SEM image showed a mixed morphology in Co/g-C₃N₄, consisting of cobalt oxide grains with an irregular polygonal crystal shape and g-C₃N₄ sheets.

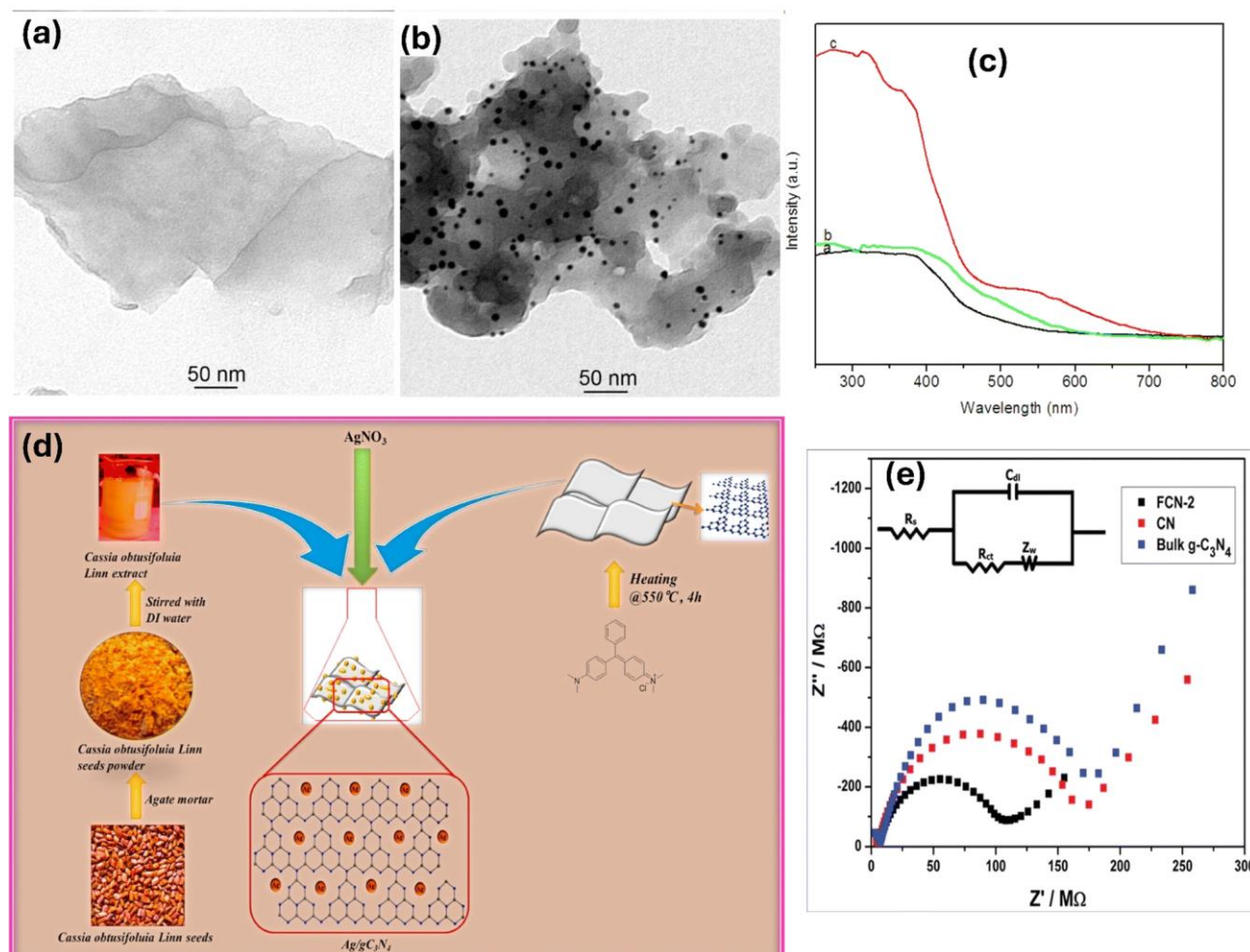


Figure 13: Tem image of (a) g-C₃N₄, (b) Au/g-C₃N₄, (c) DRS data of g-C₃N₄ nanosheets, bulk g-C₃N₄, and AuNP/g-C₃N₄ nanohybrids [183], (d) synthesis of Ag/g-C₃N₄ via green route, [184], and (e) EIS of the g-C₃N₄, and pure and Fe-doped g-C₃N₄ nanosheets, [185].

10. Modification of g-C₃N₄ by non-metallic and metallic doping

Doping involves introducing dopant into the lattice structure of g-C₃N₄ by substituting carbon or nitrogen atoms with dopant atoms. This process modifies the electronic structure and properties of g-C₃N₄ by altering the band structure, charge carrier mobility, and recombination rates. Non-metal and metal doping are the two primary types of elemental doping of g-C₃N₄. Non-metal doping has gained significant attention as a means to preserve the metal-free property of g-C₃N₄. Non-metals possess high ionization energies and electronegativities, allowing them to form covalent bonds by gaining electrons during reactions with other compounds [194-197]. This characteristic makes non-metals a suitable option for doping g-C₃N₄, as they do not introduce metal ions with varying chemical states, which could be affected by thermal variations. Various non-metal dopants, including phosphorus, sulphur, carbon, nitrogen, oxygen, boron, and halogens, have been extensively investigated for their efficacy in doping g-C₃N₄[198-200].

A facile method was employed to synthesize metal-free boron and oxygen-doped g-C₃N₄ with carbon vacancy [201]. In this method, a mixture of g-C₃N₄ and varying amounts of H₃BO₃ (1%, 2.5%, 5%, and 10%) was ground and transferred to a crucible for calcination at 500 °C for 2 hours. The resulting B and O doped g-C₃N₄ exhibited distinct morphological characteristics compared to pristine g-C₃N₄, featuring loose and irregular tissue-like structures. SEM images revealed that the B and O dopants caused

a modification in the morphology by dividing the bulk layers of g-C₃N₄ into smaller layers [201].

Phosphorus-doped g-C₃N₄ was fabricated via a simple poly-condensation strategy using dicyandiamide (or cyanoguanidine) as the precursor and 1-butyl-3-methylimidazolium hexafluorophosphate as the phosphorus source [202]. The hexafluorophosphate ions reacted with amine groups upon raising the temperature, incorporating phosphorus into the C-N framework. Analysis confirmed the formation of P-N bonds, with phosphorus likely substituting corner or bay carbon positions. Even at low doping levels, the electronic structure of g-C₃N₄ was significantly altered, leading to reduced optical band gap energy and increased electrical conductivity [202]. Furthermore, P-doped g-C₃N₄ was synthesized via a thermal polymerization method, where the P atoms were successfully introduced into the g-C₃N₄ lattice, resulting in modified electronic properties and improved suppressions of charge carrier recombination [203]. Moreover, a co-condensation approach, without the use of templates, was followed to synthesize P-doped g-C₃N₄ nanoflowers with in-plane mesopores, where the introduced phosphorus species exhibited strong chemical bonding with neighboring carbon and nitrogen atoms, leading to a forced planar coordination within the carbon nitride framework [204].

Furthermore, a single-pot pyrolysis method was employed to synthesize sulfur-doped graphitic carbon nitride porous rods (S-pg-C₃N₄) by heating a

complex of melamine and trithiocyanuric acid at various temperatures [205]. The characterization results demonstrated that S-pg-C₃N₄ exhibited a porous rod structure with a significantly higher surface area (ranging from 20 to 52 m² g⁻¹) when compared to bulk g-C₃N₄. Additionally, it was observed that the surface area of the S-pg-C₃N₄ samples increased as the heating temperature was raised [205]. On the other hand, the synthesis of oxygen-doped g-C₃N₄ using a facile H₂O₂ hydrothermal method was reported [206]. XPS analysis revealed the successful doping of oxygen into the g-C₃N₄ lattice, resulting in the formation of N–C–O bonds, where oxygen atoms were directly bonded to sp²-hybridized carbon. Notably, the oxygen doping induced a downshift of the conduction band (CB) minimum by 0.21 eV without altering the valence band (VB) maximum. This oxygen doping-induced modulation of the electronic and band structure of g-C₃N₄ led to various beneficial effects, including an increase in visible light absorption, extended surface area and enhanced photogenerated separation efficiency [206]. Otherwise, using a hydrothermal synthesis, sulfur fluoride-doped carbon nitride (F-SCN) was effectively synthesized [207]. The incorporation of fluorine and sulfur into the carbon nitride lattice resulted in a notable improvement in the photocatalytic performance by enhancing the separation of electron–hole pairs and facilitating efficient charge transfer [207].

On the other hand, the g-C₃N₄ structure has been modified via metal doping [208–211]. For example, mesoporous graphitic-carbon-nitride nanosheets doped with zinc ions (Zn-mpg-C₃N₄) were reported [212]. The surface area and porosity of g-C₃N₄ were improved by PEG-1500, whereas the electrical features of the g-C₃N₄ increased when zinc was incorporated into the g-C₃N₄ structure.

11. Modification of g-C₃N₄ by creating heterojunctions

Heterojunctions in g-C₃N₄-based photocatalysts can be classified into several types based on their structural configurations and electronic band alignments, each offering unique advantages and functionalities for photocatalytic applications. Heterojunctions are typically formed by hybridizing g-C₃N₄ with other materials, e.g., semiconductors or carbon materials, in a composite form. When these materials are nearby in a heterojunction, they maintain their distinct crystal structures and electrical properties. Different types of heterojunctions, such as Type-I, Type-II, p–n junctions, and Z and S schemes, can be used to create these connections.

11.1. Modification by creating Type-I and Type-II heterojunctions

The synergistic combination of g-C₃N₄ with another photocatalyst can give rise to Type I and Type II heterojunctions, which exhibit fascinating electrochemical and optical properties [213]. In Type I heterojunctions, the semiconductor with the wider band gap can promote efficient charge separation and migration. Specifically, when illuminated, electron–hole pairs can traverse from the VB and CB of the wider band gap semiconductor to the partner semiconductor, leading to enhanced photocatalytic performances [213,214]. Furthermore, redox processes take place on the photocatalyst with a lower redox potential, modulating the overall photocatalytic activity. This complex interplay between different semiconductors and their band gaps exemplifies the potential for advanced applications in photocatalysis. For instance, the creation of customizable heterojunction structures composed of (CoOx) encapsulated within g-C₃N₄ using a straightforward one-pot technique under various annealing environments was demonstrated [214]. A Type I heterojunction incorporating Co₃O₄/g-C₃N₄ nanotubes was established in an air setting, resulting in the aggregation of Co₃O₄ ranging from 20 to 80 nm on the nanotube surface. Another study reported the formation of type I and type II g-C₃N₄/g-C₃N₄ heterostructures for the removal of ppb-level NO in air [213]. The research findings highlight the enhanced photocatalytic activity and stability of the g-C₃N₄-based heterostructures compared to pristine g-C₃N₄ alone. The improved performance can be attributed to the promoted charge separation within the heterostructures, leading to more efficient utilization of light energy and enhanced photocatalytic efficiency in NO removal.

Conversely, misalignment of the conduction and valence band boundaries among the two materials results in the creation of Type II heterojunctions,

where the two semiconductors are interfaced while one semiconductor has a lower conduction band and the other has a higher valence band. An inherent electric field that is generated by the energy level movement at the interface may facilitate charge separation and boost charge migration across the junction. The CB potential of g-C₃N₄ typically around –1.1 eV, significantly lower than that of many other photocatalysts. Consequently, when exposed to irradiation, e⁻ excited in the CB of g-C₃N₄ can swiftly move to the CB of a secondary photocatalyst with a greater potential. In parallel, the generated holes will move in the opposite direction. The creation of a Type II junction allows for the spatial separation of photogenerated electrons and holes, which prevents them from recombining and allows them to participate in desired redox reactions efficiently. This separation of charges leads to an increased lifetime of the charge carriers and enhances the photocatalytic activity of the system. Moreover, the band alignment in Type II heterojunctions can promote interfacial charge transfer processes, such as electron or hole transfer from one component to another, further improving the overall photocatalytic efficiency. This synergistic effect between different semiconductor materials in the heterojunction structure enables better utilization of solar energy and enhances the photocatalytic performance of g-C₃N₄-based systems. This phenomenon can be validated through specific analytical techniques like steady-state/time-resolved photoluminescence (PL) spectra, photocurrent measurements, and EIS measurements. Different types of semiconductor substances have been used in combination with g-C₃N₄ to create Type II heterojunctions to reduce the recombination of the generated charges, such as TiO₂, ZnO, Fe₂O₃, MoO₃, WO₃, ZnTe, CdS, MoS₂, ZnIn₂S₄, Bi₂WO₆, and others [215–218]. For instance, various hierarchical heterojunctions of Bi₂O₃/g-C₃N₄, such as g-C₃N₄/BiOI, g-C₃N₄/Bi₄O₅I₂, and g-C₃N₄/Bi₅O₇I have been successfully developed [219]. The g-C₃N₄/BiOI is synthesized using a direct precipitation method, while g-C₃N₄/Bi₄O₅I₂ and g-C₃N₄/Bi₅O₇I are obtained through in situ calcination transformation of g-C₃N₄/BiOI at different temperatures. The g-C₃N₄/BiOI and g-C₃N₄/Bi₄O₅I₂ heterojunctions are classified as Type-I, while g-C₃N₄/Bi₅O₇I is categorized as a Type-II heterojunction. Notably, g-C₃N₄/Bi₅O₇I exhibited significantly improved performance compared to g-C₃N₄/BiOI and g-C₃N₄/Bi₄O₅I₂. The promoted activity of g-C₃N₄/Bi₅O₇I can be attributed to its surface area, promote charge separation and transfer performance, and robust charge carrier density resulting from the formation of a Type-II heterojunction.

11.2. Modification by creating p–n heterojunctions

The formation of a p–n heterojunction involves combining two different semiconductors with p-type and n-type electronic structures. This arrangement leads to a built-in electric field at the interface, which can promote charge separation and migration, thereby improving the photocatalytic performance of the material. g-C₃N₄ behaves as an n-type owing to the –NH/NH₂ groups as electron donors present in its structure. Constructing a p–n heterojunction promotes the separation of electron–hole pairs. The Fermi level of a p-type (EF,p) is near its VB, while that of an n-type (EF,n) is close to its CB. When p-type and n-type contact, electrons transfer from the n- to p-type owing to the Fermi level offset. This results in a positively charged interface for the n-type semiconductor and a negatively charged interface for the p-type semiconductor, creating a built-in electric field at the contact interface. For instance, p–n CoFe₂O₄/g-C₃N₄ heterojunctions was created using a simple one-pot coprecipitation method [220]. The development of the p–n heterojunction and the distinct structure of g-C₃N₄ facilitated charge separation and electron transfer, resulting in a remarkable enhancement in photocatalytic activity. The presence of an internal electric field at the junction boosted the accumulation of electrons and holes in the VB of g-C₃N₄ and the CB of CoFe₂O₄. This led to increased separation efficiency and a noticeable reduction in the recombination rate of electron–hole pairs. Other p–n heterojunctions, such as CuAl₂O₄/g-C₃N₄, [221] BiOCl/g-C₃N₄, [222] and MgIn₂S₄/g-C₃N₄ (ref. [223]) have also been reported.

11.3. Modification by creating Z-scheme and S-scheme heterojunctions

The Z-scheme heterojunctions were developed to address the limitations of conventional Type-II heterojunctions. In this arrangement, photogenerated electrons from photocatalyst II are transferred to the valence band (VB) of photocatalyst I. This process enhances the separation of charges in the semiconductor without altering the redox potential of the holes in the VB of photocatalyst II and the electrons in photocatalyst I. In the Z-scheme, the electrons and holes in the lower VB and higher CB levels can be utilized for generating reactive oxygen species (ROS). By maintaining the strong oxidative and reductive properties of the electrons and holes, this heterojunction is preferred over Type-II heterojunctions [224]. However, some charge recombination between the lower VB and higher CB levels may still occur. In the direct Z-scheme, the transfer of electrons from one photocatalyst to another occurs directly through a physical contact or a solid-state interface between the two photocatalysts. This direct transfer of electrons enables efficient separation and utilization of charges for photocatalytic reactions. In the mediator Z-scheme, an additional mediator component is introduced between the two photocatalysts to facilitate the transfer of electrons. This mediator component acts as a shuttle, transferring electrons between the two photocatalysts, thus enabling efficient charge separation and reaction enhancement. The mediator Z-scheme provides flexibility in controlling and optimizing the electron transfer process in photocatalytic systems. For instance, 2D/2D Z-scheme BiOI-XBr/g-C₃N₄ with oxygen vacancies (OVs) was successfully fabricated [225]. The introduction of OVs promoted visible-light absorption, acting as an electron mediator to accelerate the separation rate of photogenerated carriers in the Z-scheme. The optimal ratio of the heterostructures exhibited a high photodegradation activity for RhB, which was attributed to the synergistic effects of the 2D/2D Z-scheme heterostructure and OVs.

It is worthy to mention that metal oxides heterostructures can not only enhance the visible light absorption ability of g-C₃N₄ due to their unique band structures but also facilitate the separation and transfer of photogenerated electron-hole pairs, as well as improve the stability and reusability of g-C₃N₄ photocatalysts. The metal oxides act as protective layers, preventing the photocorrosion of g-C₃N₄ and enhancing its durability under harsh reaction conditions. This is particularly advantageous for long-term applications and practical implementation. The method used to incorporate the metal oxide into g-C₃N₄ can significantly impact the distribution and interaction between the two components, which ultimately affects the photocatalytic efficiency. For instance, TiO₂ is a widely favored

photocatalyst due to its excellent chemical stability, affordability, and suitable valence band (VB) and conduction band (CB) positions that facilitate redox reactions [226,227]. Thus, a highly efficient heterojunction photocatalyst was developed by combining TiO₂ nanotubes with g-C₃N₄ through a thermal deposition approach [228]. In this process, a solution containing 100 mg of TiO₂ nanotubes and 4 mg of g-C₃N₄ in 20 mL of distilled water was subjected to stirring at 80 °C for 6 hours. The HRTEM analysis confirmed the close attachment between TiO₂ and g-C₃N₄, indicating a strong solid interaction and successful formation of the heterojunction [228]. In a separate study, an S-scheme heterojunction of mesoporous/macro TiO₂/g-C₃N₄ was fabricated using a straightforward chemical vapor deposition technique [229]. The research revealed that by adjusting the melamine dosage, the microstructure of the samples could be readily controlled [229]. Similarly, ZnO/g-C₃N₄ photocatalyst, consisting of ZnO loaded onto g-C₃N₄, was fabricated using an ex-situ crystallization strategy [230]. The images revealed that ZnO particles were present on the g-C₃N₄ layers, distinguishing it from pure g-C₃N₄ (Fig. 14a and b). [230]. XPS analysis confirmed the presence of Zn in the modified catalyst, indicating the successful combination of ZnO with g-C₃N₄ (Fig. 14c). Moreover, coral-like WO₃/g-C₃N₄ were fabricated using a wet chemistry strategy, with different mass ratios of WO₃ to g-C₃N₄ (1: 1, 1: 3, and 3: 1). TEM images revealed that g-C₃N₄ appeared as ribbon-like sheets, surrounded by plate-like particles of WO₃[232]. The measurements of the crystallographic particle spacing between 0.20 and 0.39 nm suggest the existence of tiny crystalline zones in the g-C₃N₄ nanosheets. This close contact between g-C₃N₄ and WO₃ facilitates the good separation of photo-excited carriers [232]. Further, TiO₂/g-C₃N₄ composites containing 20–50% TiO₂ by weight were fabricated using a hydrothermal process by dispersing TiOSO₄ in DI water, followed by the addition of g-C₃N₄ and ultrasonication for 30 minutes [231]. The mixture was then heated in an autoclave at 180 °C for 4 hours. The resulting powder was dried at 65 °C. XRD patterns of the composites displayed peaks from both g-C₃N₄ and TiO₂, with no shifting in the TiO₂ peaks demonstrating that the TiO₂ lattice structure was not impacted by the coupling with g-C₃N₄ (Fig. 14d). This lack of influence on the lattice structure is beneficial for photocatalytic activity. Moreover, among the composites, 40% TiO₂/g-C₃N₄ had the lowest bandgap energy at 2.89 eV (Fig. 14e) [231]. In another study, MoO₃/g-C₃N₄ was fabricated by combining 0.01 g of Mo₂N with varying quantities of g-C₃N₄ and the resulting mixtures were subjected to calcination at 350 °C for 240 minutes [233].

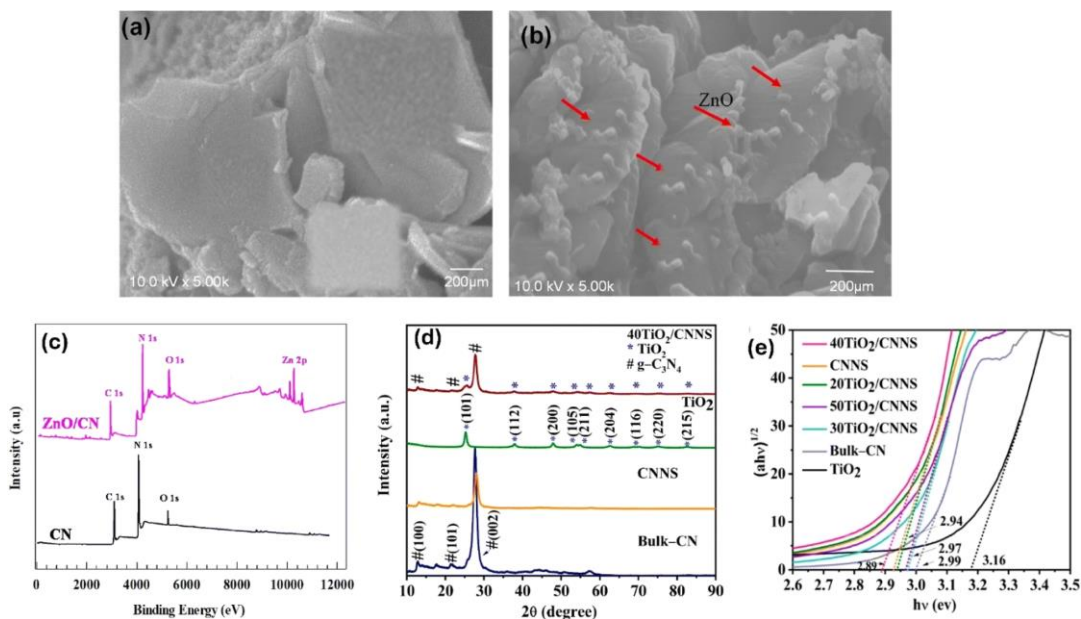


Figure 14: Surface morphology of (a) g-C₃N₄ and (b) ZnO/g-C₃N₄ and (c) XPS of g-C₃N₄ ZnO/g-C₃N₄, [230]; (d) PXRD patterns of bulk-g-C₃N₄ (CN), g-C₃N₄ nanosheets (CNNS), TiO₂, and 40TiO₂/CNNS, (e) Tauc plot displaying band gaps of g-C₃N₄, TiO₂ and their composites. [231]

Metal sulfides is another type of semiconductor materials, greatly enhancing the efficiency of photocatalysis [234-237]. Metal sulfides possess band structures that meet the thermodynamic requirements for water splitting and exhibit improved responses to sunlight due to the formation of a less negatively charged valence band through the (S-3p) orbitals [238]. These advantageous properties of metal sulfides significantly contribute to the superior photocatalytic performance of g-C₃N₄/metal sulfide heterojunction systems [223,239]. The incorporation of metal sulfides allows for the creation of customizable band structures, thereby providing tangible benefits for the desired photocatalytic reaction. In a study, CdS/g-C₃N₄ core/shell nanowires were synthesized using a combination of solvothermal and chemisorption methods [223]. Transmission electron microscopy (TEM) analysis revealed that g-C₃N₄ was effectively coated onto CdS nanowires, establishing intimate contact between the two materials. Additionally, the composite exhibited a higher surface area compared to pure CdS [223]. In another investigation, a one-step solvothermal strategy was utilized to synthesize ultra-thin g-C₃N₄ (UCN) and incorporate NiS onto the surface of ZnIn₂S₄ (ZIS) [240]. The resulting ternary compound, NiS/ZnIS/UCN, was designed to possess dual great-speed charge transfer channels. By combining these materials, the composite achieved improved efficiency in H₂ generation through enhanced charge transfer [240]. It is evident from the TEM picture of NiS/ZIS/UCN that some NiS is loaded onto the surface of ZIS and UCN, implying that the heterojunction ternary compound of

NiS/ZIS/UCN has been well constructed [240]. In another work, a series of CoS₂/g-C₃N₄ were fabricated through a photodeposition strategy [241]. The size of the CoS₂ species could be adjusted, ranging from single atom to nanometer scale, allowing for control over the photocatalytic features. The synthesis process involved mixing 20 mg of g-C₃N₄ with a solution containing 1 mL of 15.2 mg mL⁻¹ thiourea aqueous solution, 1 mL of 5 mg mL⁻¹ Co(CH₃COO)₂, 4 mL of ultrapure water, and 4 mL of absolute ethanol. The mixture was evacuated to remove air and then irradiated using a 300 W Xenon lamp to facilitate the deposition of CoS₂ onto the g-C₃N₄ surface [241]. In another work, a solvothermal approach was utilized to create a heterostructure photocatalyst made of g-C₃N₄/Bi₂S₃/CuS [242]. Further, NiS/g-C₃N₄, CdS/g-C₃N₄, and CdS/NiS/g-C₃N₄ were created via a simple and dependable chemical deposition technique [237]. In another study, g-C₃N₄ was coated with ternary NiCo₂S₄ using a solvent evaporation technique [243]. Whereby, 30 mL of ethanol was used to dissolve sulphide nanoparticles and g-C₃N₄ nanosheets, and the mixture was then ultrasonicated for 30 minutes to create a homogenous suspension. Subsequently, the solvent evaporated at 70 °C, yielding a ZnCo₂S₄/g-C₃N₄ photocatalyst. The ZnCo₂S₄ nanoparticles, which are in very near proximity to the 2D g-C₃N₄ flakes, have a median size of around 20 nm, as determined by TEM investigation (Figure. 15a-d). Moreover, EDS analysis, on the other hand, confirmed that C, N, Zn, Co, and S coexist in the composite and that the atomic ratios of Zn, Co, and S are around 1:2:4, which is in agreement with the ZnCo₂S₄ theoretical chemical ratio (Figure. 15e) [243].

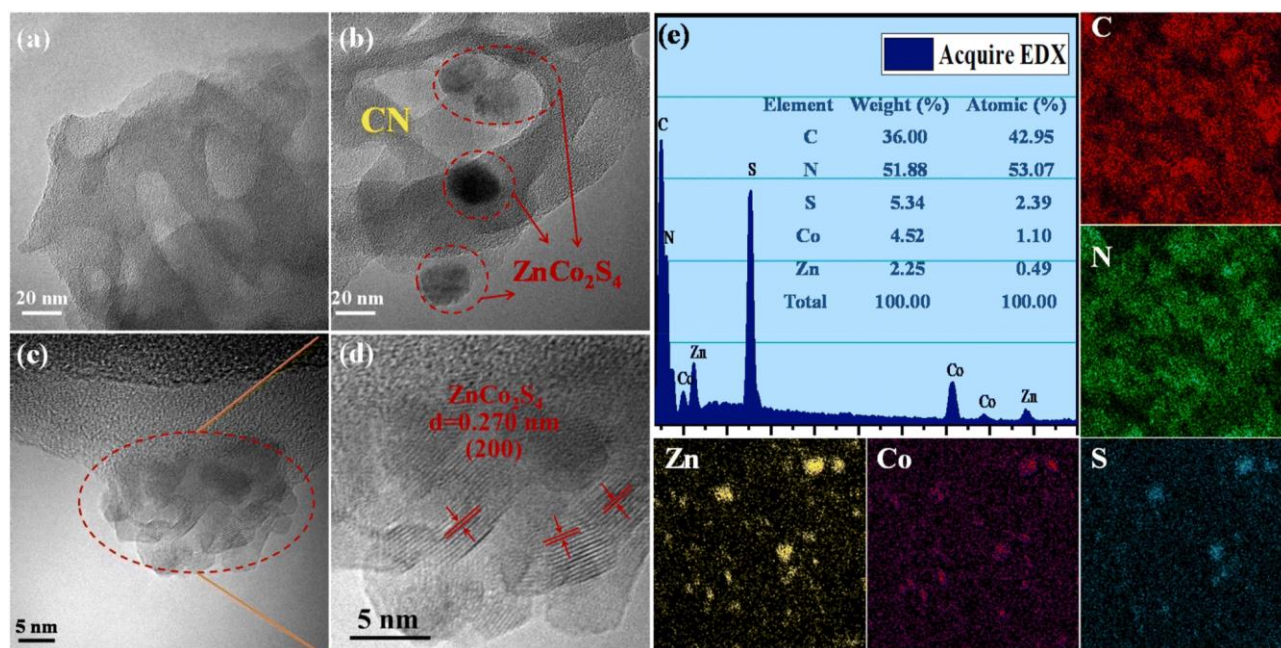


Figure 15: TEM images of (a) CN and (b) ZnCo₂S₄/CN, HRTEM images of (c-d) ZnCo₂S₄/CN, and (e) EDS spectrum of ZnCo₂S₄/CN and elemental mapping analysis, [243].

Pioneering studies constructed heterostructure with other different types of semiconductors, such as phosphides, carbonates, nitrides, halides, among others [244-248]. For instance, Ag₂CO₃/g-C₃N₄ heterojunctions were fabricated using an ultrasonic method, where Ag₂CO₃ was sonochemically targeted and fixed to the g-C₃N₄ active centers [246].

Carbon materials including graphene, carbon nanofibers, carbon nanodots, carbon nanotubes, and other forms of carbon materials, have gained significant attention for coupling with g-C₃N₄ in heterojunctions [249-252]. Carbon materials possess symmetrical molecule arrangements with unique conjugated structures, offering superior photon excitation, high surface area, thermodynamic stability, and electron transmission [253-256]. The creation of carbon-induced g-C₃N₄ photocatalysts presents a viable route for sustained improvements in photocatalytic technology as well as renewable carbon materials as an ecologically benign alternative to metal-based materials. Enhancement of photocatalytic processes has been obtained by

modifications of carbon-induced g-C₃N₄ photocatalysts by several techniques such as junction interaction, surface reconstruction, cocatalyst effects, local electric modification, and more [257-260]. For instance, g-C₃N₄/GO (graphene oxide)-wrapped melamine sponge (MS) monolith was developed through successful design and fabrication (Fig. 16) [261]. The g-C₃N₄ was uniformly distributed on the GO, ensuring efficient utilization of incident light and effective contact with pollutants. By acting as a bridge, GO facilitated the connection between the g-C₃N₄ and MS components. In another instance, g-C₃N₄/GO nanocomposite was synthesized by loading g-C₃N₄ onto GO using an electrostatic self-assembly approach [262]. Furthermore, a unique protonated g-C₃N₄/GO aerogel (p-CN/GOA) was synthesized by a direct frozen-drying technique (Fig. 17a) [263]. The protonating treatment caused a significant change in the surface electric charge of g-C₃N₄, converting it from negative to positive (p-CN), which allowed for powerful self-assembly with the negative surface of GO. This

assembly facilitated the transfer of photogenerated charge carriers. The stacking of p-CN blocks, which were several microns in size, were uniformly attached to the GO nanosheet due to the abundant surface functional groups of GO (Fig. 17c). While TEM confirmed the excellent loading of p-CN onto GO (Fig. 17d), providing further evidence of the combination between p-CN and GOA[263]. In order to enhance the efficiency of underwater photocatalysis for g-C₃N₄, a composite consisting of g-C₃N₄ and carbon nanotubes (CNT) was fabricated using an in situ solvothermal approach [264]. This composite had great surface area and improved light absorption capacity. The findings demonstrate that CNT and g-C₃N₄ exhibit good compatibility with each other. The g-C₃N₄ can grow directly on the surface of CNT, forming a stable composite structure [264]. Another study used a straightforward water bath approach to construct g-C₃N₄ that had been enhanced with carbon nanotubes (CNTs) [265]. The morphological study

showed that two materials were mixed together and that CNTs were wrapped in a lot of g-C₃N₄. This mixture promoted the movement of photogenerated electrons and aided in their separation efficiency [265]. Further, carbon fibers (CF), graphene (GN), and CNTs were introduced to modify g-C₃N₄ through a solvothermal approach [266]. The development morphology of the synthetic composites varied significantly depending on the utilized carbon substrate as shown in Fig. 18. [266]. The poor physicochemical features (e.g., SBET, particle size, pore volume, adsorptive properties, ... etc.), the limited photocatalytic activity, and stability and poor light-harvesting of pristine g-C₃N₄ are marginally boosted by proper modification and application of modified g-C₃N₄. The superior photocatalytic performance of modified g-C₃N₄ over pristine g-C₃N₄ is illustrated by various examples shown in [267].

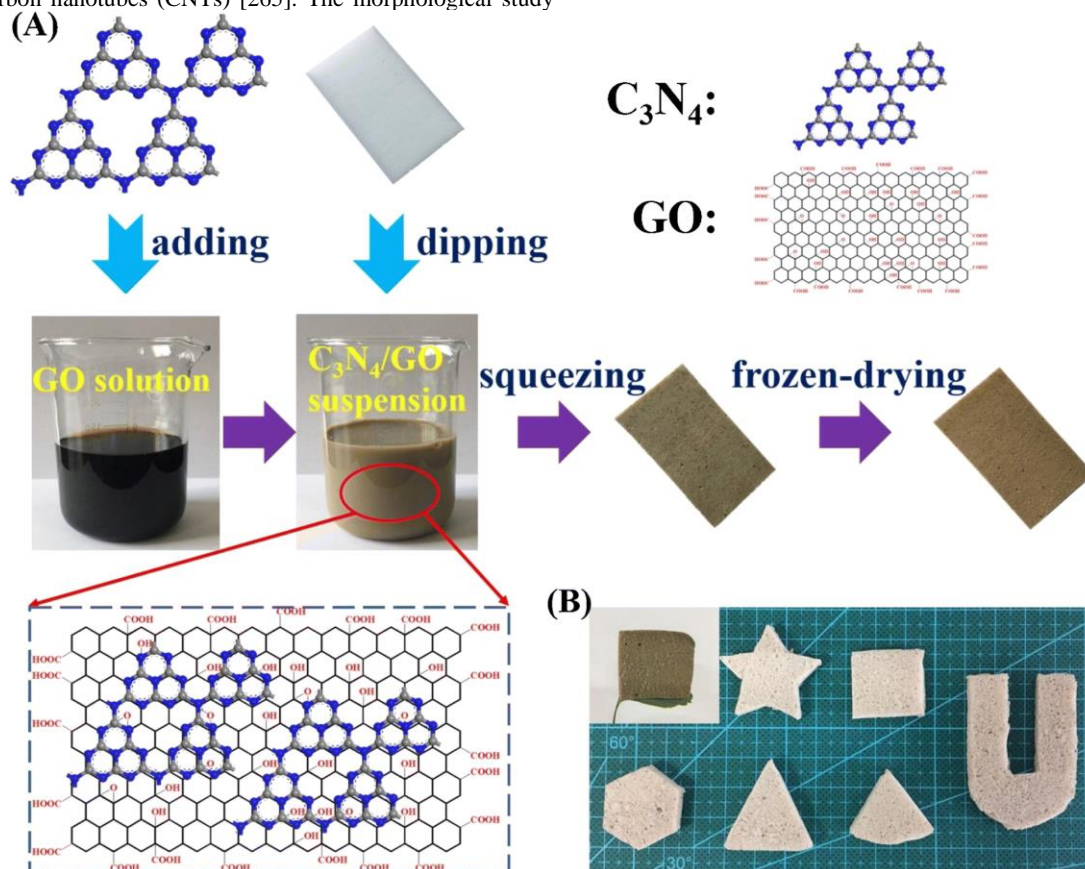


Figure 16: (a) Schematic illustration of the preparation of g-C₃N₄/GO-wrapped sponge; (B): image of different shapes of g-C₃N₄/GO-wrapped sponge, [261].

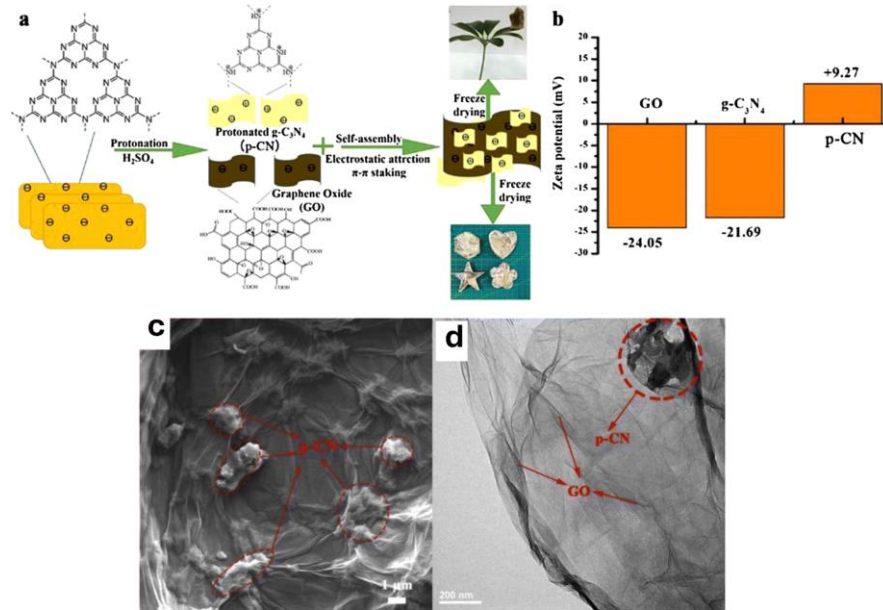


Figure 17 (a) Schematic of the fabrication of p-CN/GOA; (b) zeta potential of GO, g-C₃N₄ and p-CN, (c) the SEM of p-CN/GOA; (d) the TEM of p-CN/GOA, [263].

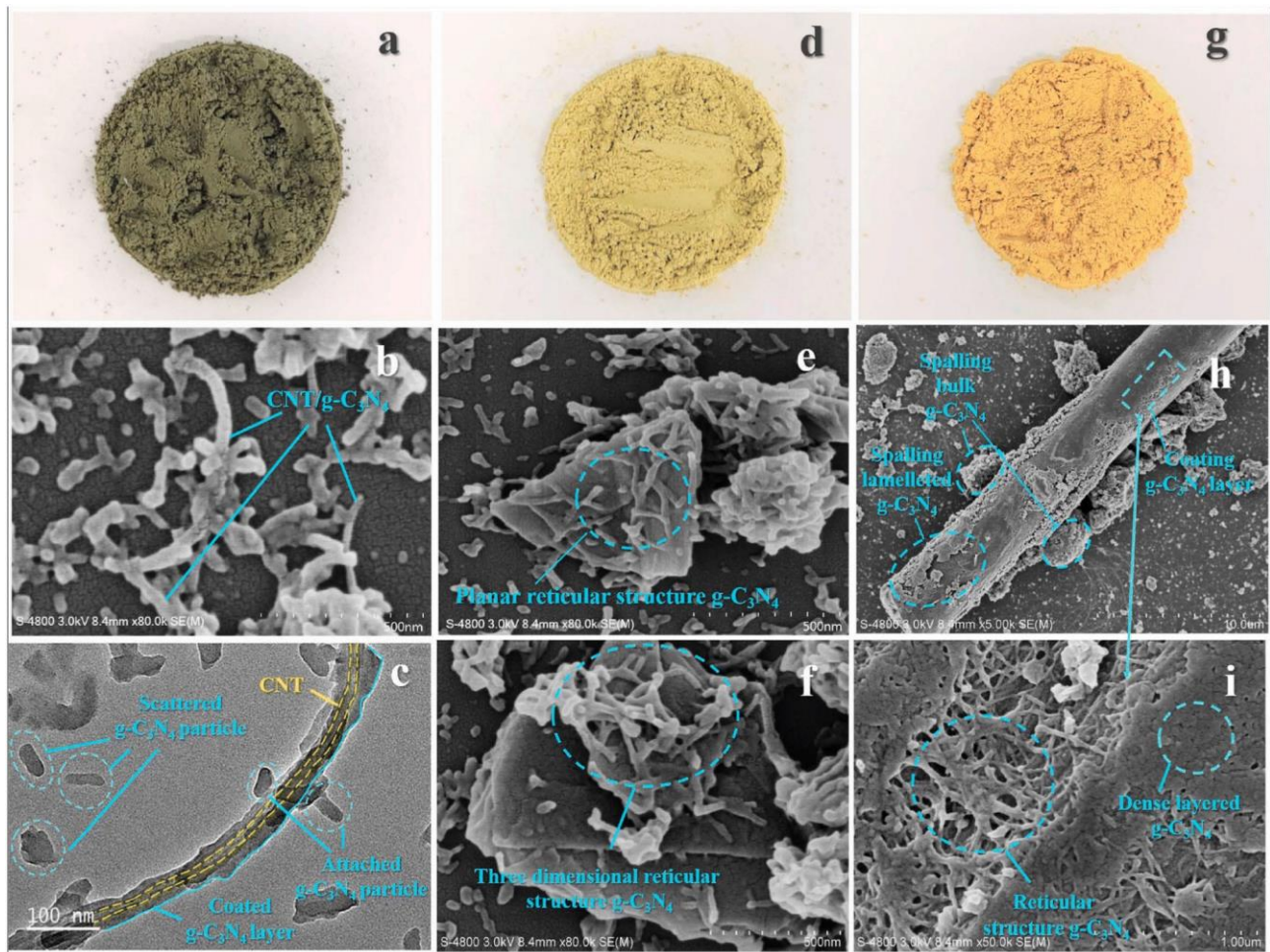


Figure 18 Macro shots of (a–c) CNT/g-C₃N₄, GN/g-C₃N₄ and CF/g-C₃N₄. SEM images of (d–f) CNT/g-C₃N₄, GN/g-C₃N₄ and CF/g-C₃N₄. TEM images of (g–i) CNT/g-C₃N₄, GN/g-C₃N₄ and CF/g-C₃N₄, [266].

12. Scientometric assessment of g-C₃N₄

A scientometric assessment was conducted to learn more about the most recent developments and uses of g-C₃N₄. This entailed the quantitative

analysis of data or information that had been recorded on a specific subject or discipline. In this study, data on the status of g-C₃N₄ applications from 2010 to 2022 were exported as a CSV file from the SCOPUS database and

imported into a VOS viewer programme for additional visualization processing. As shown in Fig. 19, g-C₃N₄ has been used in the top three disciplines of Chemistry, Chemical Engineering, and Material Science. This could be attributed to the fact that the previous two decades have been devoted to additional research on the new material (i.e., g-C₃N₄) to gain more

chemical knowledge and information about it. Now that the research community has a sufficient amount of information and data on g-C₃N₄, its application in other areas has increased, as illustrated in Fig. 19, with new disciplines such as nanomedicine, pharmacy, mathematics, and so on.

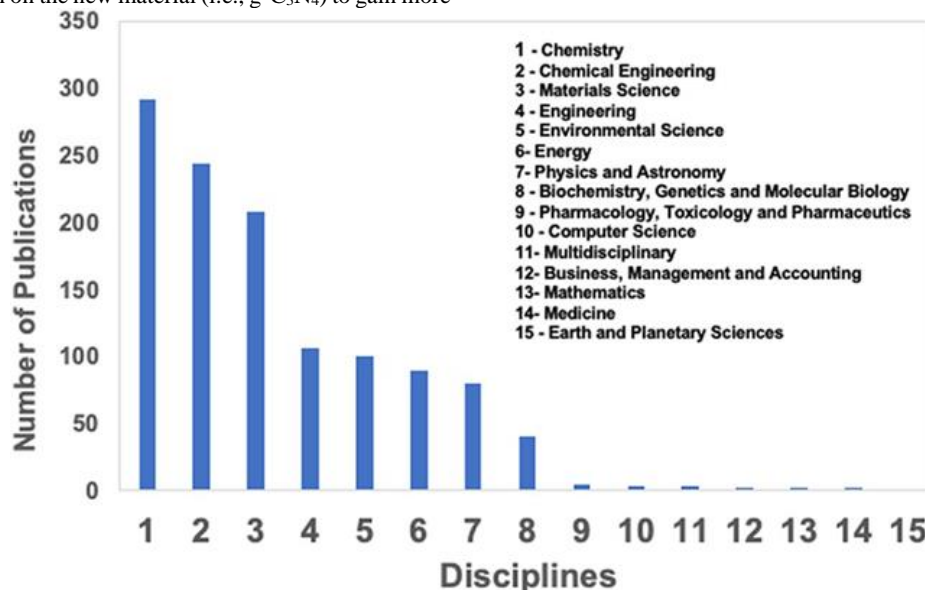


Figure 19: Global trend of publications of g-C₃N₄ in various disciplines from 2010 to 2022

13. Photoelectronic application of g-C₃N₄ in Optical sensors

Graphitic carbon nitride (g-C₃N₄) has emerged as a versatile and eco-friendly photocatalyst with a remarkable ability to address pressing environmental and energy challenges. Its wide range of applications spans various domains, each contributing to the advancement of sustainability. Here, we delve into the diverse and transformative applications of g-C₃N₄, elucidating its role in biosensors.

The addition of nitrogen into the carbon matrix brought an improvement in its electrical, structural, and mechanical properties, particularly its electronic properties, which in turn makes it a potential candidate to be used in rechargeable batteries [268], light-emitting devices [269], fuel cells [270], solar cells, and other applications [271]. Moreover, the g-C₃N₄ has been regarded as a most promising candidate in the overhead application domains. The sp² hybridization of nitrogen and carbon results in forming a π-conjugated electronic structure, which has an excellent photoelectronic characteristic.

Optical sensor systems have attracted much research interest, because of their precise and reasonable detection limit and guaranteed biocompatibility and flexibility. Usually, the optical sensor is a molecule receptor with

variable optical capabilities based on the specific visitors. Presently, fluorescent receptors are commonly used as optical sensors for detections by the interaction of fluorescent with adherent guests. The optical response is dominated by the transport of electrons from receptors to their binding guests. It is well known that g-C₃N₄ is an excellent catalyst to substantially absorb metal ions via chelation or redox reaction, since it has functions such as NH₂/NH/N over surface site. Despite many sensors with an optical receptor attaches to permeable materials, the g-C₃N₄ is the receptor itself and has excellent sensitivity. Lee et. al. investigated the possibility of using g-C₃N₄ as an optical sensor to check the presence of metal ions in an aqueous solution by examining its photoluminescence quenching effects [272]. The findings in Fig. 20 reveal that g-C₃N₄ has good Cu²⁺ sensitivity. The Cu²⁺ entirely quenches photoluminescence thru no visible interfering from other metals, because photo-generated electrons are collected by Cu²⁺. Furthermore, the Stern–Volmer equation may be used in order to quantify the degree of quenching: $I_0/I = 1 + K_{SV}[Q]$, where I₀ and I indicate the luminescence intensity in the absence and presence of metal ions, respectively. The Stern–Volmer constant [272] is denoted by [Q], which is molar concentration of the metal ion. This comparison depicts a roughly linear relationship between the effect of Cu²⁺ concentration on g-C₃N₄ photoluminescence.

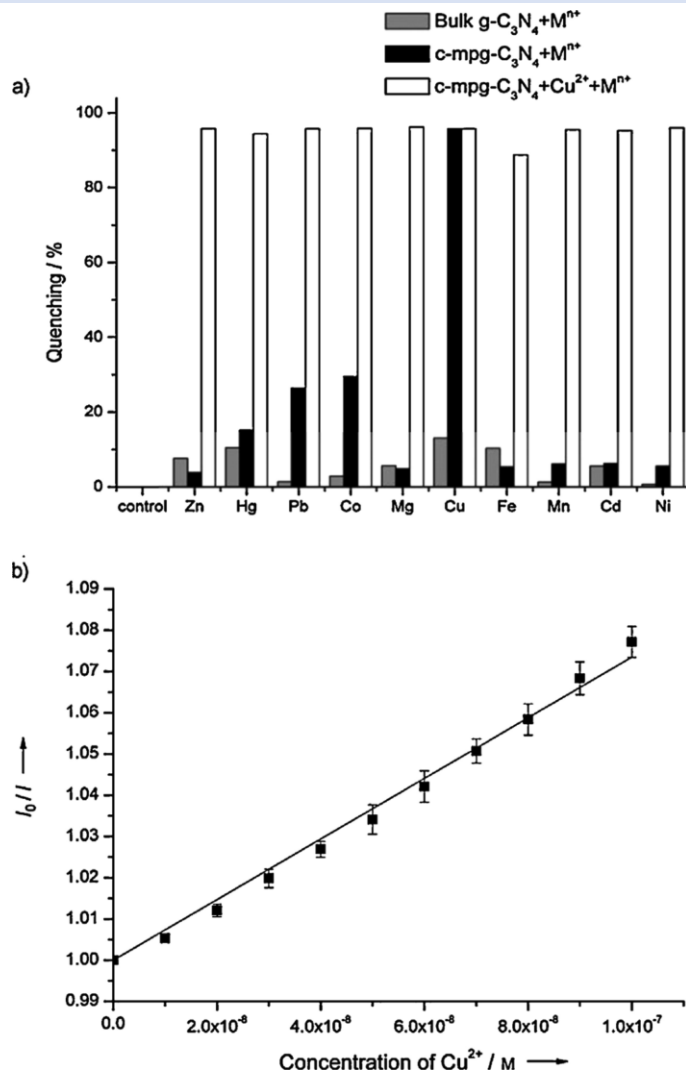


Figure 20: (a) PL spectra of both c-mpg-C₃N₄ (black bar) and bulk (gray bar) after 1 mm of metal ion solutions treatment, and (1 mm) of other metal ions intrusion with (1 mm) Cu²⁺ (white bar); (b) PL spectra of c-mpg-C₃N₄ to Cu²⁺ in 10–100 nm concentration range. Reprinted with permission from Lee (2010). Copyright © 2010 John Wiley and Sons.

Since g-C₃N₄ is biocompatible and has an appropriate electrical structure, it can be combined with a wide range of materials to perform a number of tasks in nanomedicine, sensors, food safety, and other extraterrestrial systems [273]. In this chapter, the focus was on computational analysis and photocatalytic performances in medicines and health, food safety and monitoring, and other multidisciplinary areas.

14. Application of graphitic carbon nitride (g-C₃N₄) in medicine and health

The application of g-C₃N₄ in nanomedicine has been investigated due to its distinct photocatalytic properties and simple enhancing capability. These applications include treatment of cancer cells, drug delivery systems, healing of wounds, artificial enzyme development, bioimaging, and photodynamic therapy (PDT) [27,64,273].

14.1. Application of g-C₃N₄ cancer cells treatment and photodynamic therapy (PDT)

The unique photocatalytic properties of g-C₃N₄ have favored its application in nanomedicine and health-related areas such as disease detection and treatment. In medicine, it is applied in drug delivery because of its small size, covalent bonding which is non-interfering with the drug, low level of toxicity, and excellent optical property [64]. Treatment of cancer involves shrinkage, stoppage of growth, or killing of cancer cells using radiation,

medication, surgery, and therapies [274]. Before the practical applications of g-C₃N₄ in medicine, Density Functional Theory (DFT) computational analyses were carried out. According to Perveen et al. (2020) for the first time, DFT was used to determine the efficiency drug delivery capacity of g-C₃N₄ for the cisplatin [275]. Cisplatin is known for its “cancer-penicillin” ability and has been primarily used as a chemotherapeutic agent against different cancers such as lung, bladder, stomach, head-neck, ovarian, testicular cancers, lymphomas, sarcomas, carcinomas, and pediatric malignancies (i.e., osteogenic sarcoma (OSA)) and medulloblastoma [273,276,277]. Another DFT computational analysis shows that g-C₃N₄ has a chemotherapeutic potential as a drug carrier for carboplatin in the cancer treatment [278]. These theoretical studies have provided insights for further exploration into various empirical studies.

One of the novel approaches or cutting-edge therapeutic strategies for the treatment of tumors in which reactive oxygen species (ROS) damage organelles, tissues, or organs is photodynamic therapy (PDT). This is achieved by a photocatalytic process (i.e., light irradiation of photosensitizers (PS)) that releases reactive cytotoxic oxygen species (ROS) resulting in oxidative stress and hence inhibiting and destroying cancer cells. Therefore, this process of utilizing oxidative stress to suppress the growth of cancerous cells is referred to as the photodynamic therapy [27,64,273]. A thorough study of the literature reveals that g-C₃N₄ has been shown to be quite effective for PDT. An experiment using g-C₃N₄ to mediate cancer

therapy was carried out without the use of any chemotherapeutic medications, and the results suggest that cancer cells were subjected to some degree of induced apoptosis and necrosis [279]. Similarly, PDT has been documented for tumor treatment. g-C₃N₄ up-conversion nanoparticle (UCNP) nanocomposite has been used to significantly shrink or disappear a tumor due to the generation of ROS devoid of any negative effect under the irradiation of UV light [280]. Davardoostmanesh et al. (2020) prepared g-C₃N₄ nanosheets using the electrophoretic particle size

fractionation separation technique, which demonstrated high luminescence performance than prevalent bulk carbon nitride and was effective against bone carcinoma cell line. In the future, this anti-cancer property could be widely used as a superior to the existing for cancer therapy [281]. In summary, the composite of g-C₃N₄ nanoparticles could cause the generation of ROS, apoptosis or necrosis leading to cellular membrane destruction through peroxidation and protein denaturation in some occasions resulting in the death of cancer cells [282,283] as illustrated in Figure. 21.

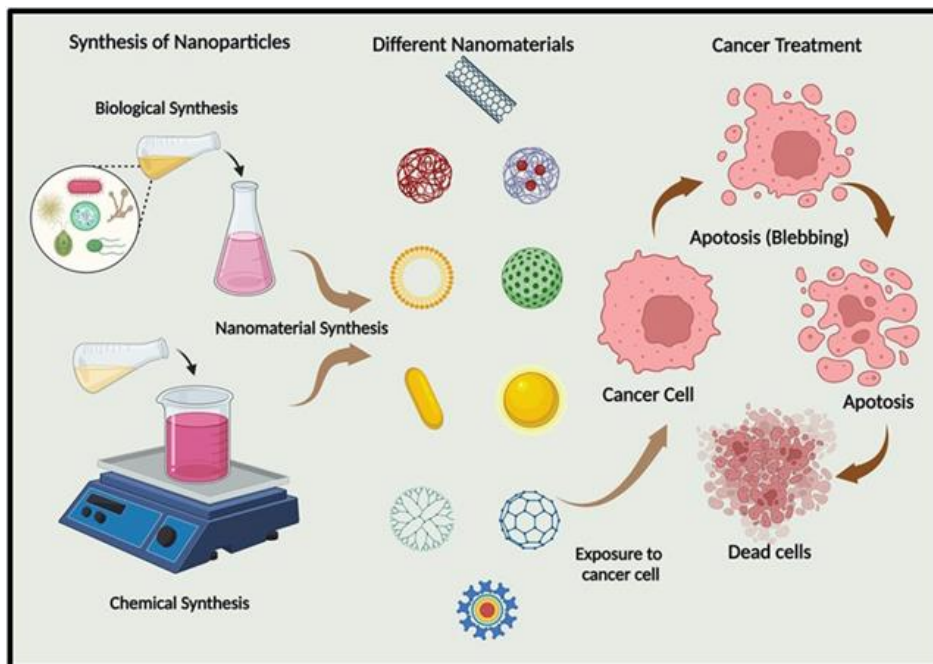


Figure 21: Summary of cancer cells treatment [282]

14.2. Application of g-C₃N₄ in drug delivery systems

Nanocarriers are utilized in the drug delivery system for responsive drug release in nanomedicine and chemotherapy [274]. g-C₃N₄ possesses certain unique features such as small size, non-toxicity, chemical and physical stability, and optical properties alongside its covalent bond favoring drug interaction. According to a study conducted by Dong et al. (2018) on a fluorescent g-C₃N₄ quantum dots (g-CNQDs) synthesized from refluxing of bulk g-C₃N₄ in nitric acid. It was then hydrothermally treated and used as a fluorescent nano-carrier (traceable drug delivery system) for doxorubicin (DOX) without any change but in a pH-responsive environment [284]. HeLa and cos-7 cells were treated with g-C₃N₄ nanoparticles that were smaller than 30 nm and exposed to visible light ($\lambda > 420$ nm). This led to the large production of ROS and the subsequent selective death of malignant cells by PDT [274,285]. Organic nanoparticles synthesized from g-C₃N₄ through the intercalation process of rod-like cyanuric acid-melamine in a mixture of LiCl-KCl (45:55 wt%) were used to destroy cancer cells by reactive oxygen species under irradiation of visible light [285]. In a study conducted by Jiang

et al. (2021) [286] where g-C₃N₄ nanosheets (CNNS) was modified with methoxy polyethylene glycol (mPEG) to obtain nanocomposites (CNNS-mPEG). The CNNSmPEG was treated with doxorubicin hydrochloride (DOX) as a model anti-cancer drug doxorubicin (DOX). Figure 22 shows that the CNNS-mPEG nanocomposites have a promising luminescence carrier for drug delivery when the pH = 5 with a release of CNNS-mPEG up to 44.7%. The time for release was 144 h which was twice that of CNNS. Perveen et al. (2020) used DFT to investigate the drug loading efficacy of graphitic carbon nitride (g-C₃N₄) for an anti-cancer drug, cisplatin, and discovered that g-C₃N₄ could be used as an efficient drug-delivery system for the cisplatin drug to treat various types of cancer. A few other significant features of cisplatin drug, g-C₃N₄ carrier, and g-C₃N₄-cisplatin complex were calculated at both excited and ground states to investigate the effectiveness of g-C₃N₄ as a drug-delivery system. Their research revealed the presence of weak noncovalent interactions. These weak interactions between the cisplatin drug and the g-C₃N₄ carrier play an important role in drug transferring at the target site [275].

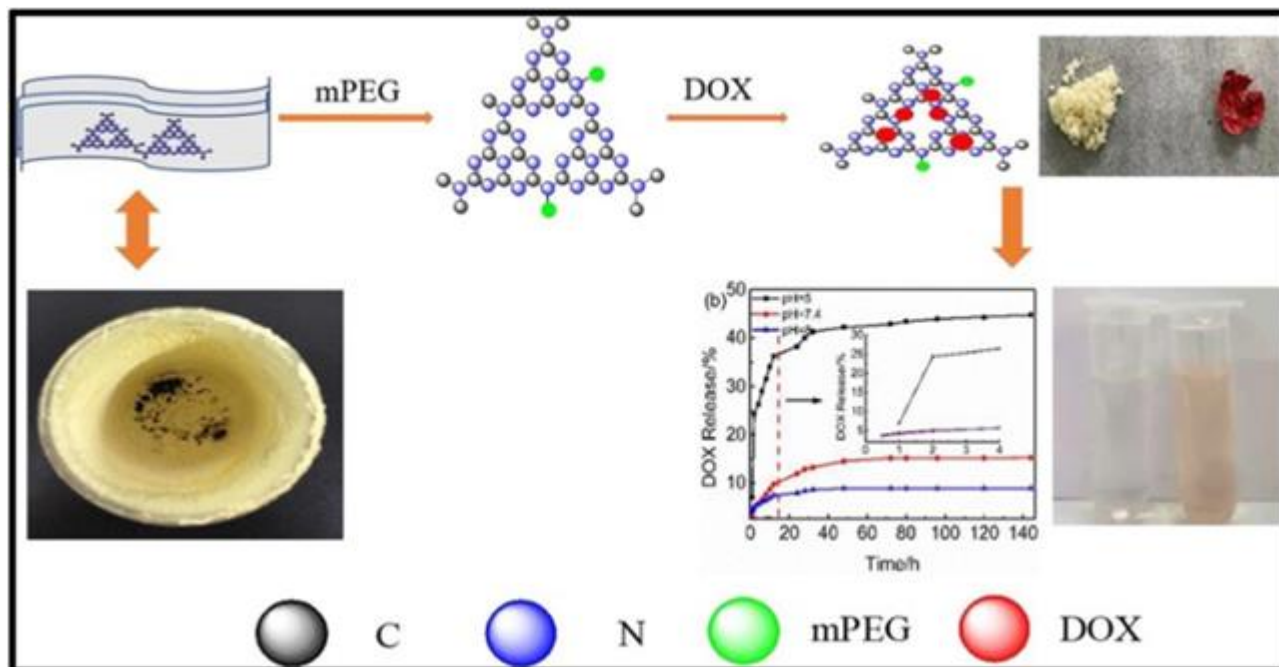


Figure 22: CNNS-mPEG nanocomposites for cancer drug delivery system [286]

14.3. Application of g-C₃N₄ in healing of wounds

Bacterial infections and wounds have posed a hazard to human health. Majority of times, bacteria exist on surfaces of wounds and cause discomfort to the individual. Normally, antibiotics are used in the treatment of wounds. However, with the emerging new trends in medicine, g-C₃N₄ nanocomposites are being applied in bacterial infection treatment including wounds because of resistance bacteria have developed against antibiotics and cell toxicity for prolonged interaction with the bacteria [64,287,288]. The advances in nanotechnology have resulted in the synthesis of g-C₃N₄ nanocomposites for wound treatment and healing. Hybrid composite nanosheets of g-C₃N₄, combined with Zn²⁺ and graphite oxide (GO g-C₃N₄-Zn²⁺@graphene oxide (SCN₂Zn²⁺@GO) was synthesized and its antibacterial property for wound healing and bacteria destruction was evaluated under exposure to two light wavelengths at 660 and 808 nm). The results indicated the synergistic effects of both photodynamic and photothermal produces ROS which causes bacterial destruction very easily and faster and hence increases the wound healing process [288]. Another study also conducted by Xiang et al. (2020) showed that a composite of ZnO/CDots/g-C₃N₄ with Z-scheme heterojunction and mechanism under visible light irradiation destroyed bacteria efficiently within a very short time of 15 min because of improved photocatalytic and photothermal effects. The combined synergistic

production of ROS and hyperthermia promote the release of Zn ions which enhance the growth of fibroblasts and thus hasten the process of wound healing [289]. An accelerated wound healing process was observed in a Z-scheme ZnO/C-dots/g-C₃N₄ ternary heterojunction composite. In this system, the C-dots serve as a bridge which enhance the migration of electrons from the ZnO conduction band to the valence band of g-C₃N₄ by reducing electron-hole pair recombination rate. This result in generation of OH· and ¹O₂ radicals leading to disinfection of 99.97% and 99.8% of *Streptococcus aureus* and *Escherichia coli*, respectively. The Zn²⁺ released intruded into the bacteria and hyperthermia effect exhibited leading to the growth of fibroblasts for a quick wound healing process [290]. Figure 23 shows the wound healing mechanism using the ZnO/C-dots/g-C₃N₄ composite. Li et al. (2017) developed Bi₂MoO₆/g-C₃N₄ heterojunctions using an in situ solvothermal method and g-C₃N₄ nanosheets. By disinfecting bacteria under visible light irradiation, the photocatalytic activities of as-prepared samples were evaluated. According to the findings, the composites' intimate contact of Bi₂MoO₆ and g-C₃N₄ nanosheets facilitates the transfer and separation of photogenerated electron-hole pairs. The heterojunction provides the most effective photocatalytic disinfection of bacteria. The generated h⁺ behaves as the dominant reactive species, potentially rendering bacteria cells inactive during the photocatalytic disinfection process [291].

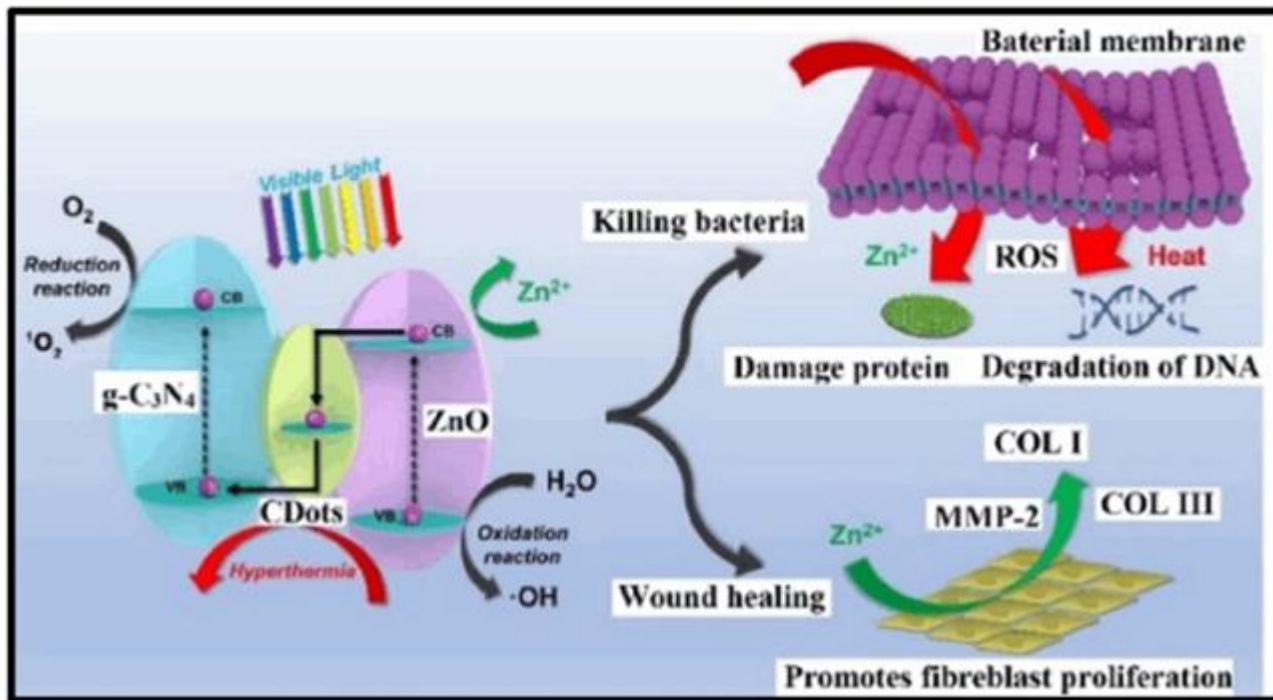


Figure 23: Wound healing mechanism using the ZnO/C-dots/g- C₃N₄ composite [290]

14.4. Application of g-C₃N₄ in artificial enzyme development

An enzyme is one of the essential components a living thing need for healthy and effective biological processes and functioning. Naturally, enzymes have high catalytic abilities and substrate specific to necessarily regulate and maintain the physiological homeostasis of living organisms [64, 274]. However, the development of nanozymes is a result of the high production

costs and instability of protein enzymes. In biomimetic chemistry, nanozymes are synthetic enzymes built from nanomaterials that imitate natural enzymes with protein substrates [64]. Figure 24 shows a brief historical evolution and progress of nanozymes [292]. The trend shows that artificial enzymes and nanozymes development started from 1965 to 1993 respectively.

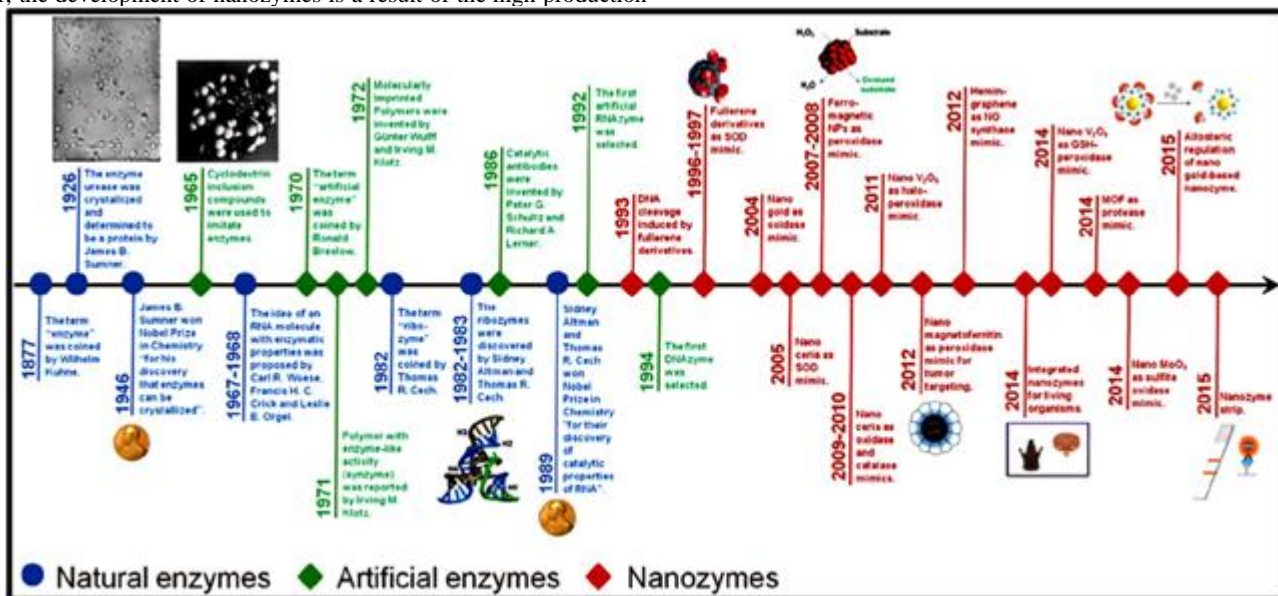


Figure 24: Historical progress of artificial enzyme and nanozymes development [292]

The exploration and applications of these nanozymes are due to their multi functions such as health monitoring and disease diagnosis. A variety of key target molecules, including metal ions, bacteria, bioactive small molecules, nucleic acids, and cancer cells, have been detected using artificial and nanozymes, according to studies. The detection of some of these substances helps in biomedical diagnosis [293-295]. A study conducted using a metal-free nanozyme synthesized from modified graphitic carbon shows its bifunctional roles mimicking enzyme. It was reported that on irradiation with

visible light, H₂O₂ was generated from a photocatalytic process of dioxygen reduction and oxidation of glucose where oxidase mimicking was observed. Furthermore, in the dark, there was peroxidase-mimicking reaction on a chromogenic substrate. This serves the dual functions for peroxidase-oxidase reactions to detect glucose effectively within 30 s. The development of this artificial modified g-C₃N₄ nanozyme has provided an insight into further exploration of mimicking natural enzymes for medical diagnosis [296,297]. In the medical industry, various studies showed that folate-modified

nanozymes have been used as a receptor to over-expressed cancer cells [298,299] as shown in Fig. 25. In the presence of light irradiation, a chitosan stabilized silver halide (AgX) nanoparticles oxidize a substrate (such as TMB) and the nanozyme folate receptor over-expressed MDA-MB-231 cancer cells [292]. With the use of the deposition-precipitation process, Wang et al. reported fabricating Au/g-C₃N₄ Hybrid Nanozyme for Bacteria Killing and Wound Disinfection. To fight bacterial infections, the hybrid AuNPs/g-C₃N₄ nanozyme triggered biologically appropriate amounts of

H₂O₂. Excellent peroxidase activity is provided by these hybrid materials, which greatly increases the efficiency with which H₂O₂ is converted to ·OH radicals. Importantly, the synergistic catalytic properties of this hybrid material allowed for the utilization of biologically appropriate H₂O₂ concentrations in bacterial killing and wound disinfection. DR Gram-positive and DR Gram-negative bacteria, as well as lung infections, were all effectively killed by this substance [300].

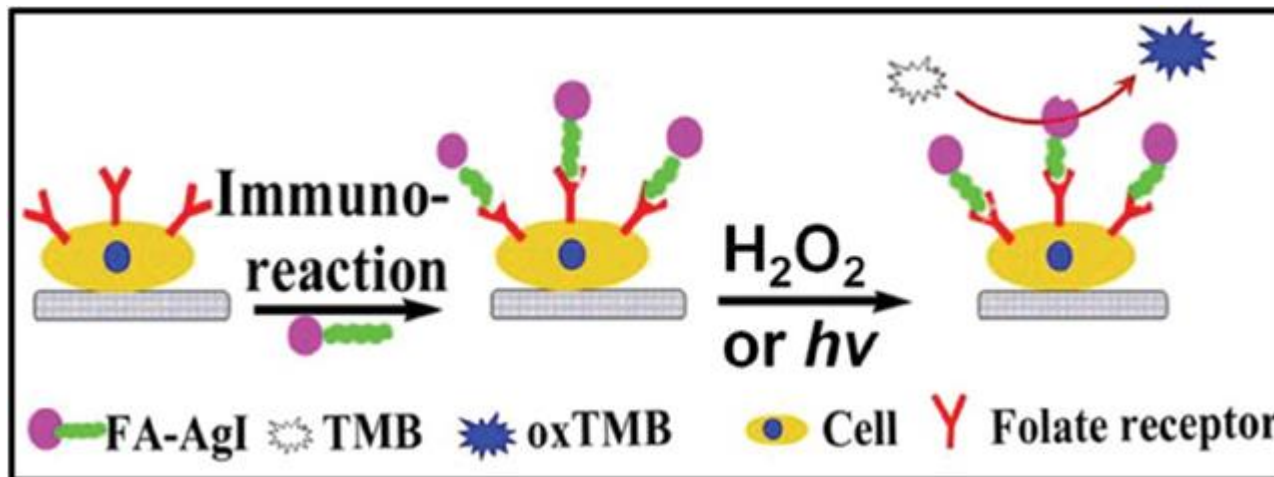


Figure 25: Cancer cell treatment by nanozyme [292]

14.5. Application of g-C₃N₄ in bioimaging

The act of perceiving and observing molecular pathways and physical occurrences in organisms' living cells is called "bioimaging." [274]. With a particle size of less than 10 nm, g-C₃N₄ is known to have considerable quantum confinement and edge effects. These unique properties led to tunable bandgap energy, optical ability, good biocompatibility and allow for different fluorescence emissions (i.e., different wavelengths of blue and green lights). These characteristics enable g-C₃N₄ to replace the use of the conventional graphene quantum dots (GQDs) in recent years [301-304]. The fluorescence ability of g-C₃N₄ enables its usage as an optical marker and hence effective in cell imaging by providing contrasting image [305]. Zhuang et al. (2018) reported the synthesis of g-C₃N₄ quantum dots (g-C₃N₄ QDs) from human urine that possesses a high quantum yield of 15.7% with reference to quinine sulphate. The as-prepared g-C₃N₄ QDs displayed excitation-wavelength dependent fluorescent emission and was successfully function as fluorescent probes for cell multicolor imaging [306]. Another study also reported the fabrication of fluorescent g-C₃N₄ quantum dots (g-C₃N₄ QDs) with an estimated yield of 20.5% through ethanolthermal treatment of bulk g-C₃N₄ in the presence of KOH. A bright blue fluorescence of HeLa cells was observed after treating them with g-C₃N₄ QDs for 5 h excited at 405 nm wavelength. This bright blue luminescence inside the cell shows that g-C₃N₄ QDs is a favorable material for bioimaging [307]. Lu et al. (2015) reported the formation of oxygen and sulfur co-doped graphitic carbon nitride quantum dots (OS-GCNQDs) through thermal treatment of citric acid and thiourea. The as-synthesized OS-GCNQDs have a high quantum yield of 14.5% which shows a bright green fluorescence after treatment with HeLa cells at a wavelength of 488 nm. This indicated that the fluorescence performance of OS-GCNQDs is favorable for probes in bioimaging [308].

In this study, phenyl-modified and sulfur doped g-C₃N₄(PhCNS) was prepared through copolymerization of 2,4-diamino-6-phenyl-1,3,5-triazine and trithiocyanuric acid. The as-prepared PhCNS was investigated by fabrication of green, yellow, and white light-emitting diodes which shows high color quality for multicolor bioimaging [309]. Li et al. (2016) reported the preparation of bright green luminescent g-C₃N₄ quantum dots (GCNQDs) doped with oxygen and sulfur using the Microwave method with the treatment of citric acid and thiourea. The GCNQDs have quantum yield of 31.67% with high fluorescence images of HeLa cells and negligible cytotoxicity. This green luminescent nanomaterial can be utilized as a fluorescent probe for bioimaging. It can be shown that the metal-free g-C₃N₄-based materials with high photoluminescence can be applied in fluorescent bioimaging [310]. Wu et al. (2016) fabricated phosphorus doped g-C₃N₄ QDs (P-g-C₃N₄ QDs) in a tuned visible region of 385–762 nm with a higher quantum yield of more than 0.90. The P-g-C₃N₄ QDs demonstrated effective application for fluorescent bio-imaging (FBI) [311] as shown in Fig. 26. Cai et al. (2021) reported the thermal treatment and alkalia-assisted hydrolysis method for the fabrication of highly cyanfluorescent g-C₃N₄ nanobelts with the PL emission wavelength higher than that of its bulk. Having their long PL emission wavelength, strong PL quantum yield, and wide excitation range, g-C₃N₄ nanobelts provided exceptional optical properties. The quantum confinement effect caused these nanobelts to appear blue-shifted to 494 nm. Because NO₂ gas caused the fluorescence quenching of nanobelts to decrease by almost 50%, compared to less than 4%, less than 25%, and less than 5% for CO₂, NH₃, and SO₂ gasses, this sensor appeared to be more sensitive to NO₂ gas. With regard to bioimaging and sensing applications, this approach might present a fresh direction for the building of carbon-nitrogen nanostructures [312].

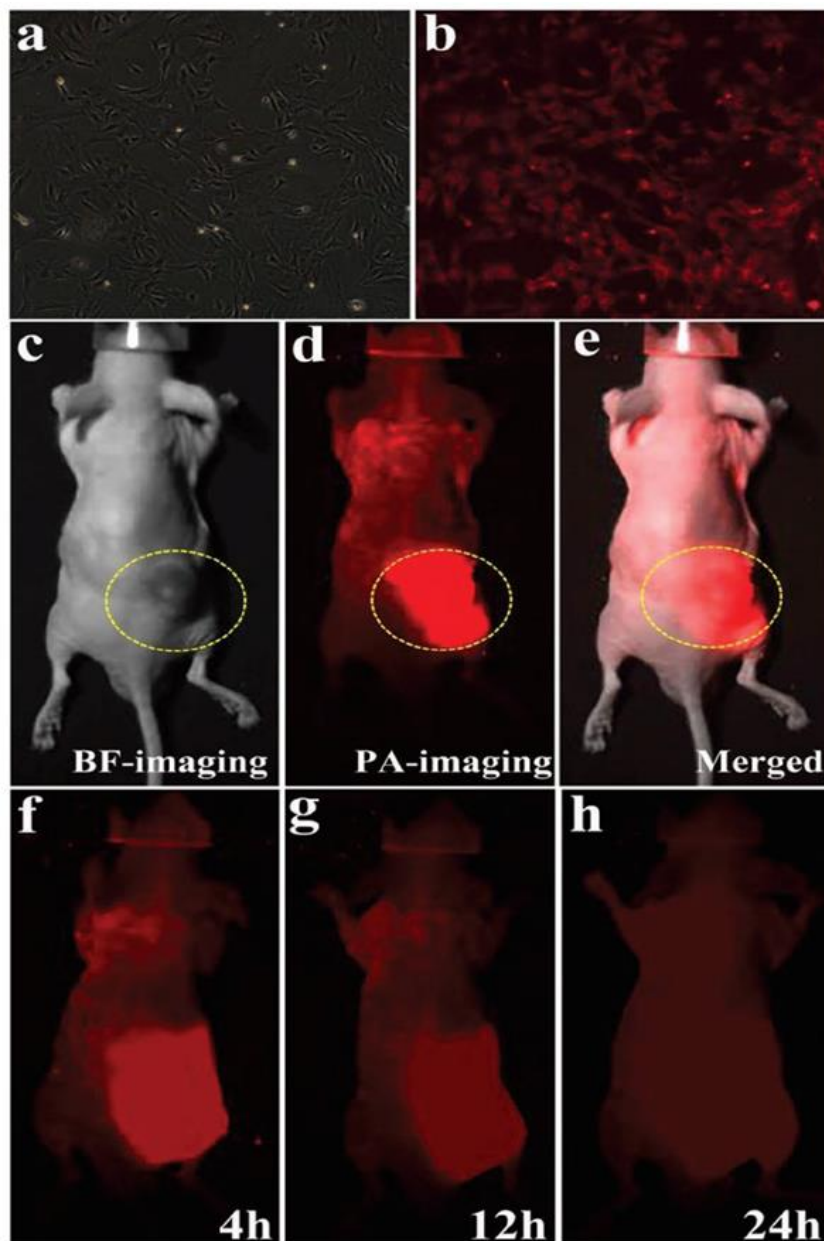


Figure 26: In vitro and in vivo bio-imaging of P-g-C₃N₄ QDs. **a** Brightfield microphotograph and **b** fluorescent microphotograph of OCM-1 cells incubated with P-g-C₃N₄ QDs-3. **c** Bright-field microphotograph of the nude mice tumor. **d** Photoacoustic image of tumor-bearing mice incubated with P-g-C₃N₄ QDs-3. **e** Bright-field and photoacoustic image of tumor-bearing mice incubated with P-g-C₃N₄ QDs-3. Yellow circles highlight the tumor site. Photoacoustic images of mice **f** 4, **g** 12, and **h** 24 h after the intratumoral injection of P-g-C₃N₄ QDs-3 (100 μ L, 0.1 mg mL⁻¹) [311]

15. Application of g-C₃N₄ in other multidisciplinary areas

Currently, g-C₃N₄ is been applied in various multidisciplinary areas such as Mathematical sciences, Computer applications etc. Muhammad et al. (2020) reported the use of g-C₃N₄ as a model material to compute topological indices. Topological indices are vital devices that help to investigate chemical compounds and to comprehend the fundamental topology of chemical structures. The topological indices show the various physical concoction properties and natural exercises that exist for the materials. This is computed mathematically in the graph theory [313]. Similarly, a calculation of topological indices of polycyclic g-C₃N₄ molecular structure was carried out by Chu et al. (2020). The results from the study enable researchers and scientists to have an excellent comprehension of the physical science and bioorganic characteristics of the material. In addition, the topological indices would offer various possibilities for the identification of drug targets for parasitic diseases [314]. Another study was also conducted

to further investigate the previously stated topological coindices of g-C₃N₄ for further synthetic atomic graphs for possible clinical utilization, synthesis, and material design. The results from this study enhance the acquisition of calculation formulae of the coindices of the physico-chemical properties of g-C₃N₄ [315]. The graphical representation of g-C₃N₄ using the M-polynomial and NM-polynomial was also computed in a study conducted by Rauf et al. (2021) to determine the topological indices for the purpose of its pharmaceutical properties as drug [316].

16. Challenges of g-C₃N₄

Challenges such as quantum efficiency and charge carrier recombination are addressed, alongside a forward-looking perspective on emerging trends and innovations. Ultimately, this chapter positions g-C₃N₄ as a sustainable game-changer in the realm of environmental and energy technologies, offering a promising path towards a more sustainable future.

Graphitic carbon nitride ($g\text{-C}_3\text{N}_4$) undoubtedly exhibits exceptional photocatalytic capabilities, yet several challenges warrant attention as we aim to harness its full potential. Foremost among these challenges is the need to enhance its quantum efficiency—the efficiency with which it utilizes incoming photons. Researchers are actively working to minimize electron–hole pair recombination rates and boost the overall photocatalytic conversion efficiency. Additionally, ensuring photostability over extended usage periods is critical. Factors such as photo-corrosion and aggregation can impact $g\text{-C}_3\text{N}_4$'s performance, necessitating the development of stable $g\text{-C}_3\text{N}_4$ materials and protective coatings. Achieving high selectivity in complex reaction mixtures remains a formidable challenge, even though $g\text{-C}_3\text{N}_4$ exhibits remarkable selectivity in many reactions. Fine-tuning the material's surface properties and optimizing reaction conditions continue to be areas of investigation. Finally, scaling up $g\text{-C}_3\text{N}_4$ production from laboratory-scale to practical, large-scale applications presents logistical challenges, requiring cost-effective manufacturing methods and seamless integration into the existing infrastructure.

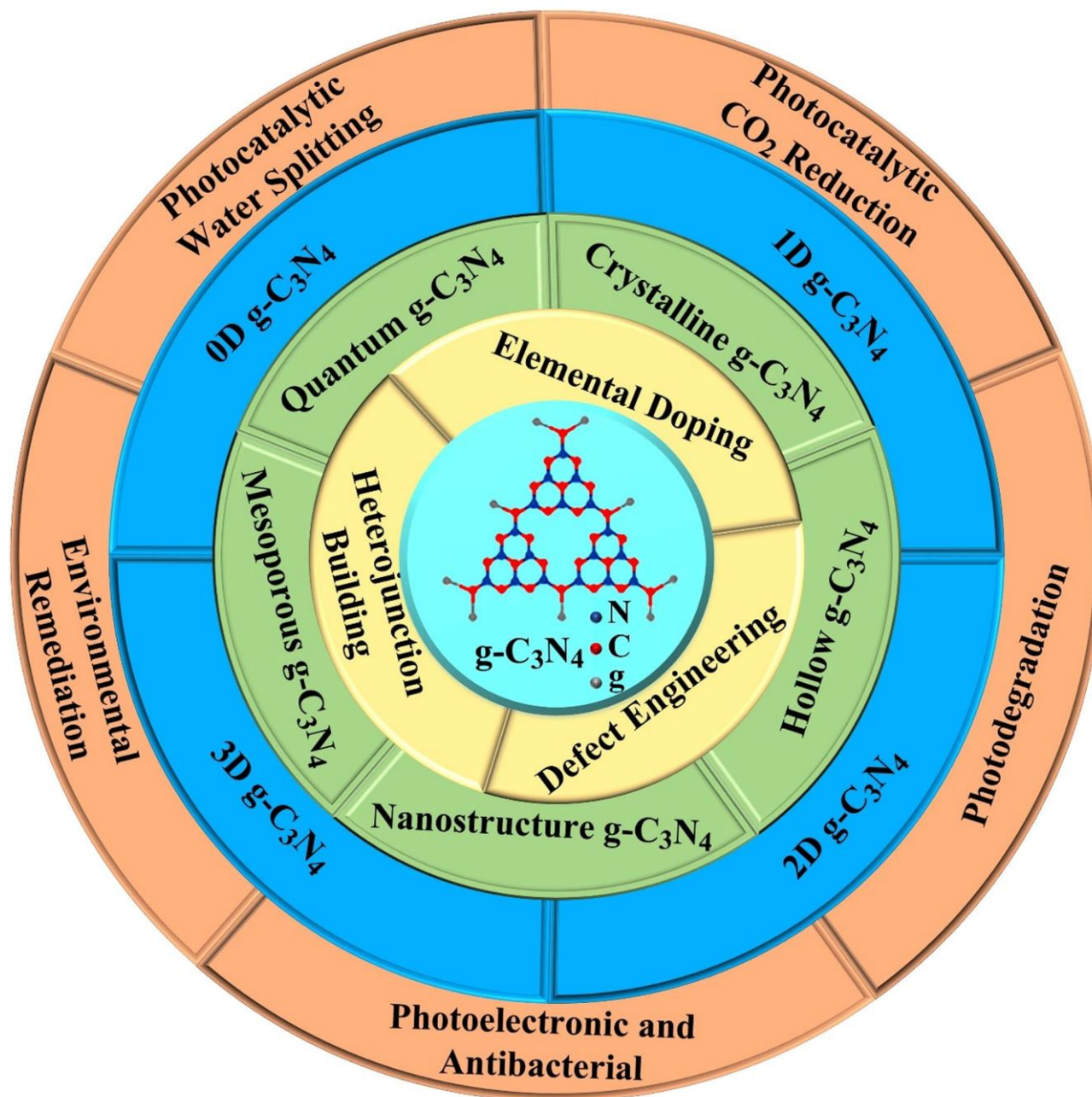
17. Conclusions and Future Perspectives

The $g\text{-C}_3\text{N}_4$ nanomaterials with their varying porosity and dimensionality and their incorporation in multi-functional nanocomposites, have brought about the significant enhancement in biosensing for biomedical applications and cancer therapeutics. Over the past three decades, graphitic carbon nitride has been studied and employed as one of the semiconductor materials with ongoing application in new disciplines. At the same time, the main difficulty still being experienced is the lack of multidisciplinary actions, and the use of sacrificial reagents to improve the photoreactor design persists. This chapter highlights and discussed the current application trends of $g\text{-C}_3\text{N}_4$ in various fields such as biosensors, medicine, bioimaging and other potential multidisciplinary areas. As mentioned above, the research fields of $g\text{-C}_3\text{N}_4$ have substantially grown over the years with a scientometric assessment indicating the applications of $g\text{-C}_3\text{N}_4$ based materials from photoelectrochemical studies etc. to other multidisciplinary areas showing the versatility of the $g\text{-C}_3\text{N}_4$. The early diagnosis of diseases is the best way to improve the treatment prognosis and decrease the side effects of illnesses. Biosensors based on nanomaterials are efficient for this approach due to the high and rapid sensitivity in diagnosing the target molecules that arises from the specific properties of nanomaterials. In recent years, the nanosheets of $g\text{-C}_3\text{N}_4$ and their derivatives have attracted a lot of interest owed to their outstanding optical properties (high photoluminescence yield), high surface area, electrical conductivity, antimicrobial activity, and good thermal and chemical stability. Several simple and high-yield methods have been used to synthesize $g\text{-C}_3\text{N}_4$ -based materials, such as the pyrolysis of low-cost materials, including melamine and urea. C_3N_4 -based materials have also been used in various biosensors (SPR, EC, PCL), which demonstrates that they are promising candidates in this field. Moreover, $g\text{-C}_3\text{N}_4$ -based biosensors show high and rapid sensitivity for detecting diseases, such as cancer; other targets in biological samples; or even the detection of pollutants. Thus, $g\text{-C}_3\text{N}_4$ is a new carbon-based 2D nanomaterial for biosensing, and it is expected that in the near future, $g\text{-C}_3\text{N}_4$ -based biosensors will be improved in order to be more sensitive in diagnosis and

functionalized in order to have more selectivity to attach the receptors. We anticipate that further research will be conducted on addressing the intrinsic shortcomings attributed to $g\text{-C}_3\text{N}_4$, including poor specific surface area, limited light absorption range, and poor dispersibility in organic and aqueous media.

The chapter discussed the history of $g\text{-C}_3\text{N}_4$ beginning with the discovery of "melon." It also focuses on current multifunctional applications of $g\text{-C}_3\text{N}_4$ in medicine and health (such as cancer cell treatment, drug delivery systems, wound healing, bioimaging, and artificial enzyme development), food safety, and other potential multidisciplinary areas. The applications in the medical and health industries are based on mechanisms of nanometric particle and human body cell interaction, which results in cell destruction as well as imaging due to the excellent optical property. Furthermore, the sensing properties of $g\text{-C}_3\text{N}_4$ -based materials enabled their use in nanotechnology for food safety and quality detection. Computational analysis in Mathematical and Computer Sciences using $g\text{-C}_3\text{N}_4$ -based nanomaterials reveals topological indices, which are important parameters in studying the chemical nature and structure of compounds. Despite the fact that this application is still in the theoretical stage, there is a lot of potential and exploration for its practical application. It is clear that $g\text{-C}_3\text{N}_4$ -based materials have been used in a variety of disciplines. Future applications of $g\text{-C}_3\text{N}_4$ -based materials must involve a wide range of stakeholders, as a shift to multidisciplinary fields is the only way forward. Chemical materials professionals and researchers must engage in more in-depth interdisciplinary exchanges and explore $g\text{-C}_3\text{N}_4$ applications.

In conclusion, this chapter has covered various aspects of $g\text{-C}_3\text{N}_4$ based nanocomposites in biosensors, including their structural properties, scientometric assessment, modifications, synthesis, and characterization methods, their medicine, health and biomedical application in cancer cells and drug delivery. Through the incorporation of dopants, metal deposition, metal chalcogenide semiconductors, and carbon materials, these nanocomposites have exhibited remarkable photocatalytic capabilities with potential for real-world environmental remediation and energy production. The synthesis and characterization techniques discussed in this article have provided valuable insights into enhancing the performance and stability of $g\text{-C}_3\text{N}_4$ -based composites. The introduction of dopants and metal deposition, as well as metal chalcogenide semiconductors have enabled the modification of the band structure and surface properties, thereby improving the separation and transfer of photogenerated charge carriers. The incorporation of carbon materials, such as graphene or carbon nanotubes, has contributed to the enhancement of photocatalytic activity by increasing the surface area and facilitating electron transfer. The investigation of factors affecting the photocatalytic process has deepened our understanding of the mechanisms involved and has highlighted the important working factors such as catalyst dose, pH, and light intensity. This knowledge can be utilized to optimize the design of $g\text{-C}_3\text{N}_4$ based nanocomposites, tailoring them for specific applications and improving their overall performance and efficiency. The main postulates of $g\text{-C}_3\text{N}_4$ are manifested in the following Scheme 3.



Scheme 3. Scheme exhibiting the applicability of $g\text{-C}_3\text{N}_4$ -based nanomaterials in photocatalysis research and the accompanying methodologies for photocatalytic efficiency improvement [317].

The future prospects for $g\text{-C}_3\text{N}_4$ photocatalysis are exceptionally promising, driven by ongoing research and innovative strategies. The integration of advanced co-catalysts, such as metal nanoparticles or semiconductor materials, holds the potential to significantly enhance charge separation and overall photocatalytic performance. The tailoring of $g\text{-C}_3\text{N}_4$ materials with specific structural and electronic properties optimized for various applications is another exciting avenue of exploration, allowing for custom-designed photocatalysts. These developments pave the way for tailored solutions to environmental and energy challenges. Moreover, the integration of $g\text{-C}_3\text{N}_4$ photocatalysis with solar cell technologies in tandem or integrated systems offers the possibility of continuous and efficient energy conversion. The exploration of $g\text{-C}_3\text{N}_4$'s application in environmental remediation, such as addressing emerging pollutants like pharmaceuticals and microplastics in water and air, remains an area of interest. Additionally, the concept of artificial photosynthesis systems, where $g\text{-C}_3\text{N}_4$ plays a pivotal role in replicating natural photosynthesis for sustainable fuel production and carbon capture, holds immense promise. As the world continues to prioritize

environmental sustainability and clean energy, $g\text{-C}_3\text{N}_4$ remains poised at the forefront of these advancements, representing a cornerstone in the journey toward a greener and more sustainable future.

Looking to the future, there are several exciting perspectives for further development in the field.

(1) The scale-up of synthesis methods and the development of cost-effective production techniques are essential for the practical application of $g\text{-C}_3\text{N}_4$ -based composites. Efforts should also be made to evaluate their long-term stability and recyclability to ensure their viability for laboratory, pilot-plant and large-scale implementation with the involvement of engineering and chemistry disciplines.

(2) In the pursuit of constructing novel $g\text{-C}_3\text{N}_4$ -based photocatalysts, there is a need for template-free and environmentally friendly synthetic approaches that can yield unique structures and exceptional intrinsic properties. However, the current methods of modifying these photocatalysts have

certain limitations. Some of the selected composite materials contain expensive and environmentally detrimental elements. Achieving precise chemical doping of g-C₃N₄ is a difficult task that often results in the introduction of impurities. Furthermore, the available techniques for controlling the structure of g-C₃N₄ are relatively limited and have only minimal effects. Additionally, achieving precise control over the microstructure of these photocatalysts remains a challenging endeavor.

(3) More detailed and specific reporting is needed to elucidate the synergistic effects that occur among the individual materials in complex heterostructures.

(4) While there is a theoretical understanding of the charge transfer and separation pathways, further experimental evidence is necessary to validate these photochemical mechanisms and establish effective photocatalytic systems on a larger scale.

(5) In the realm of photocatalytic degradation, it is crucial to address the simultaneous degradation several pollutants present in real wastewater using g-C₃N₄-based materials. Furthermore, g-C₃N₄-based photocatalysts hold significant potential for bifunctional catalysis, considering their catalytic economy and efficiency.

(6) Furthermore, it is crucial to preserve and enhance the biocompatibility and eco-friendly properties of future g-C₃N₄-based nanomaterials.

(7) To meet the industrial aim of photocatalytic hydrogen production, the solar to hydrogen (STH) efficiency must be at least 10%. Currently, the maximum efficiency attained in laboratory research is 9.2%, while the STH efficiency for g-C₃N₄ is less than 3%, indicating that much more work remains to be done. The most significant job for the g-C₃N₄ photocatalyst is to construct more efficient electron transport systems.

(8) Gaining a comprehensive understanding of the underlying mechanisms driving photocatalytic H₂O₂ production is essential. Researchers should direct their efforts towards meticulously analyzing the various factors influencing this process, such as the adsorption dynamics of O₂, the impact of the catalyst's surface properties on the adsorption and activation of O₂, the intermediate stages involved in H₂O₂ generation, and the role of active species in modulating H₂O₂ production. Despite the challenges mentioned, with continued efforts, g-C₃N₄-based materials still can hold great potential and limitless opportunities for large-scale environmental applications.

References

- Weiyu Zhu, Yanxue Yue, Huihui Wang, Bo Zhang, Rongbo Ho u, Jingting Xiao, Xinshui Huang, Alhadi Ishag, [Yubing Sun](#). Recent advances on energy and environmental application of graphitic carbon nitride (g-C₃N₄)-based photocatalysts: A review. *Journal of Environmental Chemical Engineering* Volume 11, Issue 3, June 2023, 110164
- Wang, X.; Zhou, C.; Shi, R.; Liu, Q.; Waterhouse, G.I.N.; Wu, L.; Tung, C.-H.; Zhang, T. Supramolecular precursor strategy for the synthesis of holey graphitic carbon nitride nanotubes with enhanced photocatalytic hydrogen evolution performance. *Nano Res.* 2019, 12, 2385–2389.
- Zhou, C.; Shi, R.; Shang, L.; Wu, L.-Z.; Tung, C.-H.; Zhang, T. Template-free large-scale synthesis of g-C₃N₄ microtubes for enhanced visible light-driven photocatalytic H₂ production. *Nano Res.* 2018, 11, 3462–3468.
- Yang, P.; Ou, H.; Fang, Y.; Wang, X. A Facile Steam Reforming Strategy to Delaminate Layered Carbon Nitride Semiconductors for Photoredox Catalysis. *Angew. Chem.-Int. Ed.* 2017, 56, 3992–3996.
- Perez-Molina, A.; Pastrana-Martinez, L.M.; Morales-Torres, S.; Maldonado-Hodar, F.J. Photodegradation of cytostatic drugs by g-C₃N₄: Synthesis, properties and performance fitted by selecting the appropriate precursor. *Catal. Today* 2023, 418, 114068.
- Gao, Y.; Zhu, Y.; Lyu, L.; Zeng, Q.; Xing, X.; Hu, C. Electronic Structure Modulation of Graphitic Carbon Nitride by Oxygen Doping for Enhanced Catalytic Degradation of Organic Pollutants through Peroxymonosulfate Activation. *Environ. Sci. Technol.* 2018, 52, 14371–14380.
- Li, X.; Zhang, J.; Huo, Y.; Dai, K.; Li, S.; Chen, S. Two-dimensional sulfur- and chlorine-codoped g-C₃N₄/CdSe-amine heterostructures nanocomposite with effective interfacial charge transfer and mechanism insight. *Appl. Catal. B-Environ.* 2021, 280, 119452.
- Li, G.; Tang, Y.; Fu, T.; Xiang, Y.; Xiong, Z.; Si, Y.; Guo, C.; Jiang, Z. S, N co-doped carbon nanotubes coupled with CoFe nanoparticles as an efficient bifunctional ORR/OER electrocatalyst for rechargeable Zn-air batteries. *Chem. Eng. J.* 2022, 429, 132174.
- [9] Yu, B.; Shi, J.; Tan, S.; Cui, Y.; Zhao, W.; Wu, H.; Luo, Y.; Li, D.; Meng, Q. Efficient (>20%) and Stable All-Inorganic Cesium Lead Triiodide Solar Cell Enabled by Thiocyanate Molten Salts. *Angew. Chem.-Int. Ed.* 2021, 60, 13436–13443.
- S. Vinoth, K.S. Shalini Devi, A. Pandikumar. A comprehensive review on graphitic carbon nitride based electrochemical and biosensors for environmental and healthcare applications. *TrAC Trends in Analytical Chemistry* Volume 140, July 2021, 116274,
- Juan Wang, Zhihong Liu. Recent advances in two-dimensional layered materials for photoelectrochemical sensing. *TrAC Trends in Analytical Chemistry* Volume 133, December 2020, 116089,
- Rui Zou, Xu Teng, Yanjun Lin, Chao Lu. Graphitic carbon nitride-based nanocomposites electrochemiluminescence systems and their applications in biosensors. *TrAC Trends in Analytical Chemistry* Volume 132, November 2020, 116054,
- S. Vinoth, K. Subramani, [Wee-Jun Ong](#), M. Sathish, A. Pandikumar. CoS₂ engulfed ultra-thin S-doped g-C₃N₄ and its enhanced electrochemical performance in hybrid asymmetric supercapacitor. *Journal of Colloid and Interface Science* Volume 584, 15 February 2021, Pages 204–215,
- Jing Zou, Dongpeng Mao, Arramel, Neng Li, Jizhou Jiang. Reliable and selective lead-ion sensor of sulfur-doped graphitic carbon nitride nanoflakes. *Applied Surface Science* Volume 506, 15 March 2020, 144672,
- S. Vinoth ^{a, b}, Wee-Jun Ong ^{c, d}, A. Pandikumar. Sulfur-doped graphitic carbon nitride incorporated bismuth oxychloride/Cobalt based type-II heterojunction as a highly stable material for photoelectrochemical water splitting. *Journal of Colloid and Interface Science* Volume 591, June 2021, Pages 85-95,
- Lijuan Bu, Qingji Xie, Hai Ming. Gold nanoparticles decorated three-dimensional porous graphitic carbon nitrides for sensitive anodic stripping voltammetric analysis of trace arsenic (III). *Journal of Alloys and Compounds* Volume 823, 15 May 2020, 153723,
- Yue Li, Chen Cheng, YuPeng Yang, XuJi Dun, Jianmin Gao, X iao-Juan Jin. A novel electrochemical sensor based on CuO/H-C₃N₄/rGO nanocomposite for efficient electrochemical sensing nitrite. *Journal of Alloys and Compounds* Volume 798, 25 August 2019, Pages 764-772,
- S. Vinoth ^{a, b}, P. Sampathkumar ^b, K. Giribabu ^{a, c}, A. Pandikum ar. Ultrasonically assisted synthesis of barium stannate incorporated graphitic carbon nitride nanocomposite and its analytical performance in electrochemical sensing of 4-nitrophenol. *Ultrasonics Sonochemistry* Volume 62, April 2020, 104855.
- H. M. ul Hassan, et al., Reduce the recombination rate by facile synthesis of MoS₂/g-C₃N₄ heterostructures as a solar light

- responsive catalyst for organic dye degradation, *Diamond Relat. Mater.*, 2023, 140, 110420.
20. F. Qi, et al., A CuS@ g-C₃N₄ heterojunction endows scaffold with synergetic antibacterial effect, *Colloids Surf., B*, 2023, 230, 113512.
 21. S. Mir, et al., Development of Self-Cleaning g-C₃N₄/Zn(OH)₂ Nanocomposite-Coated Mesh for Oil–Water Emulsion Separation, *Ind. Eng. Chem. Res.*, 2023, 62(28), 11096–11108.
 22. C. Chai, Photocatalytic degradation of polyethylene and polystyrene microplastics by a-Fe₂O₃/g-C₃N₄, *Environ. Sci. Pollut. Res.*, 2023, 30, 121702–121712.
 23. H. Qie, et al., High-efficiency control of pesticide and heavy metal combined pollution in paddy soil using biochar/g-C₃N₄ photoresponsive soil remediation agent, *Chem. Eng. J.*, 2023, 452, 139579.
 24. Q. Zhang, et al., Facile construction of CuO/g-C₃N₄ heterojunctions with promoted photocatalytic hydrogen generation behaviors, *Fuel*, 2023, 353, 129224.
 25. Rono, N., Kibet, J.K., Martincigh, B.S., Nyamori, V.O.: A review of the current status of graphitic carbon nitride. *Crit. Rev. Solid State Mater. Sci.* 46, 1–29 (2020).
 26. Reddy, I.N., Reddy, L.V., Jayashree, N., Reddy, C.V., Cho, M., Kim, D., Shim, J.: Vanadium-doped graphitic carbon nitride for multifunctional applications: photoelectrochemical water splitting and antibacterial activities. *Chemosphere* 264, 128593 (2021).
 27. Chan, M.H., Liu, R.S., Hsiao, M.: Graphitic carbon nitridebased nanocomposites and their biological applications: a review. *Nanoscale* 11, 14993–15003 (2019).
 28. Mohanraj, J., Durgalakshmi, D., Saravanan, R.: Water-soluble graphitic carbon nitride for clean environmental applications. *Environ. Pollut.* 269, 116172 (2021).
 29. Vinoth, S., Devi, K.S., Pandikumar, A.: A comprehensive review on graphitic carbon nitride based electrochemical and biosensors for environmental and healthcare applications. *Trends Analyt. Chem.* 140, 116274 (2021).
 30. Dong, Y., Wang, Q., Wu, H., Chen, Y., Lu, C.H., Chi, Y., Yang, H.H.: Graphitic carbon nitride materials: sensing, imaging and therapy. *Small* 12, 5376–5393 (2016).
 31. Srinivas, P.R.; Kramer, B.S.; Srivastava, S. Trends in Biomarker Research for Cancer Detection. *Lancet Oncol.* 2001, 2, 698–704.
 32. Samadi, A.; Pourmadadi, M.; Yazdian, F.; Rashedi, H.; Navaei-Nigjeh, M.; Eufrazio-da-silva, T. Ameliorating Quercetin Constraints in Cancer Therapy with PH-Responsive Agarose-Polyvinylpyrrolidone -Hydroxyapatite Nanocomposite Encapsulated in Double Nanoemulsion. *Int. J. Biol. Macromol.* 2021, 182, 11–25.
 33. [33] Ludwig, J.A.; Weinstein, J.N. Biomarkers in Cancer Staging, Prognosis and Treatment Selection. *Nat. Rev. Cancer* 2005, 5, 845–856.
 34. Azimi, S.; Farahani, A.; Sereshti, H. Plasma-functionalized highly aligned CNT-based biosensor for point of care determination of glucose in human blood plasma. *Electroanalysis* 2020, 32, 394–403.
 35. [35] Bohunicky, B.; Mousa, S.A. Biosensors: The New Wave in Cancer Diagnosis. *Nanotechnol. Sci. Appl.* 2011, 4, 1–10.
 36. Smith, D.S.; Humphrey, P.A.; Catalona, W.J. The Early Detection of Prostate Carcinoma with Prostate Specific Antigen The Washington University Experience. *Cancer* 1997, 80, 1852–1856.
 37. Sugumaran, S.; Jamlos, M.F.; Ahmad, M.N.; Bellan, C.S.; Schreurs, D. Nanostructured Materials with Plasmonic Nanobiosensors for Early Cancer Detection: A Past and Future Prospect. *Biosens. Bioelectron.* 2018, 100, 361–373.
 38. Pourmadadi, M.; Yazdian, F.; Hojjati, S.; Khosravi-Darani, K. Detection of Microorganisms Using Graphene-Based Nanobiosensors. *Food Technol. Biotechnol.* 2021, 59, 496–506.
 39. [39] Holzinger, M.; Le Goff, A.; Cosnier, S. Nanomaterials for Biosensing Applications: A Review. *Front. Chem.* 2014, 2, 63.
 40. Pandey, P.; Datta, M.; Malhotra, B.D. Prospects of Nanomaterials in Biosensors. *Anal. Lett.* 2008, 41, 159–209.
 41. Pourmadadi, M.; Nouralishahi, A.; Shalhaf, M.; Shabani Shayeh, J.; Nouralishahi, A. An electrochemical aptasensor fordetection of Prostate-specific antigen-based oncarbon quantum dots-gold nanoparticles. *Biotechnol. Appl. Biochem.* 2022, 1–9.
 42. Dinani, H.S.; Pourmadadi, M.; Yazdian, F.; Rashedi, H.; Ebrahimi, S.A.S.; Shayeh, J.S.; Ghorbani, M. Fabrication of Au/Fe₃O₄/RGO Based Aptasensor for Measurement of MiRNA-128, a Biomarker for Acute Lymphoblastic Leukemia (ALL). *Eng. Life Sci.* 2022, 22, 519–534.
 43. Pourmadadi, M.; Ahmadi, M.J.; Dinani, H.S.; Ajalli, N.; Dorkoosh, F. Theranostic Applications of Stimulus-Responsive Systems Based on Fe₂O₃. *Pharm. Nanotechnol.* 2022, 10, 90–112.
 44. Golnaz, M.; Javad, S.; Meysam, S.O.; Mehrab, P.; Fatemeh, Y.; Lobat, T. An electrochemical aptasensor for detection of prostatespecific antigen using reduced graphene gold nanocomposite and cu/carbon quantum dots. *Biotechnol. Appl. Biochem.* 2021, 1–10.
 45. Zavareh, H.S.; Pourmadadi, M.; Moradi, A.; Yazdian, F.; Omid, M. Chitosan/Carbon Quantum Dot/Aptamer Complex as a Potential Anticancer Drug Delivery System towards the Release of 5-Fluorouracil. *Int. J. Biol. Macromol.* 2020, 165, 1422–1430.
 46. Pourmadadi, M.; Shayeh, J.S.; Arjmand, S.; Omid, M.; Fatemi, F. An Electrochemical Sandwich Immunosensor of Vascular Endothelial Growth Factor Based on Reduced Graphene Oxide/Gold Nanoparticle Composites. *Microchem. J.* 2020, 159, 105476.
 47. Pourmadadi, M.; Shayeh, J.S.; Omid, M.; Yazdian, F.; Alebouyeh, M.; Tayebi, L. A Glassy Carbon Electrode Modified with Reduced Graphene Oxide and Gold Nanoparticles for Electrochemical Aptasensing of Lipopolysaccharides from Escherichia coli Bacteria. *Microchim. Acta* 2019, 186, 2–9.
 48. Aayanifard, Z.; Alebrahim, T.; Pourmadadi, M.; Yazdian, F.; Dinani, H.S.; Rashedi, H.; Omid, M. Ultra PH-Sensitive Detection of Total and Free Prostate-Specific Antigen Using Electrochemical Aptasensor Based on Reduced Graphene Oxide/Gold Nanoparticles Emphasis on TiO₂/Carbon Quantum Dots as a Redox Probe. *Eng. Life Sci.* 2021, 21, 739–752.
 49. Behboudi, H.; Mehdipour, G.; Safari, N.; Pourmadadi, M.; Saei, A.; Omid, M.; Tayebi, L.; Rahmandoust, M. Carbon Quantum Dots in Nanobiotechnology. In *Nanomaterials for Advanced Biological Applications*; Springer: Berlin/Heidelberg, Germany, 2019; pp. 145–179.
 50. Kazemi, S.; Pourmadadi, M.; Yazdian, F.; Ghadami, A. The Synthesis and Characterization of Targeted Delivery Curcumin Using Chitosan-Magnetite-Reduced Graphene Oxide as Nano-Carrier. *Int. J. Biol. Macromol.* 2021, 186, 554–562.
 51. Malmir, S.; Karbalaei, A.; Pourmadadi, M.; Hamed, J.; Yazdian, F.; Navaee, M. Antibacterial Properties of a Bacterial Cellulose CQD-TiO₂ NanocoZamani, M.; Pourmadadi, M.; Seyyed Ebrahimi, S.A.; Yazdian, F.; Shabani Shayeh, J. A Novel Labeled and Label-Free Dual Electrochemical Detection of Endotoxin Based on Aptamer-Conjugated Magnetic Reduced Graphene Oxide-Gold Nanocomposite. *J. Electroanal. Chem.* 2022, 908, 116116.
 52. Azadmanesh, F.; Pourmadadi, M.; Zavar Reza, J.; Yazdian, F.; Omid, M.; Haghirosadat, B.F. Synthesis of a Novel Nanocomposite Containing Chitosan as a Three-Dimensional

- Printed Wound Dressing Technique: Emphasis on Gene Expression. *Biotechnol. Prog.* 2021, 37, e3132.
54. Heydari Foroushani, P.H.; Rahmani, E.; Alemzadeh, I.; Vossoughi, M.; Pourmadadi, M.; Rahdar, A.; Díez-Pascual, A.M. Curcumin Sustained Release with a Hybrid Chitosan-Silk Fibroin Nanofiber Containing Silver Nanoparticles as a Novel Highly Efficient Antibacterial Wound Dressing. *Nanomaterials* 2022, 12, 3426.
55. Behboodi, H.; Pourmadadi, M.; Omid, M.; Rahmandoust, M.; Siadat, S.O.R.; Shayeh, J.S. Cu-CDs as Dual Optical and Electrochemical Nanosensor for BME Detection. *Surf. Interfaces* 2022, 29, 101710.
56. [56] Tabar, F.S.; Pourmadadi, M.; Rashedi, H.; Yazdian, F. Design of Electrochemical Nanobiosensor in the Diagnosis of Prostate Specific Antigen (PSA) Using Nanostructures. In Proceedings of the 2020 27th National and 5th International Iranian Conference on Biomedical Engineering (ICBME), Tehran, Iran, 26–27 November 2020; pp. 35–40.
57. Abolghasemzade, S.; Pourmadadi, M.; Rashedi, H.; Yazdian, F.; Kianbakht, S.; Navaei-Nigjeh, M. PVA Based Nanofiber Containing CQDs Modified with Silica NPs and Silk Fibroin Accelerates Wound Healing in a Rat Model. *J. Mater. Chem. B* 2021, 9, 658–676.
58. Kalajahi, S.T.; Mofradnia, S.R.; Yazdian, F.; Rasekh, B.; Neshati, J.; Taghavi, L.; Pourmadadi, M.; Haghirosadat, B.F. Inhibition Performances of Graphene Oxide/Silver Nanostructure for the Microbial Corrosion: Molecular Dynamic Simulation Study. *Environ. Sci. Pollut. Res.* 2022, 29, 49884–49897.
59. Dinani, H.S.; Pourmadadi, M.; Rashedi, H.; Yazdian, F. Fabrication of Nanomaterial-Based Biosensor for Measurement of a MicroRNA Involved in Cancer. In Proceedings of the 2020 27th National and 5th International Iranian Conference on Biomedical Engineering (ICBME), Tehran, Iran, 26–27 November 2020; pp. 47–54.
60. Xiong, M.; Rong, Q.; Meng, H.M.; Zhang, X.B. Two-Dimensional Graphitic Carbon Nitride Nanosheets for Biosensing Applications. *Biosens. Bioelectron.* 2017, 89, 212–223.
61. Duan, F.; Zhang, S.; Yang, L.; Zhang, Z.; He, L.; Wang, M. Bifunctional Aptasensor Based on Novel Two-Dimensional Nanocomposite of MoS₂ Quantum Dots and g-C₃N₄ Nanosheets Decorated with Chitosan-Stabilized Au Nanoparticles for Selectively Detecting Prostate Specific Antigen. *Anal. Chim. Acta* 2018, 1036, 121–132.
62. Naderian, N.; Pourmadadi, M.; Rashedi, H.; Yazdian, F. Design of a Novel Nanobiosensor for the Diagnosis of Acute Lymphoid Leukemia (ALL) by Measurement of MiRNA-128. In Proceedings of the 2020 27th National and 5th International Iranian Conference on Biomedical Engineering (ICBME), Tehran, Iran, 26–27 November 2020; pp. 41–46.
63. Sakthivel, A.; Chandrasekaran, A.; Sadasivam, M.; Manickam, P.; Alwarappan, S. Sulphur Doped Graphitic Carbon Nitride as a Dual Biosensing Platform for the Detection of Cancer Biomarker CA15-3. *J. Electrochem. Soc.* 2021, 168, 017507.
64. Ajiboye, T.O.; Kuvarega, A.T.; Onwudiwe, D.C.: Graphitic carbon nitride-based catalysts and their applications: a review. *Nano-Struct.* **24**, 100577 (2020).
65. MuhammadAsim Khan, Sadaf Mutahir, Imrana Shaheen, Yuan Qunhui, Mohamed Bououdina, Muhammad Humayun. Recent advances over the doped g-C₃N₄ in photocatalysis: A review. *Coordination Chemistry Reviews Volume 522*, 1 January 2025, 216227,
66. Ismael, M. A Review on Graphitic Carbon Nitride (g-C₃N₄) Based Nanocomposites: Synthesis, Categories, and Their Application in Photocatalysis. *J. Alloys Compd.* **2020**, 846, 156446.
67. Wang, H.; Qi, C.; He, W.; Wang, M.; Jiang, W.; Yin, H.; Ai, S. A Sensitive Photoelectrochemical Immunoassay of N6-Methyladenosine Based on Dual-Signal Amplification Strategy: Ru Doped in SiO₂ Nanosphere and Carboxylated g-C₃N₄. *Biosens. Bioelectron.* **2018**, 99, 281–288.
68. Feng, L.; He, F.; Liu, B.; Yang, G.; Gai, S.; Yang, P.; Li, C.; Dai, Y.; Lv, R.; Lin, J. G-C₃N₄ Coated Upconversion Nanoparticles for 808 Nm Near-Infrared Light Triggered Phototherapy and Multiple Imaging. *Chem. Mater.* **2016**, 28, 7935–7946.
69. Zhang, X.; Xie, X.; Wang, H.; Zhang, J.; Pan, B.; Xie, Y. Enhanced Photoresponsive Ultrathin Graphitic-Phase C₃N₄ Nanosheets for Bioimaging. *J. Am. Chem. Soc.* **2013**, 135, 18–21.
70. Zhang, M.; Wang, Q.; Xu, Y.; Guo, L.; Lai, Z.; Li, Z. Graphitic Carbon Nitride Quantum Dots as Analytical Probe for Viewing Sialic Acid on the Surface of Cells and Tissues. *Anal. Chim. Acta* **2020**, 1095, 204–211.
71. Chen, L.; Huang, D.; Ren, S.; Dong, T.; Chi, Y.; Chen, G. Preparation of Graphite-like Carbon Nitride Nanoflake Film with Strong Fluorescent and Electrochemiluminescent Activity. *Nanoscale* **2013**, 5, 225–230.
72. Ong, W.J.; Tan, L.L.; Ng, Y.H.; Yong, S.T.; Chai, S.P. Graphitic Carbon Nitride (g-C₃N₄)-Based Photocatalysts for Artificial Photosynthesis and Environmental Remediation: Are We a Step Closer to Achieving Sustainability? *Chem. Rev.* **2016**, 116, 7159–7329.
73. Vasiljević, J.; Jerman, I.; Simončič, B. Graphitic Carbon Nitride as a New Sustainable Photocatalyst for Textile Functionalization. *Polymers* **2021**, 13, 2568.
74. Alwin, E.; Kočí, K.; Wojcieszak, R.; Zieliński, M.; Edelmánová, M.; Pietrowski, M. Influence of High Temperature Synthesis on the Structure of Graphitic Carbon Nitride and Its Hydrogen Generation Ability. *Materials* **2020**, 13, 2756.
75. Thomas, A.; Fischer, A.; Goettmann, F.; Antonietti, M.; Müller, J.O.; Schlögl, R.; Carlsson, J.M. Graphitic Carbon Nitride Materials: Variation of Structure and Morphology and Their Use as Metal-Free Catalysts. *J. Mater. Chem.* **2008**, 18, 4893–4908.
76. Tian, C.; Zhao, H.; Sun, H.; Xiao, K.; Keung Wong, P. Enhanced Adsorption and Photocatalytic Activities of Ultrathin Graphitic Carbon Nitride Nanosheets: Kinetics and Mechanism. *Chem. Eng. J.* **2020**, 381, 122760.
77. Du, X.; Kleitz, F.; Li, X.; Huang, H.; Zhang, X.; Qiao, S.Z. Disulfide-Bridged Organosilica Frameworks: Designed, Synthesis, Redox-Triggered Biodegradation, and Nanobiomedical Applications. *Adv. Funct. Mater.* **2018**, 28, 1707325.
78. Dante, R.C.; Trakulmututa, J.; Meejoo-Smith, S.; Sirisit, N.; Martín-Ramos, P.; Chamorro-Posada, P.; Rutto, D.; Dante, D.G. A Solid-State Glucose Sensor Based on Cu and Fe-Doped Carbon Nitride. *Mater. Chem. Phys.* **2021**, 258, 124023.
79. Ma, T.Y.; Tang, Y.; Dai, S.; Qiao, S.Z. Proton-Functionalized Two-Dimensional Graphitic Carbon Nitride Nanosheet: An Excellent Metal-/Label-Free Biosensing Platform. *Small* **2014**, 10, 2382–2389.
80. Dhavalkumar Bhandari, Pratikumar Lakhani, Chetan K. Modi. Graphitic carbon nitride (g-C₃N₄) as an emerging photocatalyst for sustainable environmental applications: a comprehensive review. *RSC Sustainability Volume 2*, Issue 2, 7 February 2024, Pages 265-287,
81. L. Tan, et al., Novel two-dimensional crystalline carbon nitrides beyond g-C₃N₄: structure and applications, *J. Mater. Chem. A*, 2021, 9, 17–33.

82. S. Kumar, S. Karthikeyan and A. F. Lee, g-C₃N₄-based nanomaterials for visible light-driven photocatalysis, *Catalysts*, 2018, 8, 74.
83. A. Dandia, et al., Structure couture and appraisal of catalytic activity of carbon nitride (g-C₃N₄) based materials towards sustainability, *Curr. Res. Green Sustainable Chem.*, 2020, 3,100039.
84. N. S. N. Hasnan, M. A. Mohamed and Z. A. Mohd Hir, Surface Physicochemistry Modification and Structural Nanoarchitectures o g-C₃N₄ for Wastewater Remediation and Solar Fuel Generation, *Adv. Mater. Technol.*, 2022, 7, 2100993.
85. M. Ismael and Y. Wu, A mini-review on the synthesis and structural modification of g-C₃N₄-based materials, and their applications in solar energy conversion and environmental remediation, *Sustainable Energy Fuels*, 2019, 3, 2907–2925.
86. X. L. Song, L. Chen, L. J. Gao, J. T. Ren and Z. Y. Yuan, Engineering g-C₃N₄ based materials for advanced photocatalysis: recent advances, *Green Energy Environ.*, 2022, DOI: 10.1016/j.gee.2022.12.005.
87. H. B. Fang, Y. Luo, Y. Z. Zheng, W. Ma and X. Tao, Facile Large-Scale Synthesis of Urea-Derived Porous Graphitic Carbon Nitride with Extraordinary Visible-Light Spectrum Photodegradation, *Ind. Eng. Chem. Res.*, 2016, 55, 4506–4514.
88. A. Kharlamov, M. Bondarenko, G. Kharlamova and N. Gubareni, Features of the synthesis of carbon nitride oxide (g-C₃N₄)O at urea pyrolysis, *Diamond Relat. Mater.*, 2016, 66, 16–22.
89. A. Hayat, et al., Graphitic carbon nitride (g-C₃N₄)-based semiconductor as a beneficial candidate in photocatalysis diversity, *Int. J. Hydrogen Energy*, 2022, 47, 5142–5191.
90. B. Yuan, et al., Physical vapor deposition of graphitic carbon nitride (g-C₃N₄) films on biomass substrate: optoelectronic performance evaluation and life cycle assessment, *Adv. Compos. Hybrid Mater.*, 2022, 5, 813–822.
91. M. I. Chebanenko, et al., Chemical and structural changes of g-C₃N₄ through oxidative physical vapor deposition, *Appl. Surf. Sci.*, 2022, 600, 154079.
92. E. B. Chubenko, N. G. Kovalchuk, I. V. Komissarov and V. E. Borisenko, Chemical Vapor Deposition of 2D Crystallized g-C₃N₄ Layered Films, *J. Phys. Chem. C*, 2022, 126, 4710–4714.
93. R. M. Yadav, et al., Facile synthesis of highly fluorescent free-standing films comprising graphitic carbon nitride (g-C₃N₄) nanolayers, *New J. Chem.*, 2020, 44, 2644–2651.
94. A. Raza, H. Shen, A. A. Haidry and S. Cui, Hydrothermal synthesis of Fe₃O₄/TiO₂/g-C₃N₄: advanced photocatalytic application, *Appl. Surf. Sci.*, 2019, 488, 887–895.
95. A. R. Kuldeep, R. S. Dhabbe and K. M. Garadkar, Development of g-C₃N₄-TiO₂ visible active hybrid photocatalyst for the photodegradation of methyl orange, *Res. Chem. Intermed.*, 2021, 47, 5155–5174.
96. F. Idrees, R. Dillert, D. Bahnemann, F. K. Butt and M. Tahir, In-situ synthesis of Nb₂O₅/g-C₃N₄ heterostructures as highly efficient photocatalysts for molecular h₂ evolution under solar illumination, *Catalysts*, 2019, 9, 169.
97. L. Kunhikrishnan, K. Vishal and S. Palaniyappan, Mechanical and Thermal Characterization on Synthesized Silane-Treated Graphitic Carbon Nitride (g-C₃N₄) Reinforced 3D Printed Poly (Lactic Acid) Composite, *J. Inorg. Organomet. Polym. Mater.*, 2023, 33, 1234–1245.
98. S. Wu, et al., A simple synthesis route of sodium-doped g-C₃N₄ nanotubes with enhanced photocatalytic performance, *J. Photochem. Photobiol., A*, 2021, 406, 112999.
99. J. Xi, et al., Preparation of high porosity biochar materials by template method: a review, *Environ. Sci. Pollut. Res.*, 2020, 27, 20675–20684.
100. [100] K. Li, et al., Template-Assisted Surface Hydrophilicity of Graphitic Carbon Nitride for Enhanced Photocatalytic H₂ Evolution, *ACS Appl. Energy Mater.*, 2021, 4, 12965–12973.
101. [101] F. T. Li, et al., Precipitation synthesis of mesoporous photoactive Al₂O₃ for constructing g-C₃N₄-based heterojunctions with enhanced photocatalytic activity, *Ind. Eng. Chem. Res.*, 2014, 53, 19540–19549.
102. M. Hao, et al., In-situ hard template synthesis of mesoporous carbon/graphite carbon nitride (C/CN-T-x) composites with high photocatalytic activities under visible light irradiation, *Solid State Sci.*, 2020, 109, 106428.
103. J. Liu, et al., Controlled synthesis of ordered mesoporous g-C₃N₄ with a confined space effect on its photocatalytic activity, *Mater. Sci. Semicond. Process.*, 2016, 46, 59–68.
104. C. T. Yang, et al., A novel heterojunction photocatalyst, Bi₂SiO₅/g-C₃N₄: synthesis, characterization, photocatalytic activity, and mechanism, *RSC Adv.*, 2016, 6, 40664–40675.
105. T. S. Bui, P. Bansal, B. K. Lee, T. Mahvelati-Shamsabadi and T. Soltani, Facile fabrication of novel Ba-doped g-C₃N₄ photocatalyst with remarkably enhanced photocatalytic activity towards tetracycline elimination under visiblelight irradiation, *Appl. Surf. Sci.*, 2020, 506, 144184.
106. H. Starukh and P. Praus, Doping of graphitic carbon nitride with non-metal elements and its applications in photocatalysis, *Catalysts*, 2020, 10, 1–38.
107. M. A. Qamar, M. Javed, S. Shahid and M. Sher, Fabrication of g-C₃N₄/transition metal (Fe, Co, Ni, Mn and Cr)-doped ZnO ternary composites: excellent visible light active photocatalysts for the degradation of organic pollutants from wastewater, *Mater. Res. Bull.*, 2022, 147, 111630.
108. Jiang, Y. Li, D. Wang, X. Hong and B. Liang, Recent Advances in Heteroatom Doped Graphitic Carbon Nitride (g-C₃N₄) and g-C₃N₄/Metal Oxide Composite Photocatalysts, *Curr. Org. Chem.*, 2020, 24, 673–693.
109. Chen, X.; Wang, H.; Meng, R.; Chen, M. Porous Graphitic Carbon Nitride Synthesized via Using Carbon Nanotube as a Novel Recyclable Hard Template for Efficient Visible Light Photocatalytic Organic Pollutant Degradation. *Chemistryselect* 2019, 4, 6123–6129.
110. Fukasawa, Y.; Takanabe, K.; Shimojima, A.; Antonietti, M.; Domen, K.; Okubo, T. Synthesis of Ordered Porous Graphitic-C₃N₄ and Regularly Arranged Ta₃N₅ Nanoparticles by Using Self-Assembled Silica Nanospheres as a Primary Template. *Chem. Asian J.* 2011, 6, 103–109.
111. Ismael, M.: A review on graphitic carbon nitride (g-C₃N₄) based nanocomposites: synthesis, categories, and their application in photocatalysis. *J. Alloys Compd.* 846, 156446 (2020).
112. Akple, M.S., Chimmikuttanda, S.P., Takyi, G.K.S., Elloh, V.W.: Fabrication and density functional theory calculations of bromine doped carbon nitride nanosheets with enhanced photocatalytic reduction of CO₂ into solar fuels. *Biointerface Res. Appl. Chem.* 11, 14602–14619 (2021).
113. Zheng, Y.; Lin, L.; Wang, B.; Wang, X. Graphitic Carbon Nitride Polymers toward Sustainable Photoredox Catalysis. *Angew. Chem.-Int. Ed.* 2015, 54, 12868–12884.
114. Liao, G.; He, F.; Li, Q.; Zhong, L.; Zhao, R.; Che, H.; Gao, H.; Fang, B. Emerging Graphitic Carbon Nitride-Based Materials for Biomedical Applications. *Prog. Mater. Sci.* 2020, 112, 100666.
115. Wang, A.J.; Li, H.; Huang, H.; Qian, Z.S.; Feng, J.J. Fluorescent Graphene-like Carbon Nitrides: Synthesis, Properties and Applications. *J. Mater. Chem. C* 2016, 4, 8146–8160.
116. Reddy, K.R.; Reddy, C.V.; Nadagouda, M.N.; Shetti, N.P.; Jaesool, S.; Aminabhavi, T.M. Polymeric Graphitic Carbon Nitride (g-C₃N₄)-Based Semiconducting Nanostructured

- Materials: Synthesis Methods, Properties and Photocatalytic Applications. *J. Environ. Manag.* 2019, 238, 25–40.
117. Yu, H.; Shi, R.; Zhao, Y.; Waterhouse, G.I.N.; Wu, L.Z.; Tung, C.H.; Zhang, T. Smart Utilization of Carbon Dots in Semiconductor Photocatalysis. *Adv. Mater.* 2016, 28, 9454–9477.
118. Hatamie, A.; Marahel, F.; Sharifat, A. Green Synthesis of Graphitic Carbon Nitride Nanosheet (g-C₃N₄) and Using It as a Label-Free Fluorosensor for Detection of Metronidazole via Quenching of the Fluorescence. *Talanta* 2018, 176, 518–525.
119. Wang, L.; Wang, C.; Hu, X.; Xue, H.; Pang, H. Metal/Graphitic Carbon Nitride Composites: Synthesis, Structures, and Applications. *Chem.-Asian J.* 2016, 11, 3305–3328.
120. Vinoth, S.; Ramaraj, R.; Pandikumar, A. Facile Synthesis of Calcium Stannate Incorporated Graphitic Carbon Nitride Nanohybrid Materials: A Sensitive Electrochemical Sensor for Determining Dopamine. *Mater. Chem. Phys.* 2020, 245, 122743.
121. Imran, H.; Manikandan, P.N.; Dharuman, V. Highly Selective and Rapid Non-Enzymatic Glucose Sensing at Ultrathin Layered Nb Doped C₃N₄ for Extended Linearity Range. *Microchem. J.* 2021, 160, 105774.
122. Vinoth, S.; Sampathkumar, P.; Giribabu, K.; Pandikumar, A. Ultrasonically Assisted Synthesis of Barium Stannate Incorporated Graphitic Carbon Nitride Nanocomposite and Its Analytical Performance in Electrochemical Sensing of 4-Nitrophenol. *Ultrason. Sonochem.* 2020, 62, 104855.
123. Lewandowski, C.M. Surface Plasmon Resonance (SPR) Biosensor Development. *Eff. Br. Mindfulness Interv. Acute Pain Exp. Exam. Individ. Differ.* 2015, 1, 43–48.
124. Nie, W.; Wang, Q.; Zou, L.; Zheng, Y.; Liu, X.; Yang, X.; Wang, K. Low-Fouling Surface Plasmon Resonance Sensor for Highly Sensitive Detection of MicroRNA in a Complex Matrix Based on the DNA Tetrahedron. *Anal. Chem.* 2018, 90, 12584–12591.
125. Ho, A.H.P.; Kim, D.; Somekh, M.G. *Handbook of Photonics for Biomedical Engineering*; Springer: Berlin/Heidelberg, Germany, 2017; pp. 1–947.
126. Yao, Y.; Yi, B.; Xiao, J.; Li, Z.H. Surface Plasmon Resonance Biosensors and Its Application. In *Proceedings of the 2007 1st International Conference on Bioinformatics and Biomedical Engineering*, Wuhan, China, 6–8 July 2007; pp. 1043–1046.
127. Maurya, J.B.; Prajapati, Y.K. A Comparative Study of Different Metal and Prism in the Surface Plasmon Resonance Biosensor Having MoS₂-Graphene. *Opt. Quantum Electron.* 2016, 48, 1–12.
128. Miyazaki, C.M.; Shimizu, F.M.; Ferreira, M. *Surface Plasmon Resonance (SPR) for Sensors and Biosensors*; Elsevier Inc.: Amsterdam, The Netherlands, 2017; ISBN 9780323497794.
129. Lin, C.; Chen, S. Design of High-Performance Au-Ag-Dielectric-Graphene Based Surface Plasmon Resonance Biosensors Using Genetic Algorithm. *J. Appl. Phys.* 2019, 125, 113101.
130. Homola, J. Surface Plasmon Resonance Sensors for Detection of Chemical and Biological Species. *Chem. Rev.* 2008, 108, 462–493.
131. Boozer, C.; Kim, G.; Cong, S.; Guan, H.W.; Londergan, T. Looking towards Label-Free Biomolecular Interaction Analysis in a High-Throughput Format: A Review of New Surface Plasmon Resonance Technologies. *Curr. Opin. Biotechnol.* 2006, 17, 400–405.
132. Gao, Y.; Liu, M.; Zhang, Y.; Liu, Z.; Yang, Y.; Zhao, L. Recent Development on Narrow Bandgap Conjugated Polymers for Polymer Solar Cells. *Polymers* 2017, 9, 39.
133. Topkaya, S.N.; Azimzadeh, M.; Ozsoz, M. Electrochemical Biosensors for Cancer Biomarkers Detection: Recent Advances and Challenges. *Electroanalysis* 2016, 28, 1402–1419.
134. Taniselass, S.; Arshad, M.K.M.; Gopinath, S.C.B. Graphene-Based Electrochemical Biosensors for Monitoring Noncommunicable Disease Biomarkers. *Biosens. Bioelectron.* 2019, 130, 276–292.
135. Gan, T.; Shi, Z.; Sun, J.; Liu, Y. Simple and Novel Electrochemical Sensor for the Determination of Tetracycline Based on Iron/Zinc Cations-Exchanged Montmorillonite Catalyst. *Talanta* 2014, 121, 187–193.
136. Cho, I.H.; Kim, D.H.; Park, S. Electrochemical Biosensors: Perspective on Functional Nanomaterials for on-Site Analysis. *Biomater. Res.* 2020, 24, 1–12.
137. [137] Li, Y.P.; Cao, H.B.; Liu, C.M.; Zhang, Y. Electrochemical Reduction of Nitrobenzene at Carbon Nanotube Electrode. *J. Hazard. Mater.* 2007, 148, 158–163.
138. Patnaik, S.; Martha, S.; Acharya, S.; Parida, K.M. An Overview of the Modification of G-C₃N₄ with High Carbon Containing Materials for Photocatalytic Applications. *Inorg. Chem. Front.* 2016, 3, 336–347.
139. Fang, T.; Yang, X.; Zhang, L.; Gong, J. Ultrasensitive Photoelectrochemical Determination of Chromium (VI) in Water Samples by Ion-Imprinted/Formate Anion-Incorporated Graphitic Carbon Nitride Nanostructured Hybrid. *J. Hazard. Mater.* 2016, 312, 106–113.
140. Wang, X.; Maeda, K.; Thomas, A.; Takanebe, K.; Xin, G.; Carlsson, J.M.; Domen, K.; Antonietti, M. A Metal-Free Polymeric Photocatalyst for Hydrogen Production from Water under Visible Light. *Nat. Mater.* 2009, 8, 76–80.
141. Zhao, Q.; Wu, W.; Wei, X.; Jiang, S.; Zhou, T.; Li, Q.; Lu, Q. Graphitic Carbon Nitride as Electrode Sensing Material for Tetrabromobisphenol-A Determination. *Sens. Actuators B Chem.* 2017, 248, 673–681.
142. Kathiresan, V.; Rajarathinam, T.; Lee, S.; Kim, S.; Lee, J.; Thirumalai, D.; Chang, S.C. Cost-Effective Electrochemical Activation of Graphitic Carbon Nitride on the Glassy Carbon Electrode Surface for Selective Determination of Serotonin. *Sensors* 2020, 20, 6083.
143. hen, J.; Liu, Y.; Zhao, G.C. A Novel Photoelectrochemical Biosensor for Tyrosinase and Thrombin Detection. *Sensors* 2016, 16, 135.
144. Devadoss, A.; Sudhagar, P.; Terashima, C.; Nakata, K.; Fujishima, A. Photoelectrochemical Biosensors: New Insights into Promising Photoelectrodes and Signal Amplification Strategies. *J. Photochem. Photobiol. C Photochem. Rev.* 2015, 24, 43–63.
145. Abolhasan, R.; Mehdizadeh, A.; Rashidi, M.R.; Aghebati-Maleki, L.; Yousefi, M. Application of Hairpin DNA-Based Biosensors with Various Signal Amplification Strategies in Clinical Diagnosis. *Biosens. Bioelectron.* 2019, 129, 164–174.
146. Forster, R.J.; Bertonecello, P.; Keyes, T.E. Electrogenenerated Chemiluminescence. *Annu. Rev. Anal. Chem.* 2009, 2, 359–385.
147. Zhao, W.W.; Xu, J.J.; Chen, H.Y. Photoelectrochemical Immunoassays. *Anal. Chem.* 2018, 90, 615–627.
148. Victorious, A.; Saha, S.; Pandey, R.; Didar, T.F.; Soleymani, L. Affinity-Based Detection of Biomolecules Using Photoelectrochemical Readout. *Front. Chem.* 2019, 7, 617.
149. Zou, X.; Sun, Z.; Hu, Y.H. G-C₃N₄-Based Photoelectrodes for Photoelectrochemical Water Splitting: A Review. *J. Mater. Chem. A* 2020, 8, 21474–21502.
150. Zang, Y.; Ju, Y.; Hu, X.; Zhou, H.; Yang, Z.; Jiang, J.; Xue, H. WS₂ Nanosheets-Sensitized CdS Quantum Dots Heterostructure for Photoelectrochemical Immunoassay of Alpha-Fetoprotein Coupled with Enzyme-Mediated Biocatalytic Precipitation. *Analyst* 2018, 143, 2895–2900.
151. Mehrab Pourmadadi, Rajabzadeh-Khosroshahi, Fatemeh Saeidi Tabar, Narges Ajalli, Amirmasoud Samadi, Mahsa Yazdani, Fatemeh Yazdian, Abbas Rahdar, and Ana M. Díez-

- Pascual. Two-Dimensional Graphitic Carbon Nitride (g-C₃N₄) Nanosheets and Their Derivatives for Diagnosis and Detection Applications. *J. Funct. Biomater.* 2022, 13(4), 204;
152. Li, X.; Yuan, Y.; Pan, X.; Zhang, L.; Gong, J. Boosted Photoelectrochemical Immunosensing of Metronidazole in Tablet Using Coral-like g-C₃N₄ Nanoarchitectures. *Biosens. Bioelectron.* 2019, 123, 7–13.
153. Mao, L.; Xue, X.; Xu, X.; Wen, W.; Chen, M.M.; Zhang, X.; Wang, S. Heterostructured CuO-g-C₃N₄ Nanocomposites as a Highly Efficient Photocathode for Photoelectrochemical Aflatoxin B1 Sensing. *Sens. Actuators B Chem.* 2021, 329, 129146.
154. Mak, W.C.; Beni, V.; Turner, A.P.F. Lateral-Flow Technology: From Visual to Instrumental. *TrAC-Trends Anal. Chem.* 2016, 79, 297–305.
155. Zhu, H.; Fan, J.; Du, J.; Peng, X. Fluorescent Probes for Sensing and Imaging within Specific Cellular Organelles. *Acc. Chem. Res.* 2016, 49, 2115–2126.
156. Tan, G.R.; Wang, M.; Hsu, C.Y.; Chen, N.; Zhang, Y. Small Upconverting Fluorescent Nanoparticles for Biosensing and Bioimaging. *Adv. Opt. Mater.* 2016, 4, 984–997.
157. Han, J.; Burgess, K. Fluorescent Indicators for Intracellular pH. *Chem. Rev.* 2010, 110, 2709–2728.
158. Wang, H.; Wang, D.; Wang, Q.; Li, X.; Schalley, C.A. Nickel(II) and Iron(III) Selective off-on-Type Fluorescence Probes Based on Perylene Tetracarboxylic Diimide. *Org. Biomol. Chem.* 2010, 8, 1017–1026.
159. Kaczmarek, J.A.; Mitchell, J.A.; Spence, M.A.; Vongsouthi, V.; Jackson, C.J. Structural and Evolutionary Approaches to the Design and Optimization of Fluorescence-Based Small Molecule Biosensors. *Curr. Opin. Struct. Biol.* 2019, 57, 31–38.
160. Nawrot, W.; Drzozga, K.; Baluta, S.; Cabaj, J.; Malecha, K. A Fluorescent Biosensors for Detection Vital Body Fluids' Agents. *Sensors* 2018, 18, 2357.
161. Dodani, S.C.; He, Q.; Chang, C.J. A Turn-on Fluorescent Sensor for Detecting Nickel in Living Cells. *J. Am. Chem. Soc.* 2009, 131, 18020–18021.
162. Bauch, M.; Toma, K.; Toma, M.; Zhang, Q.; Dostalek, J. Plasmon-enhanced fluorescence biosensors: A review. *Plasmonics* 2014, 9, 781–799.
163. Serrano-Andrés, L.; Serrano-Pérez, J.J. Calculation of Excited States: Molecular Photophysics and Photochemistry on Display. In *Handbook of Computational Chemistry*; Springer: Berlin/Heidelberg, Germany, 2012; pp. 483–560.
164. Girigoswami, K.; Akhtar, N. Nanobiosensors and Fluorescence Based Biosensors: An Overview. *Int. J. Nano Dimens.* 2019, 10, 1–17.
165. Tao, H.; Fan, Q.; Ma, T.; Liu, S.; Gysling, H.; Texter, J.; Guo, F.; Sun, Z. Two-Dimensional Materials for Energy Conversion and Storage. *Prog. Mater. Sci.* 2020, 111, 100637.
166. Akada, K.; Terasawa, T.O.; Imamura, G.; Obata, S.; Saiki, K. Control of Work Function of Graphene by Plasma Assisted Nitrogen Doping. *Appl. Phys. Lett.* 2014, 104, 131602.
167. Paquin, F.; Rivnay, J.; Salleo, A.; Stingelin, N.; Silva, C. Multi-Phase Semicrystalline Microstructures Drive Exciton Dissociation in Neat Plastic Semiconductors. *J. Mater. Chem. C* 2015, 3, 10715–10722.
168. Lee, E.Z.; Jun, Y.S.; Hong, W.H.; Thomas, A.; Jin, M.M. Cubic Mesoporous Graphitic Carbon (IV) Nitride: An All-in-One Chemosensor for Selective Optical Sensing of Metal Ions. *Angew. Chemie-Int. Ed.* 2010, 49, 9706–9710.
169. Lv, J.; Feng, S.; Ding, Y.; Chen, C.; Zhang, Y.; Lei, W.; Hao, Q.; Chen, S.M. A High-Performance Fluorescent Probe for Dopamine Detection Based on g-C₃N₄ Nanofibers. *Spectrochim. Acta-Part A Mol. Biomol. Spectrosc.* 2019, 212, 300–307.
170. Chan, M.H.; Liu, R.S.; Hsiao, M. Graphitic Carbon Nitride-Based Nanocomposites and Their Biological Applications: A Review. *Nanoscale* 2019, 11, 14993–15003.
171. Yoo, S.M.; Jeon, Y.M.; Heo, S.Y. Electrochemiluminescence Systems for the Detection of Biomarkers: Strategical and Technological Advances. *Biosensors* 2022, 12, 738.
172. Wu, L.; Sha, Y.; Li, W.; Wang, S.; Guo, Z.; Zhou, J.; Su, X.; Jiang, X. One-Step Preparation of Disposable Multi-Functionalized g-C₃N₄ Based Electrochemiluminescence Immunosensor for the Detection of CA125. *Sens. Actuators B Chem.* 2016, 226, 62–68.
173. Wang, Y.Z.; Hao, N.; Feng, Q.M.; Shi, H.W.; Xu, J.J.; Chen, H.Y. A Ratiometric Electrochemiluminescence Detection for Cancer Cells Using G-C₃N₄ Nanosheets and Ag-PAMAM-Luminol Nanocomposites. *Biosens. Bioelectron.* 2016, 77, 76–82.
174. W. Quan, et al., 2D/2D Z-scheme photocatalyst of g-C₃N₄ and plasmonic Bi metal deposited Bi₂WO₆: Enhanced separation and migration of photoinduced charges, *J. Alloys Compd.*, 2023, 946, 169396.
175. H. Dong, et al., Insight into the activity and stability of Rh x P Nano-species supported on g-C₃N₄ for photocatalytic H₂ production, *ACS Catal.*, 2019, 10(1), 458–462.
176. H. Charles, et al., Synergistic effect of surface modification and effective interfacial charge transfer over faceted g-C₃N₄/ZnSe heterojunction to enhance CO₂ photoreduction activity, *J. Water Proc. Eng.*, 2023, 56, 104307.
177. Y. Li, et al., Crystallinity-defect matching relationship of g-C₃N₄: Experimental and theoretical perspectives, *Green Energy Environ.*, 2023, 9, 623–658.
178. M. Ismael, One-step ultrasonic-assisted synthesis of Nidoped g-C₃N₄ photocatalyst for enhanced photocatalytic hydrogen evolution, *Inorg. Chem. Commun.*, 2023, 151, 110607.
179. S. Mishra and R. Acharya, Recent updates in modification strategies for escalated performance of Graphene/MFe₂O₄ heterostructured photocatalysts towards energy and environmental applications, *J. Alloys Compd.*, 2023, 170576.
180. M. A. Ahmed, S. A. Mahmoud and A. A. Mohamed, Nanomaterials-modified reverse osmosis membranes: a comprehensive review, *RSC Adv.*, 2024, 14(27), 18879–18906.
181. K. Saravanakumar, et al., Noble metal nanoparticles (Mx =Ag, Au, Pd) decorated graphitic carbon nitride nanosheets for ultrafast catalytic reduction of anthropogenic pollutant, 4-nitrophenol, *Environ. Res.*, 2022, 212, 113185.
182. L. Ge, et al., Enhanced visible light photocatalytic activity of novel polymeric g-C₃N₄ loaded with Ag nanoparticles, *Appl. Catal., A*, 2011, 409, 215–222.
183. N. Cheng, et al., Au-nanoparticle-loaded graphitic carbon nitride nanosheets: green photocatalytic synthesis and application toward the degradation of organic pollutants, *ACS Appl. Mater. Interfaces*, 2013, 5(15), 6815–6819.
184. P. C. Nagajothi, et al., Enhanced photocatalytic activity of Ag/g-C₃N₄ composite, *Separ. Purif. Technol.*, 2017, 188, 228–237.
185. S. Tonda, et al., Fe-doped and-mediated graphitic carbon nitride nanosheets for enhanced photocatalytic performance under natural sunlight, *J. Mater. Chem. A*, 2014, 2(19), 6772–6780.
186. L. Hu, et al., Single Pd atoms anchored graphitic carbon nitride for highly selective and stable photocatalysis of nitric oxide, *Carbon*, 2022, 200, 187–198.
187. M. Z. Asghar, et al., A new Y-Zr/g-C₃N₄ nanoflakes anchored mesoporous silica composite for efficient environmental remediation applications, *Diamond Relat. Mater.*, 2023, 135, 109850.
188. Y. Liu, et al., Phenanthroline bridging graphitic carbon nitride framework and Fe (II) ions to promote transfer of

- photogenerated electrons for selective photocatalytic reduction of Nitrophenols, *J. Colloid Interface Sci.*, 2022, 608, 2088–2099.
189. X.-W. Guo, et al., Single-atom molybdenum immobilized on photoactive carbon nitride as efficient photocatalysts for ambient nitrogen fixation in pure water, *J. Mater. Chem. A*, 2019, 7(34), 19831–19837.
190. Y. Wang, et al., Synthesis of Mo-doped graphitic carbon nitride catalysts and their photocatalytic activity in the reduction of CO₂ with H₂O, *Catal. Commun.*, 2016, 74, 75–79.
191. S. Le, et al., Cu-doped mesoporous graphitic carbon nitride for enhanced visible-light driven photocatalysis, *RSC Adv.*, 2016, 6(45), 38811–38819.
192. P.-W. Chen, et al., Cobalt-doped graphitic carbon nitride photocatalysts with high activity for hydrogen evolution, *Appl. Surf. Sci.*, 2017, 392, 608–615.
193. T. H. Pham, J.-W. Park and T. Kim, Enhanced photodegradation of paracetamol from water by cobalt doped graphitic carbon nitride, *Sol. Energy*, 2021, 215, 151–156.
194. N. Paramasivam, A. Sambandan and B. Nastesan, Metalloids (B, Si) and non-metal (N, P, S) doped graphene nanosheet as a supercapacitor electrode: A density functional theory study, *Mater. Today Commun.*, 2023, 35, 105905.
195. L. Chen, et al., Phosphorus Doping Strategy-Induced Synergistic Modification of Interlayer Structure and Chemical State in Ti₃C₂T_x toward Enhancing Capacitance, *Molecules*, 2023, 28(13), 4892.
196. D. Masih, Y. Ma and S. Rohani, Graphitic C₃N₄ based noble-metal-free photocatalyst systems: a review, *Appl. Catal., B*, 2017, 206, 556–588.
197. S. Zhang, et al., Which kind of nitrogen chemical states doped carbon dots loaded by g-C₃N₄ is the best for photocatalytic hydrogen production, *J. Colloid Interface Sci.*, 2022, 622, 662–674.
198. S. Kumar, V. R. Battula and K. Kailasam, Single molecular precursors for C_xN_y Materials-Blending of carbon and nitrogen beyond g-C₃N₄, *Carbon*, 2021, 183, 332–354.
199. J. Jiang, et al., Sulfur-doped g-C₃N₄/g-C₃N₄ isotype stepscheme heterojunction for photocatalytic H₂ evolution, *J. Mater. Sci. Technol.*, 2022, 118, 15–24.
200. K. Chen, et al., 2D/2D Boron/g-C₃N₄ Nanosheet Heterojunction Boosts Photocatalytic Hydrogen Evolution Performance, *ACS Appl. Energy Mater.*, 2022, 5(9), 10657–10666.
201. K. S. Pasupuleti, et al., Boron doped g-C₃N₄ quantum dots based highly sensitive surface acoustic wave NO₂ sensor with faster gas kinetics under UV light illumination, *Sens. Actuators, B*, 2023, 378, 133140.
202. Y. Zhang, et al., Phosphorus-doped carbon nitride solid: enhanced electrical conductivity and photocurrent generation, *J. Am. Chem. Soc.*, 2010, 132(18), 6294–6295.
203. Y. Zhou, et al., Brand new P-doped gC₃N₄: enhanced photocatalytic activity for H₂ evolution and Rhodamine B degradation under visible light, *J. Mater. Chem. A*, 2015, 3(7), 3862–3867.
204. Y.-P. Zhu, T.-Z. Ren and Z.-Y. Yuan, Mesoporous phosphorus-doped g-C₃N₄ nanostructured flowers with superior photocatalytic hydrogen evolution performance, *ACS Appl. Mater. Interfaces*, 2015, 7(30), 16850–16856.
205. Q. Fan, et al., A simple fabrication for sulfur doped graphitic carbon nitride porous rods with excellent photocatalytic activity degrading RhB dye, *Appl. Surf. Sci.*, 2017, 391, 360–368.
206. J. Li, et al., A facile approach to synthesize novel oxygendoped g-C₃N₄ with superior visible-light photoreactivity, *Chem. Commun.*, 2012, 48(98), 12017–12019.
207. X. Yang, et al., Simple hydrothermal preparation of sulfur fluoride-doped g-C₃N₄ and its photocatalytic degradation of methyl orange, *Mater. Sci. Eng. B*, 2023, 288, 116216.
208. Z. Ding, et al., Synthesis of transition metal-modified carbon nitride polymers for selective hydrocarbon oxidation, *ChemSusChem*, 2011, 4(2), 274–281.
209. M. Wang, et al., Synthesis of hollow lantern-like Eu (III)-doped g-C₃N₄ with enhanced visible light photocatalytic performance for organic degradation, *J. Hazard Mater.*, 2018, 349, 224–233.
210. G. Li, et al., Er-doped g-C₃N₄ for photodegradation of tetracycline and tylosin: high photocatalytic activity and low leaching toxicity, *Chem. Eng. J.*, 2020, 391, 123500.
211. Y. Wang, et al., Bio-template synthesis of Mo-doped polymer carbon nitride for photocatalytic hydrogen evolution, *Appl. Catal., B*, 2019, 248, 44–53.
212. A. Ahmed, et al., Zinc-doped mesoporous graphitic carbon nitride for colorimetric detection of hydrogen peroxide, *ACS Appl. Nano Mater.*, 2019, 2(8), 5156–5168.
213. F. Dong, et al., A general method for type I and type II gC₃N₄/gC₃N₄ metal-free isotype heterostructures with enhanced visible light photocatalysis, *New J. Chem.*, 2015, 39(6), 4737–4744.
214. Y. Zhu, et al., Tunable Type I and II heterojunction of CoOx nanoparticles confined in g-C₃N₄ nanotubes for photocatalytic hydrogen production, *Appl. Catal., B*, 2019, 244, 814–822.
215. Y. Shi, et al., Engineering of 2D/3D architectures type II heterojunction with high-crystalline g-C₃N₄ nanosheets on yolk-shell ZnFe₂O₄ for enhanced photocatalytic tetracycline degradation, *Mater. Res. Bull.*, 2022, 150, 111789.
216. W. Shi, et al., Fabrication of ternary Ag₃PO₄/Co₃(PO₄)₂/g-C₃N₄ heterostructure with following Type II and Z-Scheme dual pathways for enhanced visible-light photocatalytic activity, *J. Hazard Mater.*, 2020, 389, 121907.
217. M. Que, et al., Recent advances in gC₃N₄ composites within four types of heterojunctions for photocatalytic CO₂ reduction, *Nanoscale*, 2021, 13(14), 6692–6712.
218. S. Obregón, et al., A novel type-II Bi₂W₂O₉/g-C₃N₄ heterojunction with enhanced photocatalytic performance under simulated solar irradiation, *Mater. Sci. Semicond. Process.*, 2020, 113, 105056.
219. H. Huang, et al., Self-sacrifice transformation for fabrication of type-I and type-II heterojunctions in hierarchical Bi_xOyIz/g-C₃N₄ for efficient visible-light photocatalysis, *Appl. Surf. Sci.*, 2019, 470, 1101–1110.
220. W. He, et al., Controllable morphology CoFe₂O₄/g-C₃N₄ pn heterojunction photocatalysts with built-in electric field enhance photocatalytic performance, *Appl. Catal., B*, 2022, 306, 121107.
221. W. Chen, et al., Accelerated photocatalytic degradation of tetracycline hydrochloride over CuAl₂O₄/g-C₃N₄ pn heterojunctions under visible light irradiation, *Sep. Purif. Technol.*, 2021, 277, 119461.
222. S. Yin, et al., Ionic liquid-assisted synthesis and improved photocatalytic activity of pn junction gC₃N₄/BiOCl, *J. Mater. Sci.*, 2016, 51, 4769–4777.
223. L. Acharya, et al., Development of MgIn₂S₄ microflowerembedded exfoliated B-doped g-C₃N₄ nanosheets: p-n heterojunction photocatalysts toward photocatalytic water reduction and H₂O₂ production under visible-light irradiation, *ACS Appl. Energy Mater.*, 2022, 5(3), 2838–2852.
224. M. A. Ahmed, M. A. Ahmed and A. A. Mohamed, Fabrication of NiO/g-C₃N₄ Z-scheme heterojunction for enhanced photocatalytic degradation of methylene blue dye, *Opt. Mater.*, 2024, 151, 115339.
225. W. Zhao, W. Wang and H. Shi, 2D/2D Z-scheme BiO1-XBr/g-C₃N₄ heterojunction with rich oxygen vacancies as electron mediator for enhanced visible-light degradation activity, *Appl. Surf. Sci.*, 2020, 528, 146925.
226. A. Behera, A. K. Kar and R. Srivastava, Oxygen vacancy-mediated Z-scheme charge transfer in a 2D/1D B-doped

- g-C₃N₄/rGO/TiO₂ heterojunction visible light-driven photocatalyst for simultaneous/efficient oxygen reduction reaction and alcohol oxidation, *Inorg. Chem.*, 2022, 61(32), 12781–12796.
227. M. Chandra, U. Guharoy and D. Pradhan, Boosting the Photocatalytic H₂ Evolution and Benzylamine Oxidation using 2D/1D g-C₃N₄/TiO₂ Nanoheterojunction, *ACS Appl. Mater. Interfaces*, 2022, 14, 22122–22137.
228. Y. R. Girish, et al., Facile and rapid synthesis of solar-driven TiO₂/g-C₃N₄ heterostructure photocatalysts for enhanced photocatalytic activity, *J. Sci.: Adv. Mater. Devices*, 2022, 7(2), 100419.
229. [229] J. Yang, et al., CVD Assisted Synthesis of Macro/Mesoporous TiO₂/g-C₃N₄ S-Scheme Heterojunction for Enhanced Photocatalytic Hydrogen Evolution, *Adv. Sustainable Syst.*, 2022, 6(8), 2200056.
230. T. H. Pham, et al., Enhanced photodegradation of tetracycline in wastewater and conversion of CO₂ by solar light assisted ZnO/g-C₃N₄, *Environ. Res.*, 2023, 217, 114825.
231. T. Kobkeathawin, et al., Photocatalytic activity of TiO₂/g-C₃N₄ nanocomposites for removal of monochlorophenols from water, *Nanomaterials*, 2022, 12(16), 2852.
232. J. Singh, A. Arora and S. Basu, Synthesis of coral like WO₃/g-C₃N₄ nanocomposites for the removal of hazardous dyes under visible light, *J. Alloys Compd.*, 2019, 808, 151734.
233. H. Wang, et al., Constructing defect engineered 2D/2D MoO₃/g-C₃N₄ Z-scheme heterojunction for enhanced photocatalytic activity, *J. Alloys Compd.*, 2022, 926, 166964.
234. S. Bellamkonda and G. R. Rao, Nanojunction-mediated visible light photocatalytic enhancement in heterostructured ternary BiOCl/CdS/g-C₃N₄ nanocomposites, *Catal. Today*, 2019, 321, 18–25.
235. H. A. Omer, et al., Design of sculptured SnS/g-C₃N₄ photocatalytic nanostructure for highly efficient and selective CO₂ conversion to methane, *Appl. Catal., B*, 2023, 324, 122231.
236. J. Song, et al., Exploration of the g-C₃N₄ Heterostructure with Ag-In sulfide quantum dots for enhanced photocatalytic activity, *ACS Appl. Electron. Mater.*, 2023, 5(8), 4134–4144.
237. Q. Wu, et al., In-situ synthesis of ternary heterojunctions via g-C₃N₄ coupling with noble-metal-free NiS and CdS with efficient visible-light-induced photocatalytic H₂ evolution and mechanism insight, *Int. J. Hydrogen Energy*, 2022, 47(30), 14063–14076.
238. Y. Ren, D. Zeng and W.-J. Ong, Interfacial engineering of graphitic carbon nitride (g-C₃N₄)-based metal sulfide heterojunction photocatalysts for energy conversion: a review, *Chin. J. Catal.*, 2019, 40(3), 289–319.
239. D. Wei, et al., Cooperative effects of zinc-nickel sulfides as a dual cocatalyst for the enhanced photocatalytic hydrogen evolution activity of g-C₃N₄, *J. Environ. Chem. Eng.*, 2022, 10(2), 107216.
240. X.-y. Ji, et al., Fabrication of a ternary NiS/ZnIn₂S₄/g-C₃N₄ photocatalyst with dual charge transfer channels towards efficient H₂ evolution, *J. Colloid Interface Sci.*, 2022, 618, 300–310.
241. S. Yang, et al., Size effect of CoS₂ cocatalyst on photocatalytic hydrogen evolution performance of g-C₃N₄, *J. Colloid Interface Sci.*, 2023, 635, 305–315.
242. D. C. Onwudiwe, et al., Dual S-scheme heterojunction g-C₃N₄/Bi₂S₃/CuS composite with enhanced photocatalytic activity for methyl orange degradation, *Inorg. Chem. Commun.*, 2023, 155, 111075.
243. C. Wang, et al., S-scheme bimetallic sulfide ZnCo₂S₄/g-C₃N₄ heterojunction for photocatalytic H₂ evolution, *Ceram. Int.*, 2021, 47(21), 30194–30202.
244. Z. Chen, et al., Single-sites Rh-phosphide modified carbon nitride photocatalyst for boosting hydrogen evolution under visible light, *Appl. Catal., B*, 2020, 274, 119117.
245. Y. Lin, et al., LaOCl-coupled polymeric carbon nitride for overall water splitting through a one-photon excitation pathway, *Angew. Chem., Int. Ed.*, 2020, 59(47), 20919–20923.
246. A. Alsulmi, et al., Engineering S-scheme Ag₂CO₃/g-C₃N₄ heterojunctions sonochemically to eradicate Rhodamine B dye under solar irradiation, *RSC Adv.*, 2023, 13(18), 12229–12243.
247. N. Tian, et al., Facet-charge-induced coupling dependent interfacial photocharge separation: a case of BiOI/g-C₃N₄ pn junction, *Appl. Catal., B*, 2020, 267, 118697.
248. A. Alsulmi, et al., Sonochemical Fabrication of S-Scheme AgI/g-C₃N₄ Heterojunction for Efficient Photocatalytic Degradation of RhB Dye, *J. Inorg. Organomet. Polym. Mater.*, 2023, 1–15.
249. R. Manjupriya and S. M. Roopan, Unveiling the Photocatalytic Activity of Carbon Dots/g-C₃N₄ Nanocomposite for the O-Arylation of 2-Chloroquinoline-3-carbaldehydes, *Catalysts*, 2023, 13(2), 308.
250. X. Zhou, et al., Superior uniform carbon nanofibers@ g-C₃N₄ core-shell nanostructures embedded by Au nanoparticles for high-efficiency photocatalyst, *J. Hazard Mater.*, 2020, 388, 121759.
251. Y. Shan, et al., Nanocellulose-derived carbon/g-C₃N₄ heterojunction with a hybrid electron transfer pathway for highly photocatalytic hydrogen peroxide production, *J. Colloid Interface Sci.*, 2021, 599, 507–518.
252. M. Inagaki, et al., Graphitic carbon nitrides (g-C₃N₄) with comparative discussion to carbon materials, *Carbon*, 2019, 141, 580–607.
253. G. Bottari, et al., Covalent and noncovalent phthalocyanine-carbon nanostructure systems: synthesis, photoinduced electron transfer, and application to molecular photovoltaics, *Chem. Rev.*, 2010, 110(11), 6768–6816.
254. Z. Li, et al., Carbon-based functional nanomaterials: Preparation, properties and applications, *Compos. Sci. Technol.*, 2019, 179, 10–40.
255. Y. Fu, et al., Photocatalytic H₂O₂ and H₂ Generation from Living *Chlorella vulgaris* and Carbon Micro Particle Comodified g-C₃N₄, *Adv. Energy Mater.*, 2018, 8(34), 1802525.
256. S. Zhao, et al., Carbon-based metal-free catalysts for key reactions involved in energy conversion and storage, *Adv. Mater.*, 2019, 31(9), 1801526.
257. T. Su, et al., 2D/2D heterojunction of Ti₃C₂/g-C₃N₄ nanosheets for enhanced photocatalytic hydrogen evolution, *Nanoscale*, 2019, 11(17), 8138–8149.
258. L. Cheng, et al., Carbon-graphitic carbon nitride hybrids for heterogeneous photocatalysis, *Small*, 2021, 17(1), 2005231.
259. Y. Xu, et al., Carbon-based nanostructures for emerging photocatalysis: CO₂ reduction, N₂ fixation, and organic conversion, *Trends Chem.*, 2022, 4, 984–1004.
260. Y. Li, et al., ZIF-67 derived Co@ NC/g-C₃N₄ as a photocatalyst for enhanced water splitting H₂ evolution, *Environ. Res.*, 2021, 197, 111002.
261. R. Zhang, et al., Multifunctional g-C₃N₄/graphene oxide wrapped sponge monoliths as highly efficient adsorbent and photocatalyst, *Appl. Catal., B*, 2018, 235, 17–25.
262. H. Wang, et al., Preparation of nanoscale-dispersed g-C₃N₄/graphene oxide composite photocatalyst with enhanced visible-light photocatalytic activity, *Mater. Lett.*, 2018, 217, 143–145.
263. R. Zhang, et al., Surface modification to control the secondary pollution of photocatalytic nitric oxide removal over monolithic protonated g-C₃N₄/graphene oxide aerogel, *J. Hazard. Mater.*, 2020, 397, 122822.

264. Z. Shi, et al., The photocatalytic activity and purification performance of g-C₃N₄/carbon nanotubes composite photocatalyst in underwater environment, *Environ. Sci. Pollut. Res.*, 2022, 29(55), 83981–83992.
265. G. Liu, et al., Enhanced photodegradation performance of Rhodamine B with g-C₃N₄ modified by carbon nanotubes, *Sep. Purif. Technol.*, 2020, 244, 116618.
266. Z. Shi, et al., Influences of different carbon substrates on the morphologies of carbon/g-C₃N₄ photocatalytic composites and the purification capacities of different composites in the weak UV underwater environment, *Chemosphere*, 2022, 308, 136257.
267. Mahmoud A. Ahmed, Safwat A. Mahmoud and Ashraf A. Mohamed. Unveiling the photocatalytic potential of graphitic carbon nitride (g-C₃N₄): a state-of-the-art review. *RSC Adv.*, 2024, 14, 25629,
268. Hao, D. et al, 2021. 2021.. A green synthesis of Ru modified g-C₃N₄ nanosheets for enhanced photocatalytic ammonia synthesis. *Energy Mater. Adv.* 2021.
269. Zhao, G. et al, 2017. Co-porphyrin/carbon nitride hybrids for improved photocatalytic CO₂ reduction under visible light. *Appl. Catal. B* 200, 141–149.
270. Liu, C. et al, 2017. Intermediate-mediated strategy to horn-like hollow mesoporous ultrathin g-C₃N₄ tube with spatial anisotropic charge separation for superior photocatalytic H₂ evolution. *Nano Energy*, 738–748.
271. Bai, Y. et al, 2016. Size-dependent role of gold in g-C₃N₄/BiOBr/Au system for photocatalytic CO₂ reduction and dye degradation. *Sol. Energy Mater. Sol. Cells* 157, 406–414.
272. You, R. et al, 2017. Graphitic carbon nitride with S and O cooping for enhanced visible light photocatalytic performance. *RSC Adv.* 7 (26), 15842–15850.
273. Zhang, J.R., Kan, Y.S., Gu, L.I., Wang, C.Y., Zhang, Y.: Graphite carbon nitride and its composites for medicine and health applications. *Asian J. Chem.* 16, 2003–2013 (2021).
274. Liu, H., Wang, X., Wang, H., Nie, R.: Synthesis and biomedical applications of graphitic carbon nitride quantum dots. *J. Mater. Chem. B* 7, 5432–5448 (2019).
275. Perveen, M., Nazir, S., Arshad, A.W., Khan, M.I., Shamim, M., Ayub, K., Khan, M.A., Iqbal, J.: Therapeutic potential of graphitic carbon nitride as a drug delivery system for cisplatin (anticancer drug): a DFT approach. *Biophys. Chem.* 267, 106461 (2020).
276. Dasari, S., Tchounwou, P.B.: Cisplatin in cancer therapy: molecular mechanisms of action. *Eur. J. Pharmacol.* 740, 364–378 (2014).
277. Duan, X., He, C., Kron, S.J., Lin, W.: Nanoparticle formulations of cisplatin for cancer therapy. *Wiley Interdiscip. Rev. Nanomed. Nanobiotechnol.* 8, 776–791 (2016).
278. Shamim, M., Perveen, M., Nazir, S., Hussnain, M., Mehmood, R., Khan, M.I., Iqbal, J.: DFT study of therapeutic potential of graphitic carbon nitride (g-C₃N₄) as a new drug delivery system for carboplatin to treat cancer. *J. Mol. Liq.* 331, 115607 (2021).
280. Taheri, H., Unal, M.A., Sevim, M., Gurcan, C., Ekim, O., Ceylan, A., Syrgiannis, Z., Christoforidis, K.C., Bosi, S., Ozgenç, O.: Photocatalytically active graphitic carbon nitride as an effective and safe 2D material for in vitro and in vivo photodynamic therapy. *Small* 16, 1904619 (2020).
281. Feng, L., He, F., Yang, G., Gai, S., Dai, Y., Li, C., Yang, P.: NIRdriven graphitic-phase carbon nitride nanosheets for efficient bioimaging and photodynamic therapy. *J. Mater. Chem. B* 4, 8000–8008 (2016).
282. Davardoostmanesh, M., Ahmadzadeh, H., Goharshadi, E.K., Meshkini, A., Sistanipour, E.: Graphitic carbon nitride nanosheets prepared by electrophoretic size fractionation as an anticancer agent against human bone carcinoma. *Mater. Sci. Eng. C* 111, 110803 (2020).
283. Das, C.A., Kumar, V.G., Dhas, T.S., Karthick, V., Kumar, C.V.: Nanomaterials in anticancer applications and their mechanism of action—a review. *Nanomed. Nanotechnol. Biol. Med.* 47, 102613 (2022).
284. Lopes, J.C., Torres, M.L.P.: Utilização de nanopartículas no tratamento do câncer: aspectos gerais, mecanismos de ação antineoplásicos e aplicabilidades tumorais. *Rev. Bras. Cancerol.* 65, 13400 (2019).
285. Dong, J., Zhao, Y., Chen, H., Liu, L., Zhang, W., Sun, B., Yang, M., Wang, Y., Dong, L.: Fabrication of PEGylated graphitic carbon nitride quantum dots as traceable, pH-sensitive drug delivery systems. *New J. Chem.* 42, 14263–14270 (2018).
286. Heo, N.S., Lee, S.U., Rethinasabapathy, M., Lee, E.Z., Cho, H.J., Oh, S.Y., Choe, S.R., Kim, Y., Hong, W.G., Krishnan, G.: Visible-light-driven dynamic cancer therapy and imaging using graphitic carbon nitride nanoparticles. *Mater. Sci. Eng. C* 90, 531–538 (2018).
287. Jiang, X., Feng, Y., Wang, J.: High-energy microwave synthesis of g-C₃N₄ nanosheets and its application as an anti-cancer drug carrier. *FlatChem* 30, 100311 (2021).
288. Kong, X., Liu, X., Zheng, Y., Chu, P.K., Zhang, Y., Wu, S.: Graphitic carbon nitride-based materials for photocatalytic antibacterial application. *Mater. Sci. Eng. R Rep.* 145, 100610 (2021).
289. Li, Y., Liu, X., Tan, L., Cui, Z., Yang, X., Zheng, Y., Yeung, K.W.K., Chu, P.K., Wu, S.: Rapid sterilization and accelerated wound healing using Zn²⁺ and graphene oxide modified g-C₃N₄ under dual light irradiation. *Adv. Funct. Mater.* 28, 1800299 (2018).
290. Xiang, Y., Zhou, Q., Li, Z., Cui, Z., Liu, X., Liang, Y., Zhu, S., Zheng, Y., Yeung, K.W.K., Wu, S.: A Z-scheme heterojunction of ZnO/CDots/C₃N₄ for strengthened photoresponsive bacteriakilling and acceleration of wound healing. *J. Mater. Sci. Technol.* 57, 1–11 (2020).
291. Hasiija, V., Singh, S.P., Nguyen, V.H., Le, Q.V., Thakur, V.K., Hussain, C.M., Selvasembian, R., Huang, C.W., Thakur, S.: Photocatalytic inactivation of viruses using graphitic carbon nitridebased photocatalysts: virucidal performance and mechanism. *Catalysts* 11, 1448 (2021).
292. Li, J., Yin, Y., Liu, E., Ma, Y., Wan, J., Fan, J., Hu, X.: In situ growing Bi₂MoO₆ on g-C₃N₄ nanosheets with enhanced photocatalytic hydrogen evolution and disinfection of bacteria under visible light irradiation. *J. Hazard. Mater.* 321, 183–192 (2017).
293. Wang, X., Hu, Y., Wei, H.: Nanozymes in bionanotechnology: from sensing to therapeutics and beyond. *Inorg. Chem. Front.* 3, 41–60 (2016).
294. Huang, X., Gu, W., Ma, Y., Liu, D., Ding, N., Zhou, L., Lei, J., Wang, L., Zhang, J.: Recent advances of doped graphite carbon nitride for photocatalytic reduction of CO₂: a review. *Res. Chem. Intermed.* 46, 5133–5164 (2020).
295. Gao, L., Zhuang, J., Nie, L., Zhang, J., Zhang, Y., Gu, N., Wang, T., Feng, J., Yang, D., Perrett, S.: Intrinsic peroxidase-like activity of ferromagnetic nanoparticles. *Nat. Nanotechnol.* 2, 577–583 (2007).
296. Wei, H., Wang, E.: Fe₃O₄ magnetic nanoparticles as peroxidase mimetics and their applications in H₂O₂ and glucose detection. *Anal. Chem.* 80, 2250–2254 (2008).
297. Zhang, P., Sun, D., Cho, A., Weon, S., Lee, S., Lee, J., Han, J.W., Kim, D.P., Choi, W.: Modified carbon nitride nanozyme as bifunctional glucose oxidase-peroxidase for metal-free bioinspired cascade photocatalysis. *Nat. Commun.* 10, 1–14 (2019).
298. Emran, M.Y., Shenashen, M.A., El Sabagh, A., Selim, M.M., El-Safty, S.A.: Enzymeless copper microspheres@carbon sensor design for sensitive and selective acetylcholine screening in

- human serum. *Colloids Surf. B Biointerfaces* 210, 112228 (2022).
299. Sun, C., Chen, X., Xu, J., Wei, M., Wang, J., Mi, X., Wang, X., Wu, Y., Liu, Y.: Fabrication of an inorganic–organic hybrid based on an iron-substituted polyoxotungstate as a peroxidase for colorimetric immunoassays of H₂O₂ and cancer cells. *J. Mater. Chem. A* 1, 4699–4705 (2013).
300. Lee, Y.C., Kim, M.I., Woo, M.A., Park, H.G., Han, J.I.: Effective peroxidase-like activity of a water-solubilized Fe-aminoclay for use in immunoassay. *Biosens. Bioelectron.* 42, 373–378 (2013).
301. Wang, Z., Dong, K., Liu, Z., Zhang, Y., Chen, Z., Sun, H., Ren, J., Qu, X.: Activation of biologically relevant levels of reactive oxygen species by Au/g-C₃N₄ hybrid nanozyme for bacteria killing and wound disinfection. *Biomaterials* 113, 145–157 (2017).
302. Zhang, X., Wang, H., Wang, H., Zhang, Q., Xie, J., Tian, Y., Wang, J., Xie, Y.: Single-layered graphitic-C₃N₄ quantum dots for two-photon fluorescence imaging of cellular nucleus. *J. Adv. Mater.* 26, 4438–4443 (2014)
303. Zhang, X., Xie, X., Wang, H., Zhang, J., Pan, B., Xie, Y.: Enhanced photoresponsive ultrathin graphitic-phase C₃N₄ nanosheets for bioimaging. *JACS* 135, 18–21 (2013).
304. Ding, H., Zhang, P., Wang, T.Y., Kong, J.L., Xiong, H.M.: Nitrogen-doped carbon dots derived from polyvinyl pyrrolidone and their multicolor cell imaging. *J. Nanotechnol.* 25, 205604 (2014).
305. Liu, T., Li, M., Dong, P., Zhang, Y., Guo, L.: Design and facile synthesis of mesoporous cobalt nitride nanosheets modified by pyrolytic carbon for the nonenzymatic glucose detection. *Sens. Actuators B Chem.* 255, 1983–1994 (2018).
306. Xu, Y., Niu, X., Zhang, H., Xu, L., Zhao, S., Chen, H., Chen, X.: Switch-on fluorescence sensing of glutathione in food samples based on a graphitic carbon nitride quantum dot (g-CNQD)–Hg²⁺ chemosensor. *J. Agric. Food Chem.* 63, 1747–1755 (2015).
307. Zhuang, Q., Guo, P., Zheng, S., Lin, Q., Lin, Y., Wang, Y., Ni, Y.: Green synthesis of luminescent graphitic carbon nitride quantum dots from human urine and its bioimaging application. *Talanta* 188, 35–40 (2018).
308. Yan, Q., Huang, G.F., Li, D.-F., Zhang, M., Pan, A.L., Huang, W.Q.: Facile synthesis and superior photocatalytic and electrocatalytic performances of porous B-doped g-C₃N₄ nanosheets. *J. Mater. Sci. Technol.* 34, 2515–2520 (2018).
309. Lu, Y.C., Chen, J., Wang, A.J., Bao, N., Feng, J.J., Wang, W., Shao, L.: Facile synthesis of oxygen and sulfur co-doped graphitic carbon nitride fluorescent quantum dots and their application for mercury (II) detection and bioimaging. *Mater. Chem. C* 3, 73–78 (2015).
310. Zhang, H., Zheng, D., Cai, Z., Song, Z., Xu, Y., Chen, R., Lin, C., Guo, L.: Graphitic carbon nitride nanomaterials for multicolor light-emitting diodes and bioimaging. *ACS Appl. Nano Mater.* 3, 6798–6805 (2020).
311. Li, H., Shao, F.Q., Huang, H., Feng, J.J., Wang, A.J.: Eco-friendly and rapid microwave synthesis of green fluorescent graphitic carbon nitride quantum dots for vitro bioimaging. *Sens. Actuators B Chem.* 226, 506–511 (2016).
312. Wu, J., Yang, S., Li, J., Yang, Y., Wang, G., Bu, X., He, P., Sun, J., Yang, Y., Deng, Y.: Electron injection of phosphorus doped g-C₃N₄ quantum dots: controllable photoluminescence emission wavelength in the whole visible light range with high quantum yield. *Adv. Opt. Mater.* 4, 2095–2101 (2016).
313. Cai, Z., Chen, J., Xing, S., Zheng, D., Guo, L.: Highly fluorescent g-C₃N₄ nanobelts derived from bulk g-C₃N₄ for NO₂ gas sensing. *J. Hazard. Mater.* 416, 126195 (2021).
314. Muhammad, M.H., Chu, Y.M., Chen, X.L., Qu, L., Yu, B., Siddiqui, M.K., Nasir, M.: On topological analysis of graphite carbon nitride via degree based coindices. *Polycycl. Aromat. Compd.* 42, 1–15 (2020)
315. Chu, Y.M., Muhammad, M.H., Rauf, A., Ishtiaq, M., Siddiqui, M.K.: Topological study of polycyclic graphite carbon nitride. *Polycycl. Aromat. Compd.* 42, 1–13 (2020).
316. Huang, R., Muhammad, M.H., Siddiqui, M.K., Nasir, M., Cancan, M.: On degree based topological co-indices of graphite carbon nitride. *Polycycl. Aromat. Compd.* 42, 1–10 (2021).
317. Rauf, A., Ishtiaq, M., Muhammad, M.H., Siddiqui, M.K., Rubbab, Q.: Algebraic polynomial based topological study of graphite carbon nitride (g-) molecular structure. *Polycycl. Aromat. Compd.* 42, 1–22 (2021).
318. Muhammad Sohail, Usama Anwar, T.A. Taha, H.I.A. Qazi, Abdullah G. Al Sehem, Sami Ullah, Hamed Algarni, I.M. Ahmed, Mohammed A. Amin, Arkom Palamanit, Waseem Iqbal, Sarah Alharthi, W. I. Nawawi, Zeeshan Ajmal, Hamid Ali, Asif Hayat. Nanostructured materials based on g-C₃N₄ for enhanced photocatalytic activity and potentials application: A review. *Arabian Journal of Chemistry* Volume 15, Issue 9, September 2022, 104070



This work is licensed under Creative Commons Attribution 4.0 License

To Submit Your Article Click Here:

Submit Manuscript

DOI:10.31579/2766-2314/150

Ready to submit your research? Choose Auctores and benefit from:

- fast, convenient online submission
- rigorous peer review by experienced research in your field
- rapid publication on acceptance
- authors retain copyrights
- unique DOI for all articles
- immediate, unrestricted online access

At Auctores, research is always in progress.

Learn more <https://www.auctoresonline.org/journals/biotechnology-and-bioprocessing>